

Stress Signaling Pathways in Metabolic Disorders

Inaugural-Dissertation

zur Erlangung des Doktorgrades

der Mathematisch-Naturwissenschaftlichen Fakultät
der Universität Köln

vorgelegt von

Martin Pal

aus Köln

Köln, Februar 2012

Berichterstatter: **Prof. Dr. Jens Brüning**
PD Dr. Thomas Wunderlich

Tag der mündlichen Prüfung: 12.04.2012

Contents

Abbreviations	x
Abstract	xii
Zusammenfassung	xiii
1 Introduction	1
1.1 Metabolic Homeostasis	1
1.2 Obesity and Type 2 Diabetes - Metabolic Threats	1
1.3 Insulin - the Metabolism's Central Hormone	3
1.4 Obesity induced Stress-Kinase Signaling	5
1.4.1 Obesity induced JNK Activation	6
1.5 Physical Exercise induced JNK Activation	8
1.6 Skeletal Muscle - an Endocrine Organ	10
1.6.1 Physical Exercise induced IL-6 activation	11
1.7 Obesity induced ER Stress	14
1.7.1 IRE1/XBP1-induced JNK activation	15
1.8 Conditional Gene Targeting	17
1.9 Objectives	19
2 Materials and Methods	20
2.1 Chemicals and Biological Material	20
2.1.1 Targeting Vectors	23
2.2 Molecular Biology	25
2.2.1 Isolation of Genomic DNA	25
2.2.2 Quantification of Nucleid Acids	25
2.2.3 Polymerase Chain Reaction	25
2.2.4 Southern Blot	27

2.2.5	Gene Expression Analysis	28
2.3	Cell Biology	30
2.3.1	Cell Culture	30
2.3.2	Immunohistochemistry	30
2.3.3	Flow Cytometry	30
2.4	Biochemistry	31
2.4.1	Enzyme-Linked Immunosorbent Assay (ELISA)	31
2.4.2	Protein Extraction	31
2.4.3	Western Blot Analysis	31
2.4.4	c-Jun N-terminal Kinase Assay	32
2.5	Mouse Experiments	33
2.5.1	Animal Care	33
2.5.2	Mice	33
2.5.3	Genotyping of Mice	35
2.5.4	Collection of Blood Samples and Determination of Blood Glucose and Lactate Levels	35
2.5.5	Analysis of Body Composition (NMR)	35
2.5.6	Glucose, Insulin, and Pyruvate Tolerance Test	35
2.5.7	Insulin Signaling	36
2.5.8	Isolation of Adipocytes and Stromal Vascular Fraction	36
2.5.9	Isolation of Primary Peritoneal Macrophages	36
2.5.10	Isolation of Kupffer Cells	37
2.5.11	Food Intake	37
2.5.12	Indirect Calorimetry	37
2.5.13	Treadmill	37
2.6	Computer Analysis	39
2.6.1	Densitometrical Analysis	39
2.6.2	Statistical Methods	39

3	Results	40
3.1	The role of skeletal muscle derived JNK in metabolic regulation	40
3.1.1	Increased JNK activity in skeletal muscle of obese mice	40
3.1.2	Generation of a skeletal muscle specific knockout of JNK-1	41
3.1.3	Unaltered energy homeostasis in JNK-1 ^{SM-KO} mice	44
3.1.4	Unaltered glucose metabolism and insulin sensitivity in JNK-1 ^{SM-KO} mice	47
3.1.5	Exercise induces activation of JNK and IL-6 in skeletal muscle of WT mice	50
3.1.6	Exercise induced IL-6 mRNA increase in skeletal muscle is blunted in JNK-1 ^{SM-KO} mice	51
3.1.7	Generation of a JNK-1 gain of function mouse in skeletal muscle .	55
3.1.8	Unaltered energy homeostasis in JNK-1 ^{SM-C} mice	56
3.1.9	Unaltered insulin sensitivity in JNK-1 ^{SM-C} mice	59
3.1.10	Hepatic glucose production of JNK-1 ^{SM-C} mice	60
3.1.11	Expression pattern of the JNK isoforms in tissues of WT mice . . .	64
3.1.12	Generation of a loxP-flanked JNK-2 allele in mice	65
3.2	Central and peripheral induction of ER stress	68
3.2.1	Targeted insertion of mXBP1s into the murine ROSA26 locus . . .	68
3.2.2	Hippocampal expression of mXBP1s results in increased expression of central and hepatic ER stress markers	70
3.3	Characterization of a novel adipose tissue specific Cre recombinase mouse line	76
3.3.1	FABP-4-2A-Cre-mediated recombination in FOXODN ^{FABP4} mice .	77
3.3.2	FABP4-2A-Cre-mediated recombination in IL-6R α ^{FABP4} mice	81
4	Discussion	84
4.1	Role of skeletal muscle specific JNK-1 in metabolic regulation	84
4.1.1	Inactivation of the JNK-1 gene specifically in skeletal muscle	84
4.1.2	Role of skeletal muscle specific JNK-1 in the regulation of energy and glucose homeostasis	85

4.1.3	Role of skeletal muscle specific JNK-1 in the regulation of exercise-induced IL-6 activation	87
4.1.4	Constitutive JNK activation in skeletal muscle	90
4.1.5	Successful generation of a conditional JNK-2 allele in mice	92
4.2	Conditional overexpression of mXBP1s protein in brain and liver	93
4.3	FABP4-2A-Cre-mediated recombination	95
	List of Figures	100
	List of Tables	101
	Bibliography	102
	Danksagung	120
	Erklärung	122
	Curriculum Vitae	123

Abbreviations

5'	sugar end of a DNA strand
3'	phosphate end of a DNA strand
°C	temperature in degrees celsius
aa	amino acid
AKT	protein kinase B
AP2	Adipocyte protein 2
BAC	bacterial artificial chromosome
BAT	brown adipose tissue
BMI	body mass index
bp	base pair
BSA	bovine serum albumin
CAG(s)	strong Chicken β -actin promoter
CNS	central nervous system
Cre	causes recombination, site-specific recombinase from phage P1
cDNA	complementary DNA
CO ₂	carbon dioxide
ddH ₂ O	double distilled water
DMEM	Dulbeccos's modified Eagle medium
DNA	desoxy ribonucleotid acid
dNTP	2' desoxyribonucleosidtriphosphate
EF	mouse embryonic fibroblasts
e.g.	<i>exempli gratia</i>
eGFP	enhanced green fluorescent protein
ES	mouse embryonic stem cells

ELISA	enzyme-linked immunosorbent assay
ER	endoplasmic reticulum
EtBr	ethidium bromide
EtOH	ethanol
FABP4	Fatty acid binding protein 4
FACS	Fluorescence-activated cell sorting
FFA	free fatty acid
FCS	fetal calf serum
Fig.	figure
floxed	flanked by loxP sites
Flp	site-specific recombinase from yeast
FOXODN	dominant negative version of the forkhead box-containing protein class O
FRT	<u>F</u> lp <u>r</u> ecognition <u>t</u> arget site
g	gramm
GTT	glucose tolerance test
h	hour
HFD	high fat diet
HGP	hepatic glucose production
H ₂ O	water molecule
IL-6	interleukin 6
IL-6R α	interleukin 6 receptor alpha
i.p.	intraperitoneal
IRES	internal ribosomal entry site
ITT	insulin tolerance test
JNK	c-Jun N-terminal kinase
kb	kilo base
kDa	kilo Dalton
KO	knockout

l	liter
IKK	I κ B kinase
IRS	insulin receptor substrate
LAH	long arm of homology
loxP	<u>l</u> ocus of <u>X</u> over in <u>P</u> I, recognition sequence of Cre
m	milli
M	Molar
MAPK	mitogen-activated protein kinase
min	minute
mRNA	messenger RNA
mXBP	murine X-binding protein
μ	micro
NCD	normal chow diet
neo ^R	neomycine resistance gene
NF κ B	nuclear factor kappa-light-chain-enhancer of activated B cells
ng	nano gramm
NMR	nuclear magentic resonance
NO	nitric oxide
nt	nucleotide
O ₂	oxygen molecule
PBS	phophate buffered saline
PCR	polymerase chain reaction
PEPCK	phosphoenolpyruvate carboxykinase
PTT	pyruvate tolerance test
RNA	<u>r</u> ibon <u>u</u> cleic <u>a</u> cid
rpm	rounds per minute
ROS	reactive oxygen species
SAH	short arm of homology

sec	second
SEM	standard error of mean
SSC	saline sodium citrate
Tab.	table
TNF- α	tumor necrosis factor alpha
U	units
UV	ultra violet
v/v	volume per volume
VO ₂	volume of oxygen
w/v	weight per volume
WAT	white adipose tissue
WHO	world health organization
WT	wild type

"If we could give every individual the right amount of nourishment and exercise, not to little and not too much, we would have found the safest way to health"

Hippocrates (460 - 377 BC)

Abstract

Obesity affects more than 30 percent of the worldwide population reaching pandemic dimensions. Furthermore, obesity is associated with the development of metabolic disorders, such as insulin resistance that is at least partly caused by an increased inflammatory state. The chronic low-grade inflammation under obese conditions induces stress signaling pathways such as c-Jun N-terminal kinase (JNK) and endoplasmic reticulum stress leading to the activation of the X-box binding protein 1 (XBP1), both might contribute to the development of obesity-associated insulin resistance. While recent studies using whole body JNK-1 knockout mice have implicated a crucial role for stress signaling induced JNK-1 in the development of obesity-associated insulin resistance, neither the metabolic tissue in which JNK-1 ablation sensitizes for insulin action nor the cell type-specific function of the other JNK isoform JNK-2 could be identified in these studies.

To this end, mouse models carrying skeletal muscle specific inactivation or constant activation of JNK-1 were analysed for alterations in energy and glucose homeostasis. While mice with a skeletal muscle specific JNK-1 deficiency or constitutive activation of JNK-1 demonstrated largely unaltered body weight gain, glucose tolerance and insulin sensitivity, JNK-1 was responsible to induce exercise-dependent increases of the myokine IL-6 in skeletal muscle. These data reveal a novel role for stress-induced JNK-1 in skeletal muscle in the context of physical activity, controlling the beneficial effects of IL-6 in response to exercise. Moreover, a conditional JNK-2 mouse line was created in this study allowing for the cell type-specific inactivation of JNK-2 in tissues that express the Cre recombinase. Furthermore, mice were generated that carry a conditional allele of the spliced and transcriptionally active form of the murine XBP1 (mXBP1s) to mimic ER stress that is associated with obesity. These mice were crossed with CAMKII-Cre and ALFP-Cre mice that resulted in mXBP1s expression and the induction of ER stress in hippocampus and liver, respectively. Surprisingly, however, qPCR analysis indicated that the central expression of mXBP1s resulted not only in the neuron-specific induction of ER stress, but also revealed upregulated CHOP and GRP78 expression in liver, implicating a crosstalk between brain and liver in the transmission of ER stress.

Also, the novel FABP4-2A-Cre mouse line was characterized using ROSA26-FOXODN and IL-6R α ^{FL} mice as reporter alleles. While FABP4-2A-Cre excised the loxP-flanked STOP sequence of ROSA26-FOXODN mice exclusively in WAT, BAT and myeloid lineage cell types, the loxP-flanked exons of the IL-6R α gene were completely excised indicating the occurrence of a transient FABP4 expression early during embryonic development.

Collectively, the herein generated mouse lines will be valuable tools for further studies addressing the cell type-specific role of stress signaling pathways in metabolic disorders.

Zusammenfassung

Adipositas breitet sich weltweit aus und betrifft mittlerweile 30 Prozent der globalen Bevölkerung. Zudem ist Fettleibigkeit mit einem erhöhten Risiko verbunden, Stoffwechselkrankheiten zu begünstigen wie die Entstehung einer Insulin-Resistenz. Die Insulin-Resistenz wird teils durch verstärkt auftretende Entzündungsprozesse bei Adipositas verursacht, die zur Aktivierung von Stress-Signal-Wegen führen, z.B. dem c-Jun N-terminalen Kinase (JNK) Signalweg oder erhöhtem Stress im endoplasmatischen Reticulum (ER), welcher in der Aktivierung des X-box bindenden Protein 1 (XBP1) resultiert. Jüngste Studien, in denen JNK-1 im ganzen Körper inaktiviert wurde, weisen daraufhin, dass JNK-1 eine zentrale Rolle bei der Entstehung der Adipositas-assoziierten Insulin-Resistenz einnimmt. Allerdings konnten diese Studien weder das Gewebe identifizieren, in welchem eine JNK-1 Inaktivierung die Insulin Wirkung sensibilisiert, noch konnte die Zelltyp-spezifische Rolle von JNK-2 aufgeklärt werden. Daher wurden in dieser Arbeit Maus-Modelle generiert, in denen JNK-1 spezifisch im Skelettmuskel inaktiviert oder konstant aktiviert wurde. Während diese Mausmutanten im Vergleich zu Wildtyp-Mäusen eine unveränderte Gewichtszunahme, sowie eine mit Wildtyp-Mäusen vergleichbare Glukosetoleranz und Insulinsensitivität zeigten, so konnte nachgewiesen werden, dass JNK-1 für die Sekretion des Myokins Interleukin 6 (IL-6) im Skelettmuskel während körperlicher Aktivität verantwortlich ist. Diese Erkenntnis belegt eine neue Rolle des Stress-induzierbaren JNK-1 Proteins während körperlicher Anstrengung, da es die vorteilhaften Effekte von IL-6 als Antwort auf diese Aktivität kontrolliert. Zusätzlich wurde eine konditionale JNK-2 Maus-Linie generiert, die es erlaubt JNK-2 in Organen zu inaktivieren, in denen die Cre-Rekombinase exprimiert wird. Weiterhin wurden Mäuse erzeugt, die ein induzierbares Allel des gespleißten und transkriptionell aktiven murinen XBP1 Proteins (mXBP1s) in ihrem Genom tragen. Das Kreuzen dieser mit Mäusen, welche die CAMKII-Cre oder die ALFP-Cre exprimieren, resultierte in der Expression von mXBP1s und der Induktion von ER Stress im Hippocampus bzw. der Leber. Überraschenderweise deutete eine Analyse mittels qPCR daraufhin, dass die zentrale Expression von mXBP1s nicht nur in neuronalen ER Stress resultiert, sondern es wurden auch erhöhte Expressionswerte von CHOP und GRP78 in der Leber dieser Tiere festgestellt. Dies deutet auf eine Verbindung zwischen Gehirn und Leber in Bezug auf die Weiterleitung des ER Stress hin. Ferner wurde die neu-entwickelte FABP4-2A-Cre Maus-Linie charakterisiert. Mit ROSA26-FOXODN und IL-6R^{FL} Mäusen als Reporter, konnte gezeigt werden, dass die loxP-flankierte STOP-Sequenz der ROSA26-FOXODN Mäuse exklusiv im weißen und braunen Fettgewebe und in Makrophagen durch die Aktivität der FABP4-2A-Cre herausgeschnitten wurde. Allerdings wurden die loxP-flankierten Exons des IL-6R^α Gens komplett deletiert. Dies legt nahe, dass FABP4 bereits früh während der Embryonalentwicklung transient exprimiert wird. Insgesamt stellen die hier präsentierten Maus-Linien ein verlässliches und nützliches Werkzeug dar, um in zukünftigen Studien die Zelltyp-spezifische Rolle von Stress-Signalwegen bei Stoffwechselkrankheiten zu untersuchen.

1 Introduction

1.1 Metabolic Homeostasis

Individuals are able to maintain a steady body weight. This tightly regulated process is dependent on compensatory signals which sense high and low energy states of the body (Schwartz, 2004, 2006). Malfunctions in this regulatory system lead towards increased energy storage, body weight gain and may eventuate in obesity. These failures in metabolic regulation are induced by environmental factors or by genetic predisposition, or the combination of both. Energy-dense food, new dietary compounds, an increased life span and insufficient physical activity all challenge the regulatory systems to maintain this homeostasis (Hill & Peters, 1998; Hill *et al.* , 2003). Studies have investigated how certain genetic factors influence this homeostasis. Mutations in the hormone leptin, which is secreted by the adipose tissue to reduce food intake and enhance physical activity, have been identified in obese patients (Barsh *et al.* , 2000). Moreover, the fat mass and obesity associated (FTO) gene was identified, which predisposes its carrier to the development of obesity (Fischer *et al.* , 2009; Frayling *et al.* , 2007). The "thrifty gene" hypothesis, which describes the evolutionary benefits of genes promoting high energy storage is now needless in developed societies where there is perpetual availability of energy dense foods (Sharma, 1998).

Understanding the regulation of metabolic balance is of crucial importance in preventing the development of obesity.

1.2 Obesity and Type 2 Diabetes - Metabolic Threats

Formerly obesity was described as a disease affecting well-developed and wealthy countries, possessing an overabundance of food and well established transportation systems (Mokdad *et al.* , 2003). However, now obesity is also prevalent in less well developed countries, leading to epidemic proportions. Estimations by the world health organization (WHO) reveal that in 2008, 1.5 billion adults were overweight, and among these 500 million people were obese. In Germany 61 % people were estimated to be overweight,

and 25 % of these obese (WHO, 2008). Furthermore, childhood obesity is steadily increasing, with 43 million children under the age of five years worldwide being overweight (WHO). This is a very worrying trend, since these children are predisposed to develop obesity later in life. Crucially, the obesity pandemic places a huge burden on health care expenditure (Pedersen, 2011). Currently, the WHO defines obesity and overweight on measures of the body mass index (BMI). The BMI is the measurement of the person's weight in kilograms divided by the square of his height in meters (kg/m^2). A BMI equal or greater than 25 defines overweight and a BMI equal or greater than 30 characterizes obesity (WHO).

Interestingly, the drastic increase in obesity is accompanied by a worldwide rise in physical inactivity. Indeed, the prevalence of obesity and the rate of physical inactivity are closely related (Fig. 1.1).

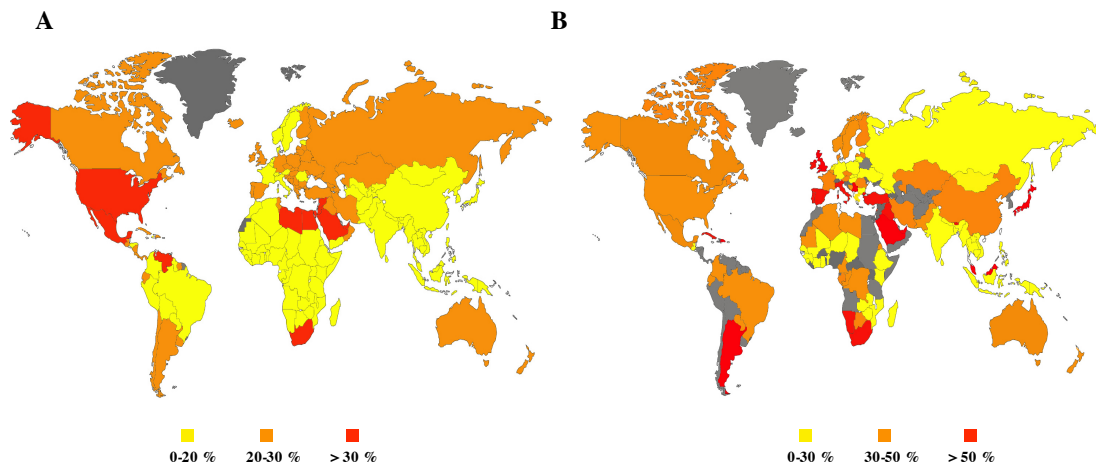


Figure 1.1: Obesity and physical inactivity are closely related.

Map of global distribution of (A) obesity and (B) physical inactivity. Colors indicate prevalence of obesity or physical inactivity in the respective countries. (grey = no data available; adapted from WHO)

30 % of the german population are physical inactive, which is associated with premature death (WHO), and a shortened life span of on average five years compared to that of physically active people (Pedersen, 2011).

Obesity is characterized by an excess accumulation of fat due to an imbalance in metabolic homeostasis and is linked to several disorders, including type 2 diabetes, cardiovascular disease, hypertension, arthritis, depression, and some forms of cancer (Pedersen, 2011). Indeed, type 2 diabetes constitutes a large portion of the obesity induced health conse-

quences (Zimmet *et al.*, 2001). Concomitantly with an increased prevalence of obesity 366 million people worldwide are projected to suffer from type 2 diabetes by the year 2030 (Wild *et al.*, 2004). A hallmark of type 2 diabetes is hyperglycemia and hyperinsulinemia, however, this endocrine disorder differs from the juvenile type 1 diabetes. In type 1 diabetes insulin producing β -cells in the pancreatic islets of Langerhans in the pancreas are destroyed by T-lymphocytes. This leads to a complete ablation of insulin secretion and is denoted as an autoimmune disease (Eisenbarth *et al.*, 1988). Type 2 diabetes, is described as an adult-onset disease, however in recent years there is an increased appearance of type 2 diabetes in younger adults (Saltiel & Kahn, 2001). Type 2 diabetes is characterized by an inability to respond appropriately to insulin (Kahn *et al.*, 1996). This inability to respond to insulin is also referred to as insulin resistance, and is induced by multiple mechanisms influenced by both genetic and environmental factors (Chan *et al.*, 1994). Huge efforts are being made to elucidate the underlying signaling pathways, and hence, to understand the development of obesity and its associated metabolic disorders.

1.3 Insulin - the Metabolism's Central Hormone

Frederick Grant Banting discovered insulin in 1921 as a substance to treat type 1 diabetes (Banting *et al.*, 1962; Majumdar, 2001). Insulin is a hormone produced in pancreatic β -cells and has several anabolic effects such as promoting glucose uptake and inhibiting gluconeogenesis and lipolysis (Kahn *et al.*, 1996; Saltiel & Kahn, 2001). In healthy individuals insulin mediates these pleiotropic effects by binding to its receptor, which results in a conformational change of the regulatory α -subunits and subsequent phosphorylation of the catalytic β -subunits (Kasuga *et al.*, 1982; Patti & Kahn, 1998). The active insulin receptor recruits and tyrosine phosphorylates proteins of the insulin-receptor-substrate (IRS) family. (Isakoff *et al.*, 1996; Myers *et al.*, 1995). These molecules serve as a docking platform for Src-homology (SH)-2 domain-containing proteins, such as the phosphatidylinositol 3 (PI₃)-kinase (Myers *et al.*, 1992, 1993) or growth factor receptor binding protein (Grb)-2. Grb-2 initiates the Ras/Raf-mitogen activated protein kinase (MAPK)-pathway, which has no role in transmitting the metabolic effects of insulin, but lead to cellular proliferation and differentiation (Chang & Karin, 2001; White, 2003).

The activation of the PI3-kinase pathway catalyzes the phosphorylation of phosphatidylinositol (4,5) bisphosphate (PIP₂) to phosphatidylinositol (3,4,5) triphosphate (PIP₃) (Whitman *et al.*, 1988). These lipids have a high affinity for the PH-domain of the protein kinase B (PKB, also known as AKT). PIP₃ mediates the translocation of AKT to the cell membrane, and AKT, in turn, co-localizes with phosphoinositide-dependent protein kinase 1 (PDK-1) (Vanhaesebroeck & Alessi, 2000). This leads to a conformational change enabling PDK-1 to activate AKT by phosphorylation. The activation cascade downstream of AKT leads to the metabolic effects of insulin, including expression of genes responsible for glucose uptake, stimulation of glycogen and lipid synthesis, and inhibition of gluconeogenesis and lipolysis (Cheatham & Kahn, 1995) (Fig. 1.2).

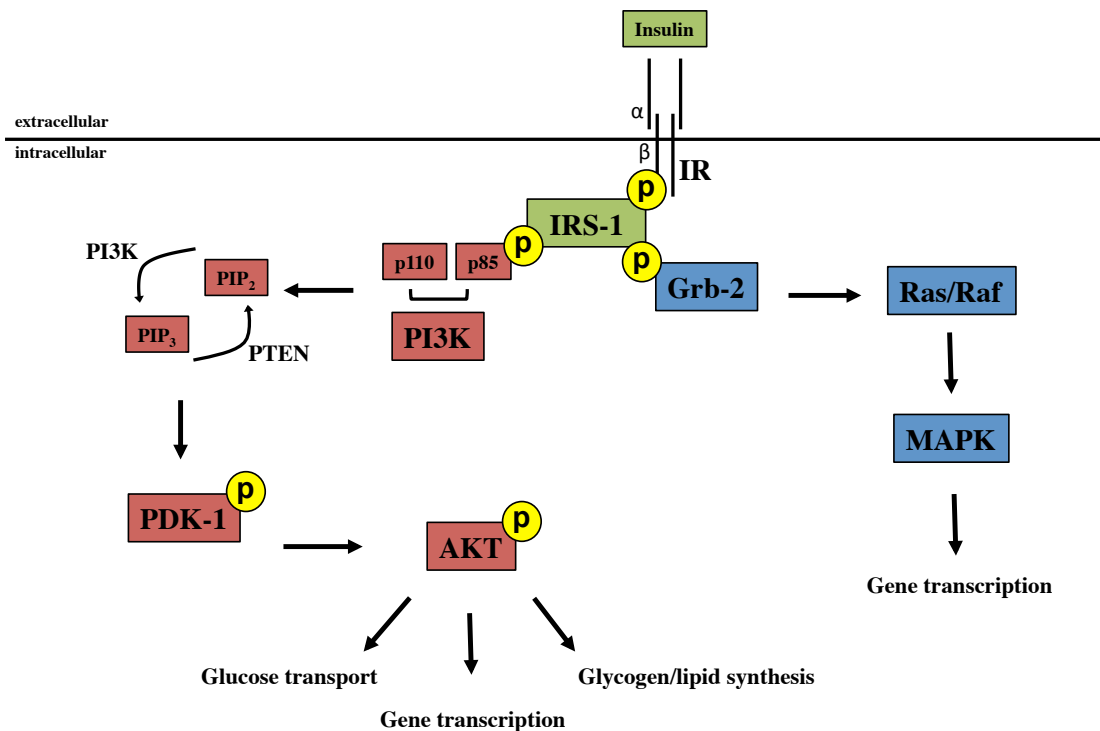


Figure 1.2: Schematic view of the insulin signaling pathway.

Binding of insulin to its receptor activates the tyrosine kinase activity. The β -subunit of the receptor is phosphorylated on three intracellular tyrosine residues, which enables the receptor to recruit and phosphorylate IRS-proteins. IRS proteins serve as a docking platform for both the p85 and p110 subunits of the PI3-kinase and the Grb-2 molecules, the latter induces the MAPK-signaling pathway. Signaling via the PI3-kinase converts PIP₂ into PIP₃, which leads to recruitment of AKT to the cell membrane via PDK-1 molecules, which further stimulate AKT activation. AKT, in turn, implements the pleiotropic metabolic effects of insulin such as glucose uptake, or inhibition of gluconeogenesis and lipolysis.

In obese individuals this insulin signaling cascade is disturbed (Prager *et al.*, 1987;

White, 2003). However, the underlying signaling pathways contributing to this disturbance are not fully understood.

1.4 Obesity induced Stress-Kinase Signaling

In 1993, a first evidence for a link between obesity and inflammatory signaling was established when Hotamisligil revealed increased expression of the tumor necrosis factor- α (TNF- α) in adipose tissue of obese mice (Hotamisligil *et al.* , 1993; Uysal *et al.* , 1997). Today, the link between obesity and inflammation is well established, but the precise underlying mechanisms remain to be elucidated (Solinas & Karin, 2010). Obesity is associated with low grade chronic inflammation, reflected by immune cell invasion into the adipose tissue. The first invading cells are T-cells, which further recruit non-resident macrophages (Lumeng *et al.* , 2009). In combination with resident macrophages they release pro-inflammatory cytokines, which lead to the activation of inflammatory signaling pathways in the adipose tissue and systemically in other metabolic tissues. This effect is further aggravated by the leakage of fat molecules from expanded adipocytes (Feuerer *et al.* , 2009). Indeed, the inhibition of insulin signaling in obesity and type 2 diabetes is largely caused by activation of two stress-sensitive kinases, namely the I κ B kinase (IKK) and the c-Jun N-terminal kinase (JNK), both of which are activated by TNF- α and interfere with insulin signaling (Arkan *et al.* , 2005; Solinas & Karin, 2010).

IKK phosphorylation is essential for the activation of the transcription factor nuclear factor κ light chain enhancer of activated B-cells (NF κ B). Under normal conditions, NF κ B is bound in a complex to the inhibitor of IKK (I κ B) (Courtois & Israël, 2011). Upon certain stress-stimuli, such as UV-light, irradiation or cytokines like TNF- α , I κ B is phosphorylated by IKK (Jimi & Ghosh, 2005). This phosphorylation of I κ B leads to its proteasomal degradation, and released NF κ B can translocate into the nucleus to activate transcription of diverse genes, such as IL-6 or IL-1 β (Courtois & Israël, 2011). Strikingly, mice with an increased hepatic activation of NF κ B signaling develop both hepatic and systemic insulin resistance (D Cai, 2005).

1.4.1 Obesity induced JNK Activation

The JNK protein family was identified in 1993 as two protein kinases, p46JNK1 and p54JNK2, phosphorylating the transcription factor c-Jun on the N-terminal Ser63 and Ser73 residues (Hibi *et al.* , 1993). Presently it is established that the JNK family comprises three genes, resulting in three proteins, namely JNK-1, JNK-2, and JNK-3 (Weston & Davis, 2007). In addition, several isoforms of JNK proteins resulting from alternative splicing, have been described (Davis, 2000). JNKs are serine/threonine kinases belonging to the mitogen-activated protein kinases (MAPK)-family, and thus are activated in a MAPK-module upon certain stimuli such as UV-light (Davis, 2000). Two upstream MAP2 kinase kinases (MKK) have been described to activate JNK, namely MKK4 and MKK7. Both phosphorylate JNK within a Thr-X-Tyr motif, with MKK4 preferring the Tyr185 site, and MKK7 the Thr183 site (Davis, 2000). These differential phosphorylation sites provide a molecular basis for the activation of JNK by various stimuli. MKK4 was shown to be activated by environmental stress and MKK7 primarily by cytokines (Tournier *et al.* , 2001). In addition, MKK7 was shown to solely phosphorylate JNK, whereas MKK4 also phosphorylates the MAPK p38 (Tournier *et al.* , 1999). Moreover, the activation of JNK is dependent on the JNK interacting protein 1 (JIP1), which ensures the local proximity of the MAP kinase module (Jaeschke *et al.* , 2004).

JNK activation then leads to induction of transcription factor activator protein 1 (AP1), which in turn leads to target gene expression.

Examination of the role of JNK in insulin-secreting cells in the pancreas revealed differential activity between the protein isoforms. While one study claimed that only JNK-1 and JNK-2 are expressed in pancreatic islets (Varona-Santos *et al.* , 2008), another study also showed the expression of JNK-3 (Abdelli *et al.* , 2009). In the latter study, JNK-3 was attributed a protective function on β -cell mass, whereas JNK-1 and JNK-2 lead to cell death (Varona-Santos *et al.* , 2008).

JNK is drastically activated during obesity (Hirosumi *et al.* , 2002). In obesity, levels of extracellular long-chain saturated free fatty acids are elevated (Weisberg *et al.* , 2003), which is thought to activate JNK signaling via Toll-like receptor (TLR)-signaling pathways (Sabio & Davis, 2010) (Fig. 1.3). Moreover, obesity-induced inflammation and increased TNF- α levels, also results in JNK activation (Sabio & Davis, 2010). Furthermore, obesity-induced ER stress is directly linked to JNK activation via the IRE1/XBP1-

pathway (Urano *et al.*, 2000), and indirectly by increasing the amount of oxidative stress, and accumulation of reactive oxygen species (ROS), such as O_2^- radicals or H_2O_2 . ROS, which also arise during oxidative phosphorylation in mitochondria, are known to activate the JNK pathway (Bouloumie *et al.*, 1999), presumably via activation of the apoptosis signal-regulating kinase 1 (ASK1) (Ichijo *et al.*, 1997; Tobiume *et al.*, 2001) (Fig. 1.3).

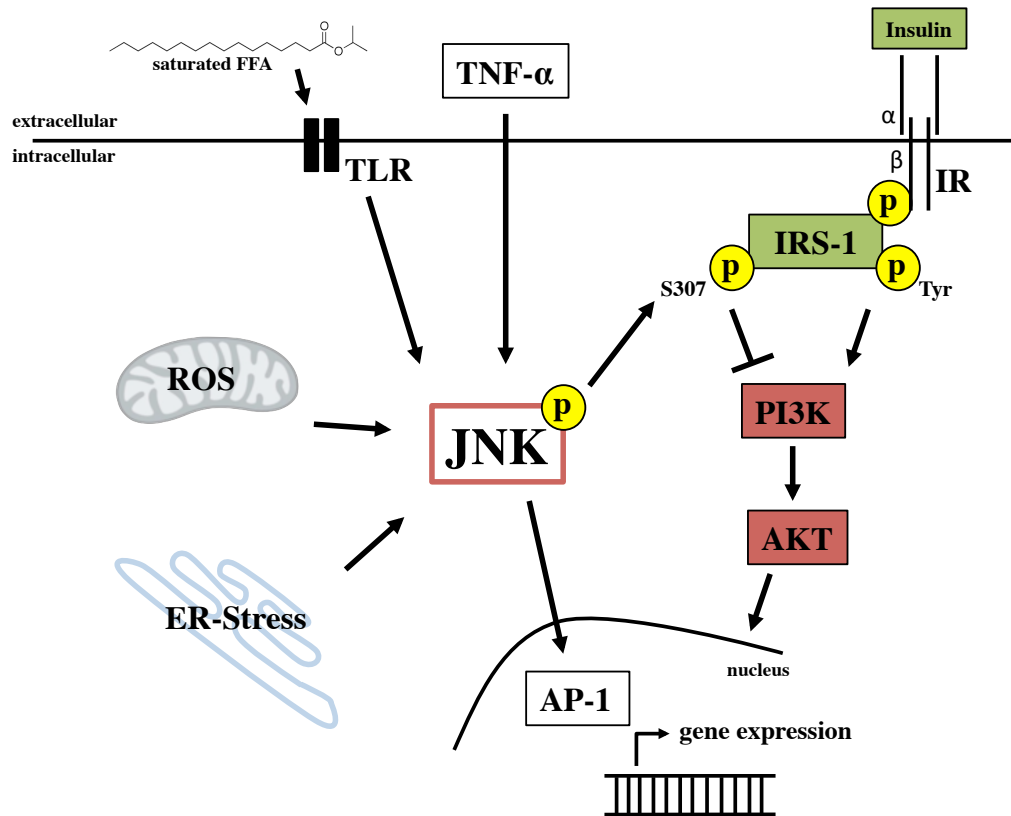


Figure 1.3: Obesity induced JNK activation leads to inhibition of the insulin signaling cascade. Obesity leads to the activation of JNK by various inducers. Obesity increases the amount of free saturated fatty acids leading to TLR-mediated JNK activation. In addition obesity-induced inflammatory cytokines, such as TNF- α , and ER stress result in increased JNK phosphorylation. Moreover, ROS are highly abundant during obesity due to enhanced oxidative phosphorylation in mitochondria and increased ER folding capacity, and may further enhance JNK activation. Activated JNK then leads to activation of AP-1 target genes and is able to interfere with insulin signaling by inhibitory phosphorylation on IRS-proteins.

As mice lacking TNF- α are protected from obesity-induced insulin resistance (Uysal *et al.*, 1997), and TNF- α is an important inducer of JNK signaling, consequently JNK possess a crucial role in the regulation of inflammation-induced insulin resistance (Sabio & Davis, 2010).

Indeed, a role for JNK to interfere with insulin signaling was shown for the JNK-1 protein isoform. It was shown that JNK-1 phosphorylates IRS1 specifically at serine residue 307, which leads to the inhibition of IRS-1 and therefore further downstream insulin signal-

ing (Aguirre *et al.* , 2000). In addition, a conventional JNK-1 knockout, but not JNK-2, in obese mice, leads to reduced adiposity and improved insulin resistance, revealing a central role for JNK-1 in metabolic regulation (Hirosumi *et al.* , 2002).

In an attempt to specify in which peripheral organ JNK-1 exerts its primary effects, JNK-1 was inactivated using several approaches in different tissues (Sabio *et al.* , 2008, 2009, 2010) (for review see (Belgardt *et al.* , 2010b)). However, none of these models recapitulated the effects seen in the conventional JNK-1 knockout (Hirosumi *et al.* , 2002).

To maintain a healthy body, JNKs play a critical role, as they are strongly activated in obesity and operate by inducing insulin resistance (Vallerie & Hotamisligil, 2010). However there is also increasing evidence that JNKs are selectively activated upon physical exercise (Goodyear *et al.* , 1996).

1.5 Physical Exercise induced JNK Activation

In the late 1990's the first evidence linking physical exercise and the activation of JNK was established in rats (Goodyear *et al.* , 1996). Treadmill exercise lead to a two-to-three fold increase of JNK activity in rat skeletal muscle. Cycle ergometer exercise in humans revealed that this exercise-induced JNK activity is an intrinsic response to exercise from the exercising leg. It was suggested that JNK could be responsible for the exercise-induced transcriptional changes within the contracting skeletal muscle (Aronson *et al.* , 1998). One year later, Boppart claimed that this exercise-induced JNK activation is a response to eccentric exercise-dependent injuries (Boppart *et al.* , 1999). Another year later, Boppart showed a 7-fold increase in JNK phosphorylation compared to basal levels in human skeletal muscle immediately after marathon running (Boppart *et al.* , 2000). Moreover, training rats on a treadmill abrogated this exercise-induced JNK activation (Boluyt *et al.* , 2003), indicating an attenuation of exercise-dependent stress responses. Additionally, central increase in JNK activity was revealed in rat brains after swim exercise (peng Shen *et al.* , 2004).

As these experiments were performed in non-obese healthy individuals, the question remains as to what the physiological and molecular consequences of this exercise-induced JNK activation are. The beneficial effects of exercise have been shown in rodent models of diet induced obesity. Physical exercise reduced TLR4-signaling, JNK and IKK β phos-

phorylation, and decreased IRS1_{S307} phosphorylation in skeletal muscle, liver, and white adipose tissue of diet induced obese rats, and thus reduces inflammation and insulin resistance (da Luz *et al.* , 2011; Oliveira *et al.* , 2011). Additionally, swim exercise of diet induced obese rats leads to a reduction of obesity-induced ER stress in adipose and hepatic tissue, accompanied by decreases in JNK and NF κ B activities and improved insulin sensitivity (da Luz *et al.* , 2011). In Zucker diabetic fatty rats, exercise lowers the levels of hepatic JNK activation and subsequently the rate of IRS1_{S307} phosphorylation (Király *et al.* , 2010).

Further beneficial effects of exercise were shown in mouse models of Alzheimer's disease. Chronic exercise decreased phosphorylation of tau-protein within the hippocampus, which correlated with a decline in JNK phosphorylation (Leem *et al.* , 2009). Moreover the protective effect of treadmill exercise in Alzheimer's disease was proven by improved cognitive function in water-maze test, and a decrease in hippocampal cell death (Um *et al.* , 2011). These findings reveal exercise as a therapeutic intervention for the prevention or treatment of Alzheimer's disease, partly by attenuating JNK activation (Leem *et al.* , 2009; Um *et al.* , 2011).

These protective effects of exercise were accompanied by a cytokine expression that differs from that induced by inflammation. In contrast to inflammation responses, which lead to a drastic increase in the pro-inflammatory cytokine TNF- α , IL-6 is the first cytokine present in the circulation during exercise, whereas the pro-inflammatory cytokines TNF- α and IL-1 β do not increase and rather decrease with exercise (Pedersen & Febbraio, 2008). In contrast to inflammation, exercise induces an increase in circulating anti-inflammatory cytokines such as IL-10, IL-1R α , and soluble TNFR- α , which is an inhibitor of TNF- α (Ostrowski *et al.* , 1999; Pedersen & Febbraio, 2008).

This picture of cytokine expression during exercise indicates that exercise triggers an anti-inflammatory environment, which may lead to the beneficial effects of physical activity on metabolic diseases (Pedersen & Febbraio, 2008).

Furthermore, this exercise-induced cytokine response is mainly initiated by skeletal muscle, which points to an endocrine function of this tissue.

1.6 Skeletal Muscle - an Endocrine Organ

Skeletal muscle is the largest organ in the human body and one of its primary functions is to manage physiological adjustments due to muscle contraction (Pedersen, 2011). In this context, skeletal muscle was characterized as an endocrine organ, due to its ability to release cytokines termed myokines (for review see (Pedersen & Febbraio, 2008)). Myokines either signal in an intrinsic fashion within the muscle, for example AMP-activated protein kinase (AMPK)-induced glucose uptake, or lead to systemic effects on other organs, such as liver or adipose tissue (Pedersen, 2011). During recent years many cytokines secreted by the skeletal muscle have been identified, particularly during fasting and exercise conditions (Pedersen & Febbraio, 2008; Pedersen, 2011). Under these conditions, the most prominent myokine released by the skeletal muscle is IL-6, and functions to stimulate glucose uptake within the skeletal muscle and enhance hepatic glucose production. Other myokines include IL-15 as a mediator of muscle to fat crosstalk (Nielsen *et al.*, 2007), and IL-8 whose expression is increased after 3 hours treadmill run (Nieman *et al.*, 2003). All of these myokines operate to implement the tasks of the working skeletal muscle.

IL-6 was discovered in 1980 (Weissenbach *et al.*, 1980) and classically signals through a gp130-receptor- β (gp130R β)/IL-6-receptor- α (IL-6R α) homodimer. Binding of IL-6 to the receptor results in homodimerization and initiates the auto-phosphorylation and activation of the Janus-activated kinase (JAK). This activation leads to the phosphorylation at Tyr757 in the murine gp130R β . JAKs then phosphorylate signal transducer and activator of transcription (STAT)-3 at tyrosine residues, which drives target genes, such as suppressor of cytokine signaling (SOCS).

Not all cell types within the body express the IL-6R α , yet they can still be stimulated by a soluble form of the IL-6R α (sIL-6R α) in the course of trans-signaling (Mackiewicz *et al.*, 1992; Taga *et al.*, 1989). The sIL-6R α is generated by shedding of the membrane-bound IL-6R α by the metalloproteinases ADAM10 and ADAM17, or by translation of alternatively spliced mRNA (Althoff *et al.*, 2000; Jones *et al.*, 2001; Matthews *et al.*, 2003). The role of IL-6 in metabolic regulation is controversially discussed, however what is clearly established is that activation of IL-6 mRNA and protein release are beneficial upon physical exercise (Pedersen & Febbraio, 2008).

1.6.1 Physical Exercise induced IL-6 activation

IL-6 has a prominent role in the metabolic adaptations to exercise, and indeed several studies claim that IL-6 is the 'exercise factor' (Pedersen & Febbraio, 2008). In 1998, Ostrowski and colleagues investigated participants of the Copenhagen marathon and observed increased plasma levels of IL-6 following the marathon (Ostrowski *et al.*, 1998). Consistent with these findings, Steensberg and colleagues showed that the contracting human skeletal muscle releases significant amounts of IL-6 into the circulation during prolonged single-limb exercise (Steensberg *et al.*, 2000). It was first thought that the exercise-induced IL-6 release was due to local damage within the working muscle, and that immune cells were responsible for this increase in IL-6 (Bruunsgaard *et al.*, 1997; Nehlsen-Cannarella *et al.*, 1997; Nieman *et al.*, 1998). However, since non-damaging muscle contractions can also induce IL-6 activation, it is now established that contracting skeletal muscle is the main source of IL-6 release upon exercise (Pedersen & Febbraio, 2008).

The intracellular pathways within the skeletal muscle leading to the activation of IL-6 upon an exercise stimulus, are controversial (Pedersen & Febbraio, 2008). The classical signaling pathway leading to the activation of IL-6, was established in macrophages, in which IL-6 activation is dependent on the activation of NF κ B signaling pathway (Pedersen, 2011). This inflammatory pathway starts with the binding of LPS (or other TLR-stimulating factors) to TLR-4, which recruits the myeloid differentiation primary-response protein 88 (MyD88) (Akira, 2003). MyD88 functions as an adapter molecule and triggers the recruitment of IL-1 receptor-associated kinase (IRAK)- 1 and TNF- α receptor-associated factor (TRAF)- 6. The interaction of the latter activates the inhibitor I κ B. Through phosphorylation of I κ B by IKK, I κ B is targeted for ubiquitination and sequential proteasomal degradation. This leads to the activation and to the release of NF κ B. NF κ B then translocates into the nucleus and activates classical inflammatory target genes, such as IL-6 or TNF- α (Akira & Takeda, 2004; Pedersen, 2011).

However, since exercise is supposed to have beneficial effects on insulin sensitivity, it would seem paradoxical that exercise induces IL-6 via the classical pro-inflammatory pathway (Pedersen, 2011). Another mechanism for IL-6 induction might involve nitric oxide (NO) production (Steensberg *et al.*, 2007). NO can directly alter signaling by either redox-sensitive modifications or by nitrosation of proteins (Hemish *et al.*, 2003). Several studies show an increase in NO production when the skeletal muscle is contracting

(Balon & Nadler, 1994; Grange *et al.*, 2001; Lau *et al.*, 1998), and importantly Steensberg revealed that inhibition of NO production during exercise leads to less increases in IL-6 mRNA in human skeletal muscle (Steensberg *et al.*, 2007).

Another stimulus for IL-6 activation upon exercise might be calcium. Mechanical load during contraction stimulates significant calcium release from the sarcoplasmic reticulum (Pedersen & Febbraio, 2008). The activity of nuclear factor of activated T-cell (NFAT) is dependent on intracellular calcium concentrations and calcineurin, which is a serine/threonine phosphatase sensitive to elevated calcium concentrations. Therefore, NFAT may represent the link between increased intramuscular calcium concentrations and the activation of IL-6 (Dolmetsch *et al.*, 1998; Fiedler & Wollert, 2004). However 60 minutes following concentric exercise IL-6 mRNA is increased without any changes in the nuclear localization of NFAT (Chan *et al.*, 2004).

Inhibition of p38 phosphorylation in the cell's nucleus leads to ablation of the IL-6 mRNA response in stimulated myotubes (Chan *et al.*, 2004). In support, a reduced intramuscular glycogen content has been found to increase the phosphorylation of p38 (Chan *et al.*, 2004). However, IL-6 transcription is rapid and in the beginning of exercise, therefore, alternative signaling pathways must be responsible for the initial exercise-induced IL-6 expression (Pedersen & Febbraio, 2008) (Fig. 1.4).

Exercise-induced IL-6 influences systemic physiology (Fäldt *et al.*, 2004). Within the contracting skeletal muscle, IL-6 acts in a paracrine manner to activate either the PI3-kinase pathway resulting in glucose uptake, or the STAT3-AMPK pathway, which results in enhanced fat oxidation within the muscle (Carey *et al.*, 2006; van Hall *et al.*, 2003; Wolsk *et al.*, 2010). Systemically it acts on the liver to increase hepatic glucose production, and to the adipose tissue to induce lipolysis (Carey *et al.*, 2006; Febbraio *et al.*, 2004; Glund *et al.*, 2007).

However, studies also show that IL-6 can have adverse effects when chronically activated, as in obesity or in patients with type 2 diabetes (Bastard *et al.*, 2000; Carey *et al.*, 2004; Vozarova *et al.*, 2001). IL-6 was shown to induce insulin resistance in skeletal muscle and liver (Kim *et al.*, 2004). In support, the action of IL-6 was shown to induce insulin resistance and to repress hepatic glucose production (Sabio *et al.*, 2008). Nonetheless, conventional IL-6 knockout mice exhibit impaired glucose tolerance that is reverted by IL-6 and also develop mature-onset obesity (Wallenius *et al.*, 2002). Moreover, hepatic

inactivation of IL-6R α increases local systemic inflammation and insulin resistance, indicating a protective role of IL-6 (Wunderlich *et al.*, 2010).

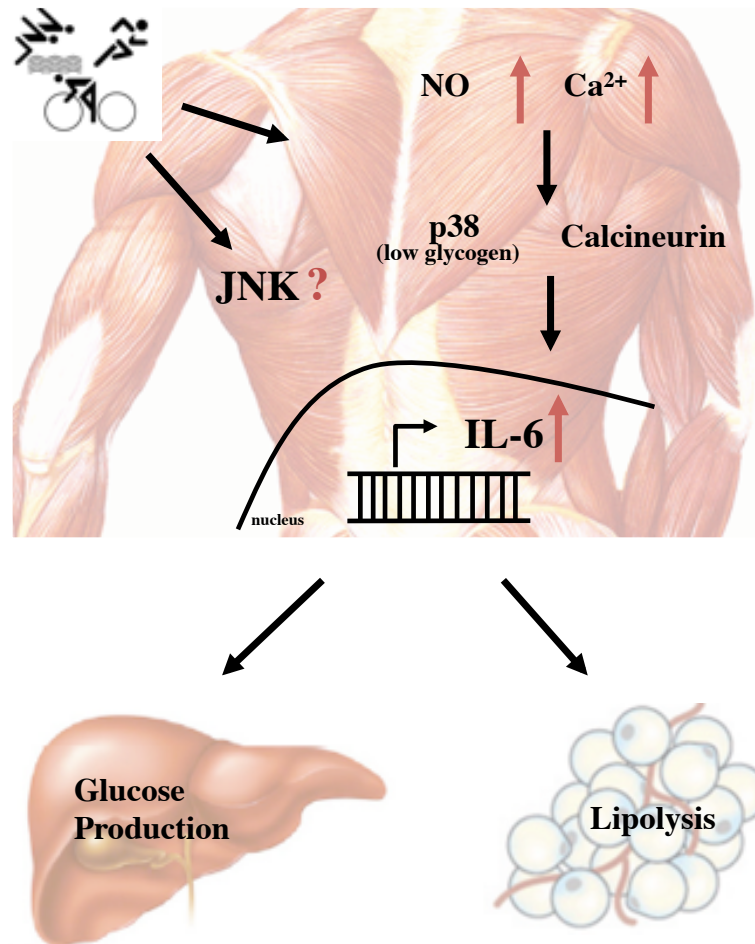


Figure 1.4: Physical Exercise induced IL-6 activation in skeletal muscle.

Physical exercise leads to activation of IL-6 by a yet undefined signaling pathway. Exercise increases the amount of nitric oxide and calcium within the muscle cells. Calcium triggers calcineurin and may lead to an increase in IL-6 mRNA transcription via the transcription factor NFAT. Additionally, low glycogen levels may represent a link between the exercise induced activation of p38 and IL-6 mRNA transcription. Studies also revealed that JNK is activated in the skeletal muscle upon an exercise stimulus. IL-6 fulfills its role in a paracrine and systemic manner, leading to glucose uptake and fat oxidation within the contracting skeletal muscle and enhanced hepatic glucose production and lipolysis in adipose tissue. (adapted from (Belgardt *et al.*, 2010b))

While acute increases in IL-6, i.e. during exercise, have a beneficial effect on peripheral metabolism, when chronically elevated, i.e. in obesity, IL-6 contributes to insulin resistance.

1.7 Obesity induced ER Stress

Incidences of metabolic diseases have strongly increased over the last years (Pedersen, 2011). Obesity induces ER stress and an increased demand on the endoplasmic reticulum (ER) is thought to be a primary contributing factor to metabolic dysfunction (Hummasti & Hotamisligil, 2010; Ozcan *et al.*, 2004). The ER functions to balance calcium levels and regulating folding, maturation, quality control, and trafficking of proteins (Hotamisligil, 2010). However, metabolic disorders are characterized by conditions challenging the ER. These conditions include an increase in newly synthesized, unfolded proteins in the ER lumen. To cope with these conditions of stress, the ER evolved the unfolded protein response (UPR). The UPR is mediated by three ER membrane-associated proteins: inositol requiring enzyme (IRE) 1, PKR-like eukaryotic initiation factor 2 α kinase (PERK), and activating transcription factor (ATF) 6. In stress-free conditions these transmembrane proteins are bound by chaperones (Fig. 1.5) (for review see (Hotamisligil, 2010)).

Upon activation, the endoribonuclease activity of IRE1 cleaves a 26 bp segment from the mRNA of the X-box binding protein (XBP) 1, which creates an alternatively spliced form of the transcription factor, XBP1s (Sidrauski & Walter, 1997). This excision results in conversion of a 267 amino acid unspliced XBP1 protein (XBP1u) to a 371 amino acid spliced XBP1 protein (XBP1s) (Glimcher, 2010). XBP1s then triggers a transcriptional program and produces chaperones and proteins of the ER-associated protein degradation (ERAD) to combat the ER's stress situation (Hotamisligil, 2010).

Furthermore ER stress involves the activation of transmembrane protein ATF6. To be fully functional, ATF6 needs to be reduced and can then translocate to the Golgi apparatus. Here, ATF6 is processed by the serine protease site-1 protease (S1P) and the metalloprotease site-2 (S2P) to produce an active transcription factor (Chen *et al.*, 2002). Once activated ATF6 stimulates the expression of genes containing ER stress elements (Hotamisligil, 2010).

Moreover, ER stress leads to the phosphorylation of eukaryotic translational initiation factor (eIF2)- α at serine 51 by PERK (Shi *et al.*, 1998). This serine phosphorylation induces eIF2 α to reduce the rate of ternary complex formation, thereby inhibiting global protein synthesis, which further attenuates the levels of stress on the ER (Harding *et al.*, 1999). If the UPR is not able to counteract and relieve ER stress, apoptosis is initiated (Hetz *et al.*

, 2006; Rao *et al.*, 2004). The induction of the UPR in the course of obesity-induced ER stress, is able to attenuate stress-levels within the cell. However, activated UPR pathways may also lead to a further manifestation of obesity-induced deteriorations, partly by activating JNK signaling via the IRE1 pathway.

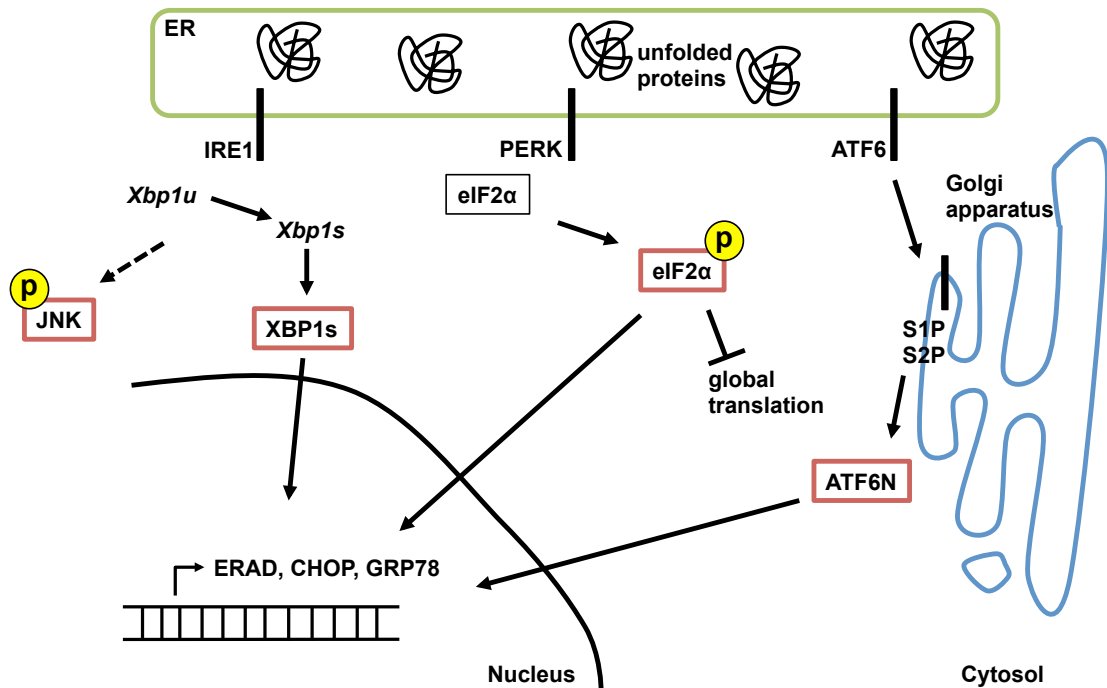


Figure 1.5: ER stress activates the UPR.

An accumulation of unfolded proteins within the ER-lumen results in activation of the three UPR pathways. The endonuclease activity of IRE1 cleaves *xbp1u* mRNA to yield the active form *xbp1s*. XBP1s transcription factor then translocates to the nucleus and induces gene expression for ERAD and chaperone proteins. The transmembrane kinase PERK phosphorylates eIF2 α , which leads to inhibition of global translation activities. Additionally, ATF6 is reduced upon UPR activation, and translocates to the Golgi apparatus, in which it is processed to an active transcription factor by S1P and S2P. Moreover, IRE1/XBP1-activity leads to induction of JNK signaling.

1.7.1 IRE1/XBP1-induced JNK activation

XBP1 was discovered over 20 years ago when attempting to define regulators of the major histocompatibility complex (MHC) class 2 gene expression (Boothby *et al.*, 1988; Liou *et al.*, 1988, 1990; Ono *et al.*, 1991). It belongs to the basic region-leucine zipper family of transcription factors (Clauss *et al.*, 1996; Glimcher, 2010), and while is ubiquitously expressed in all tissues, it is most abundant in the liver (Clauss *et al.*, 1993; Reimold *et al.*, 2000). XBP1 was previously described for its role in immune function and plasma cell differentiation (for review see: (Glimcher, 2010) and (He *et al.*, 2010).

Interestingly, IRE1/XBP1-signaling was also shown to activate the JNK pathway. Mice

with XBP1-deficiency in the intestinal epithelium induced constitutive activation of IRE1, which lead to JNK activation and TNF- α release (Podolsky, 2002). IRE1 induces JNK activation by recruiting the TRAF-2 (Urano *et al.* , 2000). Brain deficient XBP1 mice indicated a link between ER stress and the development of insulin and leptin resistance, which is accompanied by increased food intake and body weight in these mice (Ozcan *et al.* , 2009; Zhang *et al.* , 2008). Furthermore, IRE1 and JNK are strongly activated in liver and adipose tissue of obese mice (Ozcan *et al.* , 2004, 2006).

Recently, it was established that the pathways implicated in the UPR are not solely activated during ER-stress. Several studies also indicate a role for the IRE1/XBP1-signaling in the regulation of glucose homeostasis. It was shown that genes involved in glucose disposal and glycogen synthesis, e.g. glycogen synthase 1, are direct targets of XBP1 (Acosta-Alvear *et al.* , 2007; Lee *et al.* , 2008). A recent study established an interaction between XBP1s and the Forkhead box O1 (FoxO1) transcription factor, which directs FoxO1 to proteasomal degradation, and leads to improved serum glucose concentrations in mouse models of insulin resistance, without affecting the XBP1s function on enhancing ER folding capacity (Zhou *et al.* , 2011).

In addition to its role on glucose homeostasis, XBP1 also affects lipid metabolism (Hotamisligil, 2010), by regulating the transcription of genes involved in fatty acid synthesis. This was shown in mice XBP1 deficiency specifically in the liver (Lee *et al.* , 2008). These mice exhibit reductions in serum triglycerides and cholesterol, and when placed on a high carbohydrate diet, the liver specific XBP1 deficient mice did not develop hepatic steatosis (Lee *et al.* , 2008).

Taken together, these data demonstrate that UPR is linked to the development of obesity and insulin resistance and furthermore XBP1 may contribute to changes in glucose and lipid metabolism independently of the classical UPR signaling. However, further investigations using transgenic mouse model systems are required to validate these findings.

1.8 Conditional Gene Targeting

The development of the the Cre/loxP-technology represents a milestone in conditional gene targeting strategies (Kühn *et al.* , 1995; Rajewsky *et al.* , 1996). This system requires both a mouse line with a loxP-flanked allele of the target gene (Sternberg & Hamilton, 1981; Sternberg *et al.* , 1986), and a mouse line expressing the Cre recombinase (Hoess *et al.* , 1984, 1982), usually under the control of a tissue-specific promotor. Cre mediated recombination between the two loxP sites then results in the excision of the targeted exon (Hoess & Abremski, 1984) (Fig. 1.6 A).

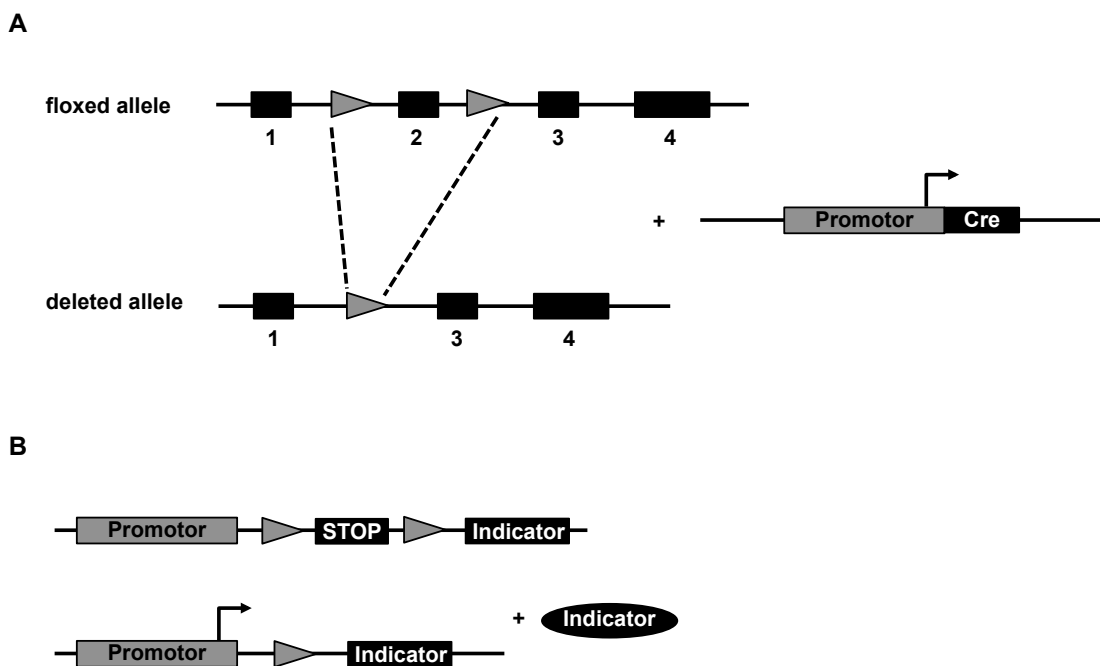


Figure 1.6: Cre mediated recombination.

(A) Expression of the Cre recombinase is driven by a tissue-specific promotor. Cre mediated recombination between the two loxP sites (grey triangles) leads to complete deletion of the targeted exon. (B) Expression of the indicator gene is prevented by a loxP flanked STOP-cassette. Cre mediated recombination between the two loxP sites leads to complete deletion of the STOP-cassette and expression of the indicator gene, resulting in a detectable indicator protein, e.g. eGFP. (adapted from (Wunderlich, 2004))

For assuring a correct recombination by Cre, in terms of time- and tissue inducibility, it is pivotal to monitor Cre mediated recombination events of indicator genes *in vivo* (Wunderlich *et al.* , 2001). To this end, reporter mice lines represent a necessary tool, in which the expression of an indicator gene is prevented by a loxP-flanked STOP-cassette. Cre mediated recombination between the loxP sites leads to deletion of the STOP-cassette, and to expression of the indicator mRNA (Fig. 1.6 B). Appropriate indicator genes in-

clude β -galactosidase or enhanced green fluorescent protein (eGFP) (Kühn *et al.* , 1995; Stoller *et al.* , 2008). Indeed, the eGFP gene is widely used and is easily detectable without further enzymatic reactions (Heim *et al.* , 1995). The eGFP protein is derived from the jellyfish *Aequorea victoria* and owes its fluorescence to a chromophore (Chalfie *et al.* , 1994). However, to detect eGFP fluorescence, it must be highly expressed within the cell, which requires the use of strong promoters to visualize Cre activity, e.g. the strong chicken β -actin promoter (Rizzuto *et al.* , 1995).

1.9 Objectives

Recent work has demonstrated that obesity-associated insulin resistance develops as a consequence of inflammation-driven stress signaling pathways. Amongst them, JNK signaling and ER stress play a prominent role. In order to gain mechanistical insights into the stress signaling pathways that link obesity and inflammation, this thesis aims at generating mouse models that carry genetic modifications in specific cell types to analyze the development of obesity-induced insulin resistance.

Firstly, as the skeletal muscle presents the largest organ of the body and implements key functions in maintaing whole body metabolic homeostasis, the stress-sensitive kinase JNK-1 should be genetically ablated as well as constitutively activated in skeletal muscle tissue of mice, to analyze the physiological consequences in these animals. Moreover, to exclude synergistic activities between the JNK-1 and JNK-2 isoforms, a conditional JNK-2 knockout mouse should be generated that would be useful to analyze the cell-type specific effects of complete JNK inactivation in metabolic disorders.

Secondly, obesity and other metabolic disorders lead to induction of ER stress that manifests as overabundance of unfolded proteins in the ER and leads to the activation of the transcription factor XBP1. Here, a mouse model should be generated allowing for the cell-type specific activation of the UPR-induced murine XBP-1 (mXBP1s) to analyze the physiological consequences of ER stress-induced mXBP1s expression in numerous organs.

Thirdly, a novel Cre mouse strain should be generated that carries a 2A-Cre insertion into the endogenous FABP4 STOP-codon, for its use to conditionally modify genes within the adipose tissue.

2 Materials and Methods

2.1 Chemicals and Biological Material

All chemicals are listed in table 2.1 and all enzymes are listed in table 2.2. Size markers for agarose gel electrophoresis (Gene Ruler DNA ladder mix) as well as size markers for SDS- polyacrylamide gel electrophoresis (Prestained protein ladder mix) were purchased from Fermentas, St. Leon-Rot, Germany. Solutions were prepared with double distilled water.

Table 2.1: Chemicals

Chemical	Supplier
β -Mercaptoethanol	AppliChem, Darmstadt, Germany
ϵ -aminocaproic acid	Sigma-Aldrich, Seelze, Germany
0.9 % saline (sterile)	Delta Select, Pfullingen, Germany
1,4-Dithio-DL-threitol (DTT)	Sigma-Aldrich, Seelze, Germany
2,2,2-Tribromethanol (Avertin)	Sigma-Aldrich, Seelze, Germany
Acetic acid	Merck, Darmstadt, Germany
Acrylamide	Roth, Karlsruhe, Germany
Agarose	Peqlab, Erlangen, Germany
Agarose (Ultra Pure)	Invitrogen, Karlsruhe, Germany
Ammonium Acetate	Merck, Darmstadt, Germany
Ammoniumpersulfate (APS)	Sigma-Aldrich, Seelze, Germany
Aprotinin	Sigma-Aldrich, Seelze, Germany
Avidin Biotin Complex-Vectastatin Elite	Vector, Burlingame, USA
Bacillo [®]	Bode Chemie, Hamburg, Germany
Barium hydroxide	Fluka, Sigma-Aldrich, Seelze, Germany
Benzamidine	Sigma-Aldrich, Seelze, Germany
Bovine serum albumin (BSA)	Sigma-Aldrich, Seelze, Germany

2 Materials and Methods

Bromphenol blue	Merck, Darmstadt, Germany
Calcium chloride	Merck, Darmstadt, Germany
Chloroform	Merck, Darmstadt, Germany
Complete Mini Protease Inhibitor Cocktail Tablets	Roche, Basel, Switzerland
Count off™	NEN® Research Products, Boston, USA
Desoxy-Ribonucleotid-Triphosphates (dNTPs)	Amersham, Freiburg, Germany
Dextran sulfate	Roth, Karlsruhe, Germany
Dimethylsulfoxide (DMSO)	Merck, Darmstadt, Germany
di-Sodiumhydrogenphosphat	Merck, Darmstadt, Germany
Enhanced chemiluminescence (ECL) Kit	Perbio Science, Bonn, Germany
Ethanol, absolute	AppliChem, Darmstadt, Germany
Ethidium bromide	Sigma-Aldrich, Seelze, Germany
Ethylendiamine tetraacetate (EDTA)	AppliChem, Darmstadt, Germany
Forene (isoflurane)	Abbot GmbH, Wiesbaden, Germany
Glucose (20%)	DeltaSelect, Pfullingen, Germany
Glycerol	Serva, Heidelberg, USA
Glycine	AppliChem, Darmstadt, Germany
HEPES	AppliChem, Darmstadt, Germany
Hydrochloric acid (37%)	KMF Laborchemie, Lohmar, Germany
Hydrogen peroxide	Sigma-Aldrich, Seelze, Germany
Insulin	Novo Nordisk, Bagsvaerd, Denmark
Isopropanol (2-propanol)	Roth, Karlsruhe, Germany
Magnesium chloride	Merck, Darmstadt, Germany
Methanol	Roth, Karlsruhe, Germany
Nitrogen (liquid)	Linde, Pullach, Germany
Phenol	AppliChem, Darmstadt, Germany
Phenylmethylsulfonylfluorid (PMSF)	Sigma-Aldrich, Seelze, Germany
Phosphate buffered saline (PBS)	Gibco BRL, Eggenstein, Germany

2 Materials and Methods

Potassium chloride	Merck, Darmstadt, Germany
Potassium hydroxide	Merck, Darmstadt, Germany
Pyruvate	Sigma-Aldrich, Seelze, Germany
Ready Safe™, Liquid Scintillation Cock- tail	Beckman Coulter, Fullerton, USA
Salmon Sperm DNA sodium salt	Biomol, Hamburg, Germany
Sodium acetate	AppliChem, Darmstadt, Germany
Sodium chloride	AppliChem, Darmstadt, Germany
Sodium citrate	Merck, Darmstadt, Germany
Sodium dodecyl sulfate	AppliChem, Darmstadt, Germany
Sodium fluoride	Merck, Darmstadt, Germany
Sodium hydroxide	AppliChem, Darmstadt, Germany
Sodium orthovanadate	Sigma-Aldrich, Seelze, Germany
Spermidine	Sigma, Steinheim, Germany
Tetramethylethylenediamine (TEMED)	Sigma-Aldrich, Seelze, Germany
Tissue Freezing Medium	Jung, Heidelberg, Germany
Trishydroxymethylaminomethane (Tris)	AppliChem, Darmstadt, Germany
Triton X-100	AppliChem, Darmstadt, Germany
Tween 20	AppliChem, Darmstadt, Germany
Western Blocking Reagent	Roche, Mannheim, Germany

Table 2.2: Enzymes

Name	Company
AscI	NEB, Frankfurt, Germany
AsiSI	NEB, Frankfurt, Germany
BamHI	NEB, Frankfurt, Germany
Bca DNA polymerase	Takara, Otsu, Japan
BglII	Fermentas, St. Leon-Rot, Germany
DNase, RNase-free	Promega, Madison, WI, USA
EcoCRI	Fermentas, St. Leon-Rot, Germany
EcoRI	Fermentas, St. Leon-Rot, Germany
EcoRV	NEB, Frankfurt, Germany
HindIII	NEB, Frankfurt, Germany
MultiScript Reverse Transcriptase	Applied Biosystems, Darmstadt, Germany
NcoI	NEB, Frankfurt, Germany
Proteinase K	Roche, Basel, Switzerland
RNase Inhibitor	Applied Biosystems, Darmstadt, Germany
SacI	NEB, Frankfurt, Germany
SacII	NEB, Frankfurt, Germany
Trypsin	Gibco, Paisley, UK
XbaI	NEB, Frankfurt, Germany

2.1.1 Targeting Vectors

JNK-2 targeting vector was obtained from the European Conditional Mouse Mutagenesis Program (EUCOMM, order PG00006A1D05). A detailed vector map is included in Figure 2.1 A. mXBP1s targeting vector was generated by Bruno Klisch. Hereto, the cDNA of mXBP1s was cloned into the common STOP-eGFP-ROSA-CAGs (SERCA) vector (Klisch, 2006). A detailed vector map is included in Figure 2.1 B.

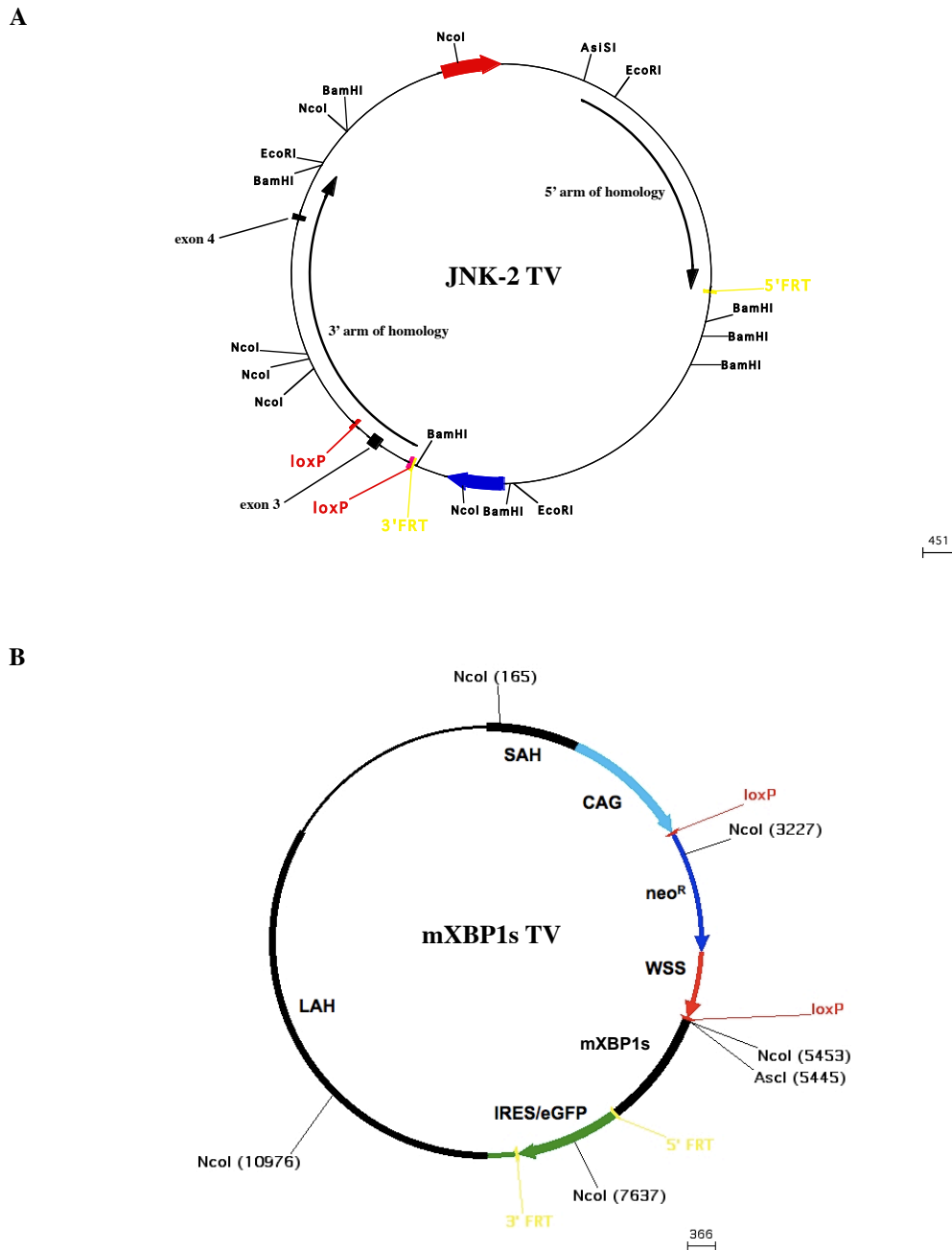


Figure 2.1: JNK-2 and mXBP1s targeting vectors

(A) Map of the JNK-2 targeting vector used for the generation of a conditional JNK-2 allele. Indicated are 5' and 3' arms for homologous recombination, FRT flanked neomycin resistance gene (colored blue), loxP flanked exon 3, the gene for diphtheria toxin A (colored red), as well as sites for restriction enzymes. (B) Map of the mXBP1s targeting vector used for targeted insertion of mXBP1s into the murine ROSA26 locus. The cDNA of mXBP1s was previously cloned into the SERCA vector (Klisch, 2006). Indicated are short (SAH) and long (LAH) arms of homology, strong chicken β -actin promoter (CAG) (colored light blue), neomycin resistance gene (neo^R) (colored dark blue), Westphal-Stop-Sequence (WSS) (colored red, later referred to as STOP-cassette), cDNA for mXBP1s (black), IRES/eGFP-cassette (colored green), and FRT- and loxP-sites as well as sites for restriction enzymes.

2.2 Molecular Biology

Standard methods of molecular biology were performed according to protocols described by J. Sambrook, unless otherwise stated (J. Sambrook, 2001).

2.2.1 Isolation of Genomic DNA

For isolation of genomic DNA mouse tail biopsies were digested overnight in lysis buffer (100 mM Tris pH 8.5, 5 mM EDTA, 0.2 % (w/v) SDS, 0.2 M NaCl, 500 mg/ml Proteinase K) in a thermomixer (Eppendorf, Hamburg, Germany) at 56 °C. On the next day, DNA was precipitated by adding an equivalent volume of 2-Propanol (100 %). DNA was washed in 70 % (v/v) ethanol and the dried DNA pellet was redissolved in TE-buffer (10 mM Tris pH 8.5, 5 mM EDTA, 500 mg/ml RNase A). A phenol/chloroform-extraction step was added after overnight lysis for isolation of genomic DNA from tissues.

2.2.2 Quantification of Nucleid Acids

DNA and RNA concentrations were quantified by using a NanoDrop ND-1000 UV-Vis Spectrophotometer (Peqlab, Erlangen, Germany). Sample absorptions at 260 nm and 280 nm were measured and an optical density of 1 corresponds to approximately 50 $\mu\text{g}/\text{ml}$ of double stranded DNA and to 38 $\mu\text{g}/\text{ml}$ of RNA. To assess purity of nucleic acids, the ratio of absorptions at 260 nm and 280 nm was calculated, as proteins absorb maximum at 280 nm. An $\text{OD}_{260}/\text{OD}_{280}$ ratio of 2 refers to pure nucleic acids, lower values display protein contaminations.

2.2.3 Polymerase Chain Reaction

PCR analysis was performed to detect loxP-flanked or Cre-targeted alleles. Customized primers for PCR analysis were obtained from Eurogentec (Eurogentec, Cologne Germany), and are listed in table 2.3. Reactions were done in a Thermocycler iCycler PCR machine (Biorad, Munich, Germany). Amplifications were performed in volumes of 25 μl , containing a minimum of 50 ng template DNA, 25 pmol of each primer, 25 μM dNTP mix, 10 \times polymerase reaction buffer, and 1 unit of DNA polymerase. Standard PCR programs started with 4 minutes of denaturation at 95 °C, followed by 25-40 cycles consisting of denaturation at 95 °C for 45 seconds, annealing at primer-specific temperatures

for 30-45 seconds, and elongation at 68 or 72 °C for 30 seconds, and a final elongation step at 72 °C for 10 minutes.

Table 2.3: Primers used for genotyping

Name	Sequence	Targeted allele
5Cre	ACGAGTGATGAGGTTTCGCA	ALFP-Cre
3Cre	ATGTTTAGCTGGCCCAAATGT	ALFP-Cre / FABP4-2A-Cre
FABP4-E1for	GTGGGAACCTGGAAGCTTG	FABP-2A-Cre
mck5	GTTCTTAAGTCTGAACCCGG	MCK-Cre
mck3	GTCTGAGATGACATCGTCCAG	MCK-Cre
Cre-intern-rev3	ATGTTTAGCTGGCCCAAATGT	MCK-Cre
TL3472	GCACCTGGATGCTGACGAAG	CAMKII-Cre
TL3473	CGCATAACCAGTGAAACAGCA	CAMKII-Cre
JNK1loxNT	ACATGTACCATGTACTGACCTAAG	JNK-1
JNK1deltaNT	CATTACTCTACTCACTATAGTAAC	JNK-1
JNK1forNT	GATATCAGTATATGTCCTTATAG	JNK-1
JNK2F3	GGTGTGACCAGACCGAAGATTG	JNK-2
JNK2R4	ACTGACCTGAGTGAGATCCCAGAGT	JNK-2
5Flp	GGCAGAAGCACGCTTATCG	FLP-Del
3Flp	GACAAGCGTTAGTAGGCACAT	FLP-Del
Typ-rev-CAGS	TGTCGCAAATTAAGTGTGAATC	mXBP1s
Typ-rev-wt	GATATGAAGTACTGGGCTCTT	mXBP1s
Typ-fwd	AAAGTCGCTCTGAGTTGTTATC	mXBP1s
5GK12	CCGCGGGCGATCGCCTAGG	IL-6R α
5IL6Ex3	CCAGAGGAGCCCAAGCTCTC	IL-6R α
3IL6A	TAGGGCCCAGTTCCTTTAT	IL-6R α

2.2.4 Southern Blot

For Southern blot analysis, 10-15 μg of genomic DNA were digested over night with the appropriate restriction enzyme. The DNA fragments were separated by agarose gel electrophoresis and transferred onto Hybond-XLTM-membranes (Amersham, Illinois, USA) by alkaline capillary transfer. 80-100 ng DNA of the appropriate probe was radioactively labeled with 2.5 mCi ^{α 32P}dCTP (Amersham, Braunschweig) using the LaddermanTM Labeling Kit (Takara, Japan). Primers for the generation of Southern blot probes are listed in table 2.4.

Table 2.4: Primers used for the generation of Southern blot probes

Probe	Primer	Sequence
JNK1PA	5J1PA	GATATCAGCTAGCTGAAGTGT
	3J1PA	GATATCATGGCTAAGCTGACAGACTCGG
JNK2P5	5J2P5	GCTTTGTGGAATAACAAGAACT
	3J2P5	CACTAATTTTATGGTAATGTATTATG
JNK2P3	5J2P3	GCCTGCGGTGTTGCTTTTAATCTAAG
	3J2P3	TAGACCTCTGGGTAGCAGCACACA
Neo ^R	5neo	TGAATGAACTGCAGGACGAGGCA
	3neo	GCCGCCAAGCTCTTCAGCAAT
IL-6R ^{α}	IL-6R-5-probe-fwd	TTGTAGTCTCCACCCACAAGCC
	IL-6R-5-probe-rev	AGCGAGCAACCTCAGACTCAGA

Probes targeting the ROSA26 locus were generated by restriction digest and are listed in table 2.5. The DNA containing membranes were hybridized with the probes over night at 65 °C in a hybridization oven. On the following day, unspecific bound probes were washed off by using stringent solutions of SSC and SDS, ranging from 2 x SSC/ 0.1 % SDS to 0.5 x SSC/ 0.1 % SDS. Radioactivity was proven with a Kodak MS film, incubated on -80 °C together with the membrane in a film cassette.

Table 2.5: Restriction enzymes used for the generation of Southern blot probes

Name	Enzymes	Origin	Size
ROSA26 probe	EcoRI	A-04 plasmid (Mao et al., 1999)	1200 bp
	BamHI		
p26.1	SacII	pROSA26-1 (Soriano, 1999)	1000 bp
	XbaI		

2.2.5 Gene Expression Analysis

Quantitative expression for mRNAs were determined by using whole-muscle isolated by TRIzol (Invitrogen) or whole-liver, and hippocampus RNA isolated by RNeasy Kit (Qiagen, Hilden, Germany). Therefore the tissues were homogenized using an Ultra Turrax homogenizer (IKA, Staufen, Germany). This RNA isolation followed a step of DNase digestion (Promega GmbH, Germany). RNA was reversely transcribed with High Capacity cDNA Reverse Transcription Kit (Applied Biosystems, Foster City, USA) and amplified by using TaqMan Universal Master Mix (Applied Biosystems). Relative expression of mRNAs was determined by using standard curves based on cDNA derived from the respective tissues, and samples were adjusted for total RNA content by house-keeping gene hypoxanthine guanine phosphoribosyl transferase (HPRT) 1 quantitative PCR. The real-time probes used in this study are listed in table 2.6.

For genes for which no commercial probe was available, custom probes were designed (Tab. 2.7). Calculations were performed by a comparative cycle threshold (Ct) method. This means that the starting copy number of test samples was determined in comparison with the known copy number of the calibrator sample (ddCt). The relative gene copy number was calculated as 2^{-ddCT} . Quantitative PCR was performed on an ABI PRISM 7900 Sequence Detector (Applied Biosystems). Assays were linear > 4 orders of magnitudes.

Table 2.6: Realtime PCR probes

All realtime PCR probes were obtained from Applied Biosystems, Foster City, USA.

Name	Cat.-No.
mapk8	Mm00489514_m1
mapk8 human	Hs01548508_m1
mapk9	Mm00444231_m1
mapk10	Mm00436518_m1
IL-6	Mm00446190_m1
XBP1	Mm00457359_m1
Dnajb9	Mm01622956_s1
Ddit3	Mm00492097_m1
Hspa5	Mm00517691_m1
Hprt1	Mm00446968_m1
Gusb	Mm00446953_m1

Table 2.7: Custom-made realtime PCR probes

Probe	Primer	Sequence
JNK1 (Δ)	Probe	AGTGTGTGCAGCTTATGATGCC
	5JNK1	ATTGGAGATTCTACATTCACAGTCCTA
	3JNK1	CATTCTGAAATGGCCGGCT
XBP1s	Probe	CGCAGCAGGTGCAGGCCCA
	XBP-Sense	GAATGGACACGCTGGATCCT
	ABP-Antisense	CAGAATCTGAAGAGGCAACAG

2.3 Cell Biology

2.3.1 Cell Culture

Handling and passaging of cells was performed under a sterile hood (Hera Safe KS 12, Heraeus Instruments) as previously described (Pal, 2008) unless otherwise stated. Embryonic stem and embryonic fibroblast cells were maintained in an environment comprising 95 % humidity, 37 °C, and 10 % CO₂ saturation. The medium of ES cells was changed every day, the medium of EF cells every 2-3 days. ES cell colony growth was stopped before they became confluent and to maintain their pluripotency they were cultured in the presence of leukaemia inhibiting factor (LIF) containing ES cell medium (DMEM, 15 % ES-fetal calf serum (FCS), 1 x non-essential amino acids, 1 mM sodium pyruvate, 2 mM L-glutamine, 0.1 mM β -mercaptoethanol, 10 U/ml LIF supernatant). All targetings were performed in Bruce4 embryonic stem cells (F Köntgen, 1993). 10⁷ ES cells were transfected with 40 μ g of targeting vector DNA and were exposed to selection with geneticin (G418) and/or ganciclovir. Selected clones were injected into blastocysts to give rise to chimeric mice containing the desired transgene. Embryonic fibroblast cells were cultured in DMEM-medium supplemented with 1 mM sodium pyruvate and 2 mM L-glutamine, and were used as feeder cells for ES cell culture. Feeder cells are mitomycin C (mmc) treated cells and were passaged three times.

2.3.2 Immunohistochemistry

White and brown adipose tissue of FABP4-2A-Cre mice was dissected and fixed overnight in 4 % PFA and embedded for paraffin sections. Afterwards, 7 μ m thin sections were deparaffinized and stained for GFP expression using rabbit anti-GFP antibody (Invitrogen, Karlsruhe, Germany). A Zeiss Axioskop equipped with a Zeiss AxioCam for acquisition of digital images using Spot Advanced 3.0.3 software was used to view the slides.

2.3.3 Flow Cytometry

Isolated peritoneal macrophages and Kupffer cells were analysed on a FACSCalibur and data with regard to GFP fluorescence were evaluated using CellQuest software (Becton Dickinson, Mountain View, USA).

2.4 Biochemistry

2.4.1 Enzyme-Linked Immunosorbent Assay (ELISA)

Values for serum insulin and serum leptin were examined by ELISA (mouse/rat insulin ELISA, #INSKR020, Crystal Chem., Downers Grove, USA; mouse leptin ELISA #900-019, Ann Arbor, USA) according to the manufacturer's protocol. The absorbance was determined in a Precision Microplate Reader (Emax, Molecular Devices GmbH, Munich, Germany).

2.4.2 Protein Extraction

Whole tissues (e.g. skeletal muscle) were homogenized with a polytron homogenizer (IKA, Staufen, Germany) in protein lysis buffer (50 mM HEPES pH 7.4, 1 % Triton X-100, 0.1 M NaF, 10 mM EDTA, 50 mM NaCl, 0.1 % SDS, proteinase and phosphatase inhibitor cocktail tablets (Roche, Mannheim, Germany)). Lysates were cleared by centrifugation and protein concentration were determined using a NanoDrop ND-1000 UV-Vis spectrophotometer (Peqlab, Erlangen, Germany). Protein solutions were diluted with 4 x SDS sample buffer (125 mM Tris-HCL pH 6.8, 5 % SDS, 43.5 % glycerol, 100 mM DTT, 0.02 % bromphenol blue) to a final concentration of 10 mg/ml protein.

2.4.3 Western Blot Analysis

Isolated proteins were separated by SDS-polyacrylamide gel electrophoresis (10 %) and transferred to PVDF membranes (Bio-Rad, Munich, Germany). Membranes were blocked with 1 % of blocking reagent (Roche, Mannheim, Germany) for 1 hour at room temperature. Membranes were probed overnight at 4 °C with primary antibodies. A secondary antibody was applied for 1 hour at room temperature. In between the incubation of first and second and after the second antibody, membranes were washed with TBS-Tween (TBS-T, 1 % Tween). After the last washing step, membranes were incubated for 1 minute in Pierce ECL Western Substrate (Perbio Science, Bonn, Germany) and were exposed to chemiluminescence films (Amersham, Braunschweig, Germany). Films were then developed in an automatic developer (Kodak, Germany). Antibodies were obtained from Cell Signaling or Santa Cruz Technologies and are listed in table 2.8.

Table 2.8: Primary antibodies used for Western blot

Name	Origin	Company
JNK-1/3	rabbit	#sc-474, Santa Cruz Biotech., Santa Cruz, USA
p-JNK	rabbit	#4668, Cell Signaling, Danvers, USA
pan-AKT	rabbit	#4685, Cell Signaling, Danvers, USA
p-AKT	rabbit	#9271, Cell Signaling, Danvers, USA
PEPCK	rabbit	#sc-32879, Santa Cruz Biotech., Santa Cruz, USA
Calnexin	rabbit	#20880, Calbiochem, Darmstadt, Germany
p-IKK α/β	rabbit	#2697, Cell Signaling, Danvers, USA
p-I κ B	mouse	#9246, Cell Signaling, Danvers, USA
I κ B	rabbit	#4812, Cell Signaling, Danvers, USA
XBP-1	rabbit	#sc-7160, Santa Cruz Biotech., Santa Cruz, USA

2.4.4 c-Jun N-terminal Kinase Assay

SAPK/JNK assays were performed according to the manufacturer's protocol (#9810, Cell Signaling,). For this matter, tissues were homogenized in assay buffer and incubated with c-Jun fusion beads protein overnight. After washing the protein-c-Jun fusion beads were incubated with kinase buffer containing ATP, enabling bound c-Jun N-terminal kinases to phosphorylate c-Jun. After 30 minutes the reaction was stopped and the samples were loaded onto a 10 % SDS gel. Western blots were performed by using phospho-c-Jun antibody.

2.5 Mouse Experiments

General animal handling was performed as described by Hogan and Silver (B. Hogan, 1986; Silver, 1995).

2.5.1 Animal Care

All mice were cared within institutional care committee guidelines. All animal procedures were conducted in compliance with protocols and approved by local government authorities (Bezirksregierung Köln, Cologne, Germany). The procedures were also in accordance with National Institutes of Health guidelines. Mice were fed either normal chow diet (NCD) (Teklad Global Rodent 2018, Harlan) or a high fat diet (HFD) (C1057, Altromin). Normal chow diet contains 53.5 % carbohydrates, 18.5 % proteins, and 5.5 % fat (12 % of calories from fat). High fat diet contains 32.7 % carbohydrates, 20 % proteins, and 35.5 % fat (55.2 % of calories from fat). Mice were housed in groups of 3 to 5 individuals in a virus-free facility at 22 °C to 24 °C on a 12 h light / 12 h dark cycle. All mice had access to water and food *ad libitum*. At the end of the study period, mice were sacrificed by lethal CO₂ anaesthesia. Relevant organs were dissected and after shock-freezing in liquid nitrogen stored at -80 °C until further preparation.

2.5.2 Mice

All mice were backcrossed on a C57/BL6 background. In all experiments, littermates carrying the loxP-flanked alleles but not expressing Cre recombinase were used as control WT animals. Littermates containing both, the targeted loxP-flanked allele and the Cre allele, were used for analysis at all times.

In this thesis, the following mouse models were used:

- (A) To generate mice which lack JNK-1 specifically in skeletal muscle, mice expressing the Cre recombinase from the promotor of the muscle creatine kinase (MCK) (Brüning *et al.*, 1998) were crossed to mice carrying a loxP-flanked exon 2 of the JNK-1 gene (JNK-1^{FL/FL} mice, (Belgardt *et al.*, 2010a)). Resulting offspring was intercrossed to create JNK-1^{SM-KO} male mice. JNK-1^{FL/FL} mice served as wild type control (WT) animals throughout the experiments.

- (B)** To generate mice which heterozygously express a Cre inducible constitutively active form of JNK-1 (JNK-1^C) specifically in skeletal muscle, MCK-Cre mice were crossed to homozygous JNK-1^C mice. JNK-1^C mice were kindly provided by Dr. Claudia Wunderlich and PD Dr. Thomas Wunderlich. In JNK-1^C mice, JNK-1 is fused to a mutated version of its upstream kinase MKK7, which results in a constant phosphorylation of JNK independent of intra-or extracellular stimuli.
- (C)** Heterozygous mXBP1s mice were generated in this thesis and crossed to heterozygous CAMKII-Cre mice (Casanova *et al.*, 2001), or ALFP-Cre mice (Kellendonk *et al.*, 2000), respectively, to generate a brain (mXBP1s^{CAMKII})- or liver (mXBP1s^{ALFP}) specific overexpression of mXBP1s from the murine ROSA26 locus.
- (D)** To characterize newly generated FABP4-2A-Cre mice, animals were crossed with two control mouse lines, a conditional knockin of FOXODN into the ROSA26 locus, and a conditional knockout of the IL-6R α gene, respectively.
- (I) ROSA26-FOXODN mice were kindly provided by Dr. Marianne Ernst and PD Dr. Thomas Wunderlich. FOXODN is a loss of function mutant of FOXO1. The characteristic of FOXODN variants is a C-terminal truncation of the transcriptional activation domain (TAD) at (Δ 256) of FOXO1 (Nakae *et al.*, 2001). By this truncation in the FOXODN mouse mutant it functions as a dominant negative (DN) inhibitor of transcription. The binding of endogenous FOXO1 and presumably other FOXO proteins to responsive DNA elements is inhibited without the requirement of a stimulatory insulin signal (Belgardt *et al.*, 2008). In this thesis, ROSA26-FOXODN mice served as a control to test the functionality of the newly generated FABP4-2A-Cre mice. For this, homozygous ROSA26-FOXODN mice were crossed to heterozygous FABP4-2A-Cre mice. Offspring with a heterozygous allele of FOXODN served as control WT mice, offspring with both a heterozygous FOXODN allele, and an allele for the FABP4-2A-Cre (FOXODN^{FABP-4}) were used to characterize the FABP4-2A-Cre mouse.
- (II) IL-6R α ^{FL/FL} mice were kindly provided by Dr. Peter Ströhle and PD Dr. Thomas Wunderlich ((Wunderlich *et al.*, 2010)). In this thesis, IL-6R α ^{FL/FL} mice served as a control to test the functionality of the newly generated FABP4-2A-Cre

mice. For this, homozygous IL-6R α ^{FL/FL} mice were crossed to heterozygous FABP4-2A-Cre mice. Offspring with a heterozygous allele of IL-6R α ^{FL/+} served as control WT mice, offspring with both a heterozygous IL-6R α ^{FL/+} allele, and an allele for the FABP4-2A-Cre (IL-6R α ^{FABP-4}) were used to characterize the FABP4-2A-Cre mouse.

2.5.3 Genotyping of Mice

Genotyping for the different Cre lines and the targeted alleles was performed on genomic DNA isolated from tail biopsies by PCR analysis using the primer listed in table 2.3. Germline deletion for JNK-1^{FL/FL} mice was excluded by using three primers within PCR, one binding upstream the first loxP site and the others flanking the second loxP site.

2.5.4 Collection of Blood Samples and Determination of Blood Glucose and Lactate Levels

Tail bleeding of mice was performed according to Hogan and Silver (B. Hogan, 1986; Silver, 1995). Blood glucose and blood lactate values were determined from whole venous blood using an automatic glucose monitor (GlucoMen, A Menarini Diagnostics, Florence, Italy) or an automatic lactate monitor (Accutrend Plus, Roche Diagnostics, Mannheim, Germany).

2.5.5 Analysis of Body Composition (NMR)

Whole body composition of live animals was determined *in vivo* by nuclear magnetic resonance (NMR) using the NMR Analyser Minispec (Minispec mq 7.5, Bruker Optik, Ettlingen, Germany). Radiofrequency pulse sequences are transmitted into mouse tissue, which are then retransmitted by hydrogen atoms in the tissue. These are the signals the minispec detects. Amplitude and duration of the signals are related to properties of the material.

2.5.6 Glucose, Insulin, and Pyruvate Tolerance Test

Glucose and pyruvate tolerance tests (GTT, PTT) were performed on animals fasted for 16 h prior the experiment. For the insulin tolerance tests (ITT) random fed mice were

used. Animals were injected with either 2 g/kg body weight of glucose or pyruvate (2 g/kg dissolved in 0.9 % saline solution) or 0.75 units/kg body weight of human regular insulin (Novo Nordisk, Bagsværd, Denmark, diluted in 0.9 % saline solution) into the peritoneal cavity. Blood glucose concentrations were determined from tail blood by using an automated glucose monitor (GlucoMen, A Menarini Diagnostics, Mannheim, Germany) for the indicated time points.

2.5.7 Insulin Signaling

To directly test insulin signaling, 16 h fasted mice were anesthetized by intraperitoneal injection of Avertin (Sigma-Aldrich, Seelze, Germany). Samples (125 μ l) of 0.9 % saline with/without 5 U of insulin (Novo Nordisk, Bagsværd, Denmark) were injected into the inferior *vena cava*. Samples were collected 2 (liver) and 5 (skeletal muscle) minutes after injection.

2.5.8 Isolation of Adipocytes and Stromal Vascular Fraction

For the isolation of adipocytes and stromal vascular fraction, epigonadal fat pads of mice were removed and subsequently incubated in collagenase solution (1 mg/ml in DMEM/F12 1:1 medium) for 45 minutes at 37 °C to isolate adipocytes. Digested tissues were centrifuged for 5 minutes at 2.500 rpm. The upper phase contains adipocytes, whereas the pellet represents the stromal vascular fraction including preadipocytes, macrophages and other cell types. The adipocytes were further centrifuged (5 min, 13.000 rpm) to extract the nuclei. The pellet of the stromal vascular fraction was resuspended in erythrocyte lysis buffer (154 mM NH₄Cl, 10 mM KHCO₃, 0.1 mM EDTA) and incubated for 10 min at room temperature to destroy erythrocytes.

2.5.9 Isolation of Primary Peritoneal Macrophages

For the isolation of primary peritoneal macrophages, mice were injected intraperitoneally with 2 ml of thioglycolate medium (4 % in PBS) to induce a sterile peritonitis. 4 days after injection the mice were sacrificed and cells were collected by peritoneal lavage with sterile PBS. After a subsequent centrifugation step, the cells were resuspended in erythrocyte lysis buffer for 3 minutes at room temperature. Cells were then subjected to FACS analysis.

2.5.10 Isolation of Kupffer Cells

For the isolation of Kupffer cells, mice were anesthetized and the liver was floated with 10 ml of sterile PBS via the *vena carva*. Next, the liver was dissected and meshed up using 2ml DMEM and a cell strainer. Cells were centrifuged for 5 minutes at 600 rpm. The resuspended cell pellet was subjected to FACS analysis.

2.5.11 Food Intake

Daily food was calculated as the average intake of chow from custom made food racks within the time stated. For this manner, mice were acclimated to the settings for at least five days. Weight of the racks was determined daily.

2.5.12 Indirect Calorimetry

The Phenomaster system (TSE Systems, Bad Homburg, Germany) was used to determine indirect calorimetry, food intake and calorimetry of the mice. The parameters were measured with the help of Dr. Hella Brönneke and Jens Alber as previously described (Belgardt *et al.* , 2010a). The system allows measurement of metabolic performance and activity-monitoring by an infrared light-beam frame. Mice were allowed to adapt to the system chambers in training cages for five days. Food and water were provided *ad libitum* in the appropriate devices and were measured by the build-in automated instruments. Presented data are average values obtained in these recordings.

2.5.13 Treadmill

Exercise experiments were performed on a treadmill (TSE Systems, Bad Homburg, Germany) with the help of Dr. Hella Brönneke and Jens Alber (Fig. 2.2). An electrical stimuli was triggered and applied (0.2 mA, max. 8 sec) every time a mouse stopped running due to falling or exhaustion. Mice used in this study were only familiarized to but not trained on the treadmill. Therefore, the mice were adapted and familiarized to sound and movement of the treadmill on the first four days.

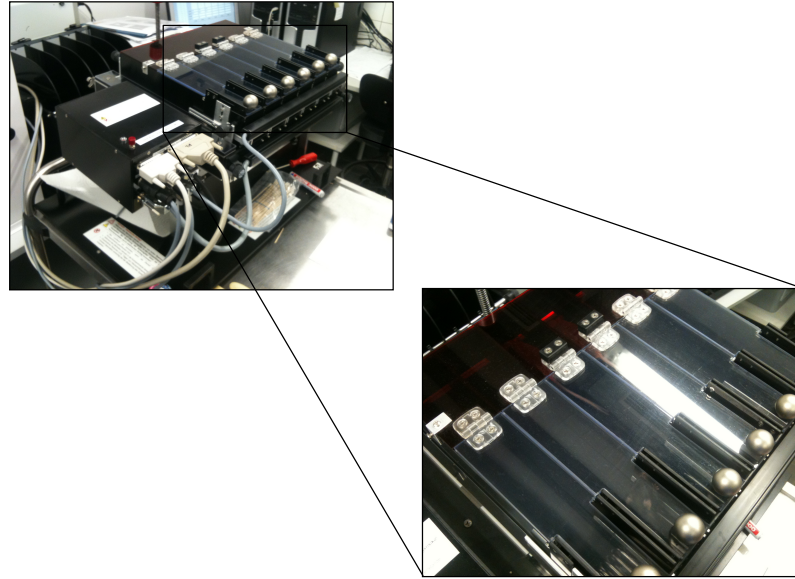


Figure 2.2: Treadmill

For exercise experiments mice were forced to run a treadmill (TSE Systems, Bad Homburg, Germany). Indicated are the running lanes for the analysis of six mice in parallel.

On the experimental day 5, the mice were forced to run for 30 minutes or 60 minutes, respectively (Tab. 2.9).

Table 2.9: Treadmill Protocol

Day	Velocity (m/s)	Time (min)	Sound	Electric Stimulation
1	none	10	none	none
	none	10	Yes	none
2	none	15	Yes	none
	0.05	15	Yes	none
3	0.05	15	Yes	none
	0.1-0.12	15	Yes	Yes
4	0.15-0.17	15	Yes	Yes
	0.17-0.22	15	Yes	Yes
5 (Test)	0.22-0.25	30 / 60	Yes	Yes

The velocity was starting at 0.22 m/s and reached a final pace of 0.25 m/s. Immediately after running, serum lactate and glucose values of the mice were determined by tail blood and the mice were sacrificed using CO₂ anesthesia .

2.6 Computer Analysis

2.6.1 Densitometrical Analysis

To determine the intensity per mm² of Western or Southern blot bands, the Quantity One Software (Biorad, Munich, Germany) was used. After background subtraction, each sample was normalized to an internal loading control (e.g. Calnexin, unphosphorylated protein).

2.6.2 Statistical Methods

Data sets were analyzed for statistical significance by using two-tailed unpaired Students's t test. *P* values below 0.05 were considered significant. All displayed values are means ± SEM. **p* ≤ 0.05, ***p* ≤ 0.01, ****p* ≤ 0.001. For visual clarity, instead of standard deviations, means ± standard errors of the mean (SEM) are depicted in all figures.

3 Results

Whole body JNK-1 knockout mice revealed a central role for JNK-1 in linking inflammatory pathways to the pathogenesis of obesity and insulin resistance, as the mice were protected from these diseases. To understand the cell-type specific functions of JNK-1 in metabolic regulation *in vivo*, mice which lack or constitutively active JNK-1 specifically in skeletal muscle were generated, and analyzed in terms of energy homeostasis. JNK-1 deficient mice were further utilised to understand synergistic activities between skeletal muscle derived JNK-1 and the myokine IL-6 during physical activity.

ER stress is a central response of the cell to obesity. To further understand the UPR *in vivo*, mice were generated with a brain- or liver specific overexpression of mXBP1s, and were analyzed in terms of central and peripheral ER stress.

Many of the metabolic dysregulations associated with obesity originate within the adipose tissue. To investigate these signaling pathways, *in vivo* genetic tools for specific gain- or loss of function in adipose tissue is crucial. Therefore, mice expressing the Cre recombinase from the promotor of the adipose tissue derived FABP-4 protein were characterized.

3.1 The role of skeletal muscle derived JNK in metabolic regulation

A crucial role for JNK-1 in obesity-associated insulin resistance was first shown in 2002 (Hirosumi *et al.*, 2002). Hirosumi and co-workers could establish that JNK-1 plays a central role in obesity and obesity-induced insulin resistance. This thesis aims at exploring the cell-type specific role of JNK-1 in the skeletal muscle, through analyzing genetically engineered loss and gain of function approaches of JNK-1.

3.1.1 Increased JNK activity in skeletal muscle of obese mice

JNK is a stress-sensitive kinase which becomes activated upon stress-stimuli such as activation of inflammatory mediators or free fatty acids, both of which are increased under

obesity conditions (Vallerie & Hotamisligil, 2010). To this end, WT mice were exposed to a high fat diet (HFD) from 3 weeks of age until 17 weeks of age. In order to show an increased inflammation status of mice fed a HFD compared to mice exposed to a normal chow diet (NCD), JNK-activity in skeletal muscle of these mice was examined. JNK-activity was determined by the status of JNK phosphorylation and the degree of c-Jun phosphorylation by performing a kinase assay. Skeletal muscle of mice fed a HFD showed increased JNK phosphorylation (Fig. 3.1). In addition, increased phosphorylation of JNKs downstream target c-Jun in a kinase assay indicated a higher JNK-activity upon HFD (Fig. 3.1).

These data demonstrate an elevated JNK activity in skeletal muscle during HFD- induced obesity.

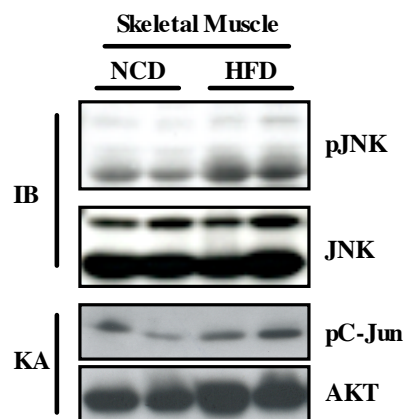


Figure 3.1: JNK activity in skeletal muscle is elevated in HFD-induced obesity.

Activation of JNK in skeletal muscle tissue in wild type mice is increased in mice fed a HFD compared to mice fed a NCD, indicated by western blot analysis (IB) and JNK kinase activity assay (KA). For western blot analysis antibodies against phosphorylated JNK and unphosphorylated JNK were used. Antibodies detecting phosphorylated c-Jun were used to show increased JNK activity on HFD in kinase assay. Antibodies against AKT were used as loading control.

3.1.2 Generation of a skeletal muscle specific knockout of JNK-1

In order to investigate the cell-type specific role of JNK-1 in skeletal muscle, mice were created with a selective loss of JNK-1 in skeletal muscle. To this end, mice with a conditional JNK-1 allele, in which exon 2 was flanked by loxP sites (JNK-1^{FL/FL} mice, (Belgardt *et al.*, 2010a)) were crossed with mice harboring the Cre recombinase under the control of the muscle creatine kinase (MCK) promotor (Brüning *et al.*, 1998) (Fig. 3.2). The expression of MCK is highly restricted to skeletal muscle and heart, and reaches its maximum at

10 days after birth (Brüning *et al.*, 1998; Johnson *et al.*, 1989). JNK-1^{FL/FL} mice harboring the MCK-Cre allele (JNK-1^{SM-KO}) were used for analysis whereas JNK-1^{FL/FL} mice served as wild type controls (WT) throughout the experiments.

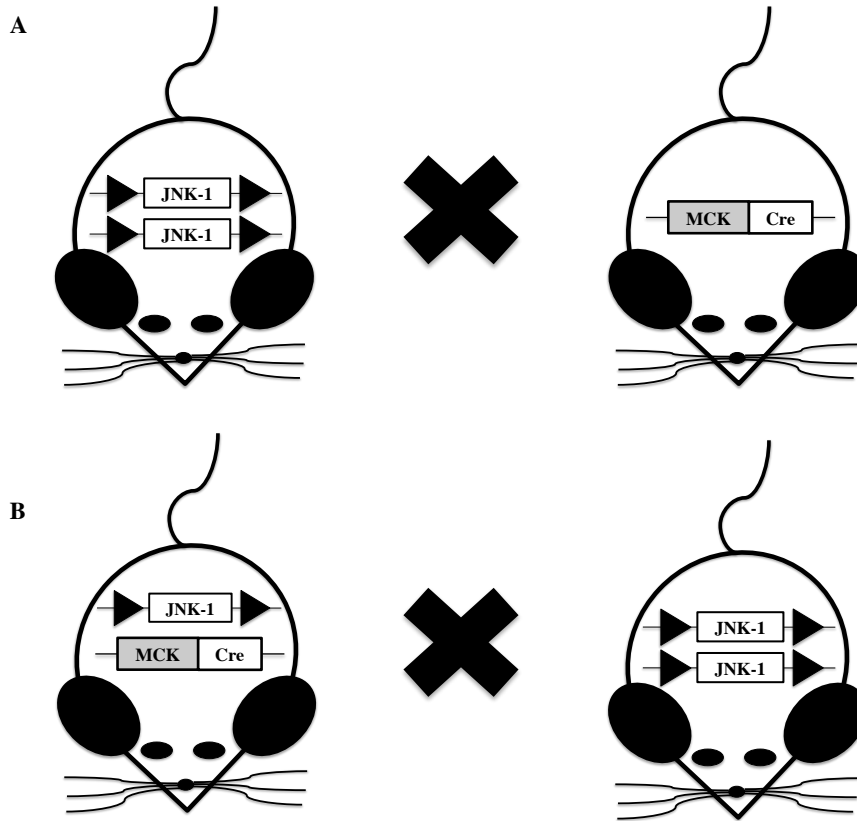


Figure 3.2: General scheme of mice with a selective deletion of JNK-1 in skeletal muscle.

(A) Mice, homozygous for a loxP-flanked allele of JNK-1 (JNK-1^{FL/FL}) were crossed with mice expressing Cre under the control of the MCK promoter. **(B)** Mice, heterozygous for both, a loxP-flanked JNK-1 allele and MCK-Cre, were further intercrossed resulting in mice which lack JNK-1 specifically in skeletal muscle tissue (JNK-1^{SM-KO} mice).

The loss of JNK-1 was confirmed by Southern blot, quantitative realtime PCR, and western blot analysis from skeletal muscle extracts (Fig. 3.3). Using probe A in Southern blot analysis yielded DNA fragments of 5.3 kb in size for the targeted allele (FL) and of 4.8 kb when the targeted allele was deleted by Cre-mediated recombination of exon 2 (Δ) (Fig. 3.3 A). Knockout of JNK-1 was only accomplished in skeletal muscle of JNK-1^{SM-KO} mice but not in liver or white adipose tissue (WAT) (Fig. 3.3 B). To confirm these data on mRNA level, quantitative realtime PCR analysis was performed using probes specific for JNK-1 and JNK-2, respectively. Expression of JNK-1 mRNA was diminished by 95 % in skeletal muscle of JNK-1^{SM-KO} mice whereas expression of JNK-2 remained unchanged between the genotypes (Fig. 3.3 C). Moreover, Western blot analysis confirmed the ab-

sense of JNK-1 protein in skeletal muscle of JNK-1^{SM-KO} mice, whereas JNK-1 protein expression in the liver was comparable between WT and JNK-1^{SM-KO} mice (Fig. 3.3 D).

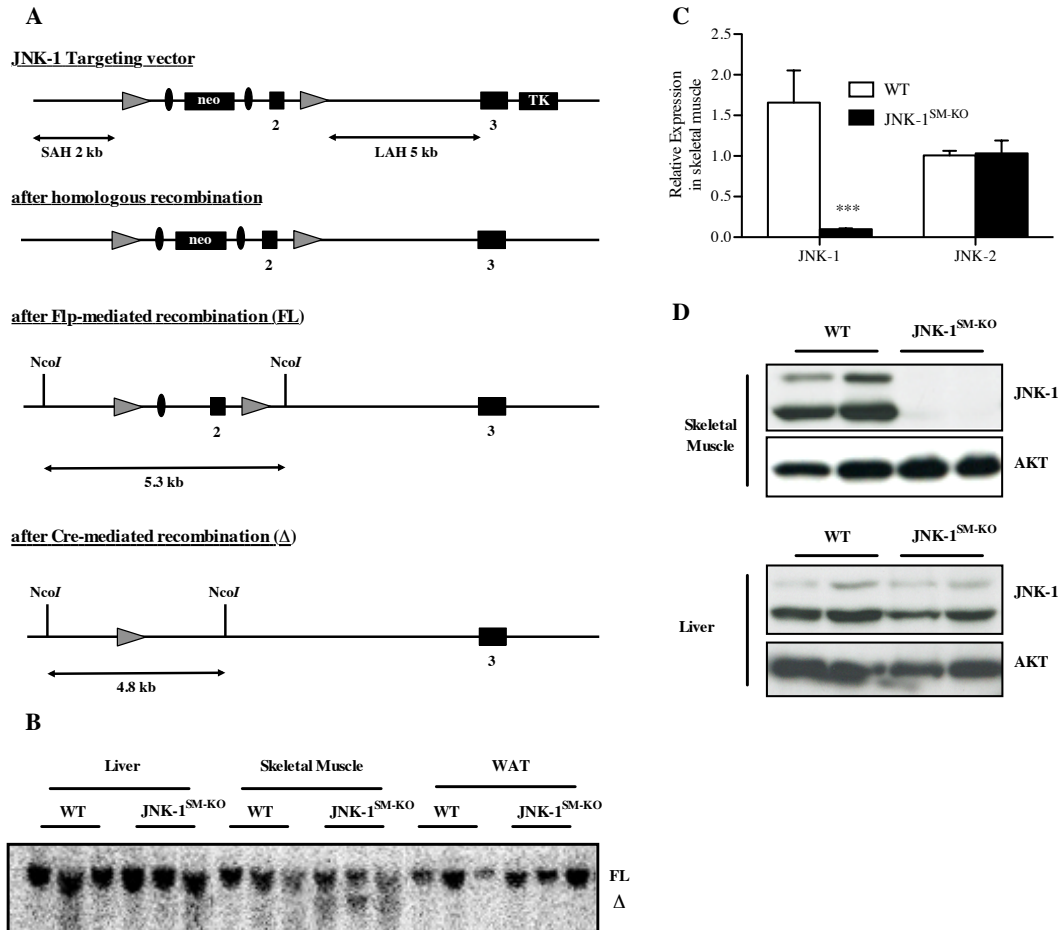


Figure 3.3: Loss of JNK-1 specifically in skeletal muscle.

(A) Targeting strategy for conditional inactivation of the JNK-1 gene. Targeting vector containing a FRT-flanked (black ovals) neomycine resistance cassette, loxP-flanked (black triangle) exon 2 and the gene for thymidine kinase (TK) essential for negative selection. Flp-mediated recombination of the neomycine resistance cassette and *NcoI* digest results in a 5.3 kb DNA fragment (FL) when using probe A in Southern blot analysis. *NcoI* digest after Cre-mediated recombination produces a 4.8 kb fragment (Δ) using the same strategy. (B) Southern blot analysis of genomic DNA isolated from liver, skeletal muscle, and WAT of WT and JNK-1^{SM-KO} mice using the beforementioned strategy. (C) Determination of relative JNK-1 and JNK-2 mRNA concentrations in skeletal muscle of WT and JNK-1^{SM-KO} mice by quantitative realtime PCR (n=6). (D) Western blot analysis of protein lysates isolated from skeletal muscle (upper panel) and liver (lower panel) of WT and JNK-1^{SM-KO} mice using JNK-1 and AKT (loading control) antibodies. Values are means \pm SEM; ***, $p \leq 0.001$.

Taken together, these data confirm a sufficient deletion of JNK-1 specifically in skeletal muscle tissue of mice and represent a reasonable model to investigate a skeletal muscle specific JNK-1 deficiency.

3.1.3 Unaltered energy homeostasis in JNK-1^{SM-KO} mice

JNK-1 complete knockout mice exhibit a decrease in body weight gain and show decreased levels of body fat under obese conditions (Hirosumi *et al.*, 2002). To investigate the impact of JNK-1 in skeletal muscle on the development of obesity, body weight gain of male WT mice and JNK-1^{SM-KO} mice was monitored from week 3 of age until week 17 of age when feeding both, NCD and HFD. However, this analysis revealed no differences between the genotypes on NCD (Fig.3.4 A). Furthermore, when feeding a HFD, JNK-1^{SM-KO} mice developed obesity similar to WT mice (Fig.3.4 B).

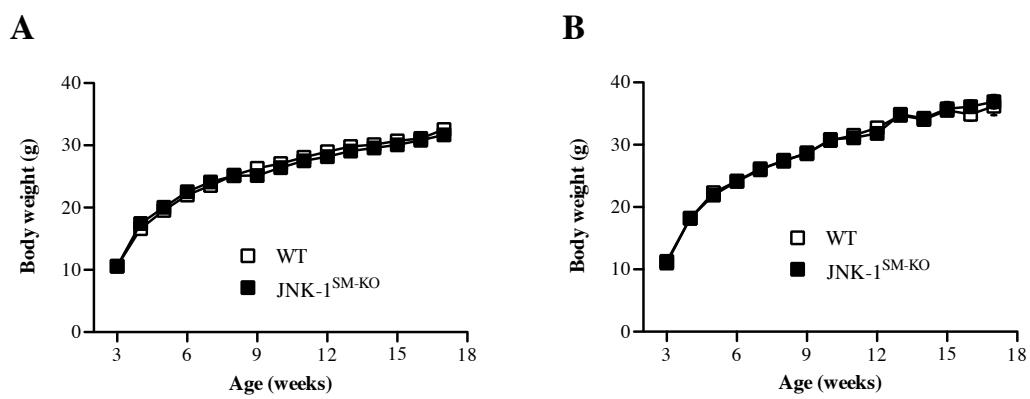


Figure 3.4: Body weight of JNK-1^{SM-KO} mice.

(A) Average body weight of WT (open squares) and JNK-1^{SM-KO} mice (black squares) fed a NCD (n=16). (B) Average body weight of WT and JNK-1^{SM-KO} mice fed a HFD (n=23). Values are means \pm SEM.

Consistent with these findings, body fat content of JNK-1^{SM-KO} mice was indistinguishable from that of WT mice, although both, JNK-1^{SM-KO} and WT mice displayed similar increases in body fat content under HFD conditions when compared to NCD (Fig. 3.5 A). In addition, the weight of epigonadal fat pads was unchanged between WT and JNK-1^{SM-KO} mice under both NCD and HFD, respectively (Fig. 3.5 B). In line with these data, the concentrations of circulating serum leptin, an indirect measurement for body fat content, were unaltered between WT and JNK-1^{SM-KO} mice, and significantly increased to the same extent upon HFD in both genotypes (Fig. 3.5 C).

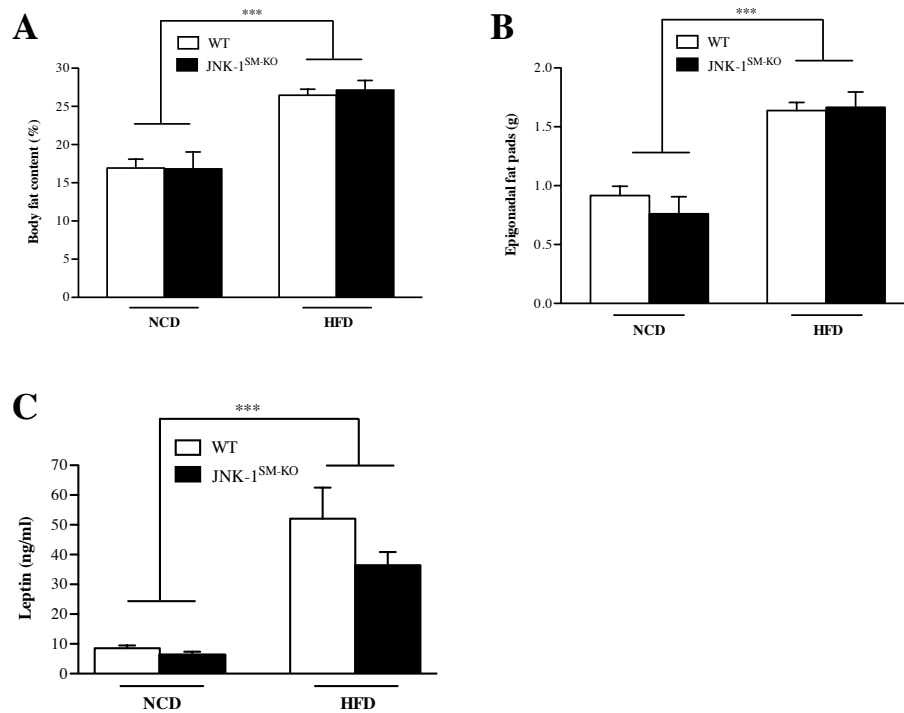


Figure 3.5: Unaltered adiposity in JNK-1^{SM-KO} mice.

(A) Body fat content of WT and JNK-1^{SM-KO} mice fed a NCD and HFD was determined by NMR at week 17 of age (n=25). (B) Weight of epigonadal fat pads from WT and JNK-1^{SM-KO} mice fed a NCD and HFD at week 17 (n=25). (C) Serum leptin concentrations of WT and JNK-1^{SM-KO} mice fed a NCD and HFD at the age of 17 weeks were determined by ELISA (n=10). Values are means \pm SEM. ***, $p \leq 0.001$.

Next, naso-anal length of JNK-1^{SM-KO} and WT mice was measured, since mice with a deletion of JNK-1 in the central nervous system (CNS) and pituitary showed reduced somatic growth (Belgardt *et al.*, 2010a). Here, although HFD caused a significant increase in length in JNK-1^{SM-KO} and WT mice, no alterations were detectable in body length between the genotypes, indicating that skeletal muscle derived JNK-1 does not influence somatic growth (Fig. 3.6).

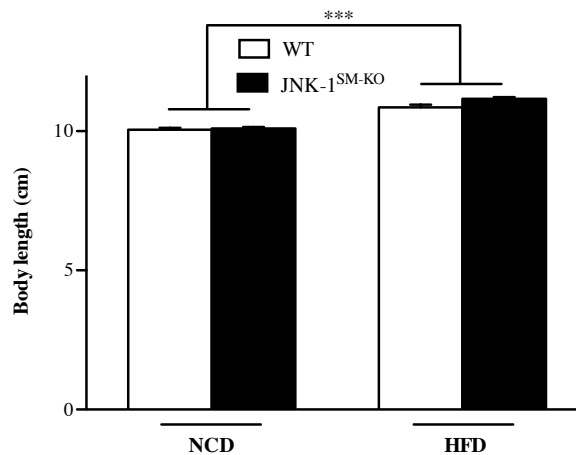


Figure 3.6: Body length of JNK-1^{SM-KO} mice.

Naso-anal length of WT and JNK-1^{SM-KO} mice fed a NCD and HFD at week 17 of age (n=25). Values are means \pm SEM. ***, $p \leq 0.001$.

According to unchanged body weight and body fat mass in JNK-1^{SM-KO} mice, determination of daily food intake revealed no alteration between the genotypes, although food intake was significantly increased upon HFD in both, WT and JNK-1^{SM-KO} mice (Fig. 3.7 A).

As energy intake was not affected, energy expenditure was assessed in WT and JNK-1^{SM-KO} mice. This analysis revealed unaltered oxygen consumption and carbon dioxide production in JNK-1^{SM-KO} mice during both day and night phases under both nutritional states (Fig. 3.7 B). In line with these findings, an unaltered ratio was observed between O₂ and CO₂ depicted in the respiratory exchange ratio (RER) between the genotypes. However, RER was decreased upon HFD in both genotypes demonstrating the effect of feeding a HFD since a RER value close to 0.8 represents the intake of more fat as a food source (Fig. 3.7 C). Moreover, basal heat production in JNK-1^{SM-KO} mice was indistinguishable to WT animals during both day and night phase upon NCD and HFD (Fig. 3.7 D).

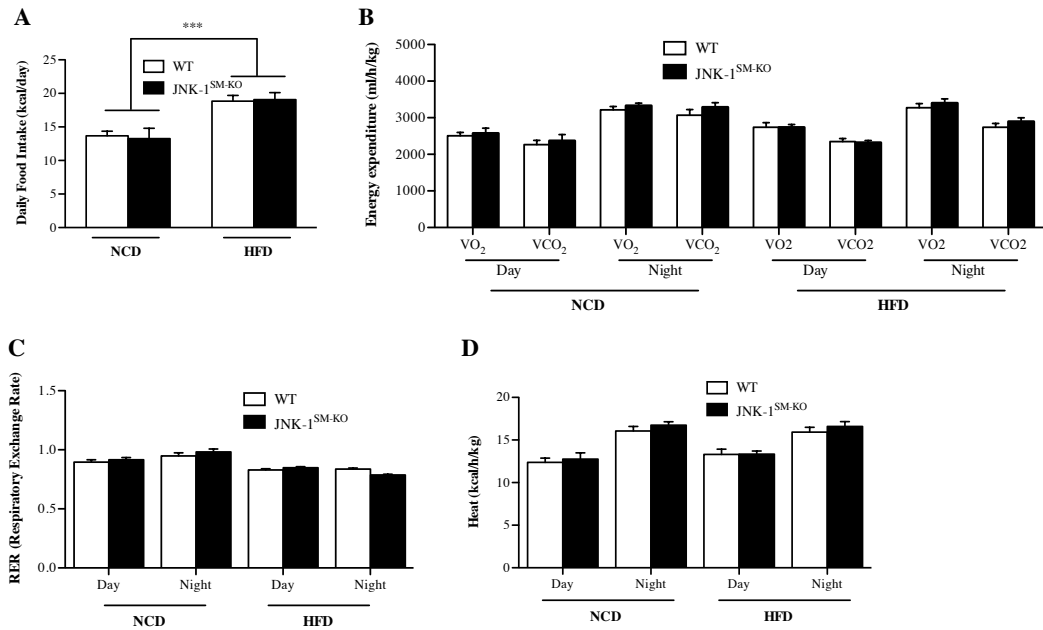


Figure 3.7: Food intake and energy expenditure of JNK-1^{SM-KO} mice.

(A) Daily food intake of WT and JNK-1^{SM-KO} mice at the age of 14 weeks under both NCD and HFD (n=8). (B) Energy expenditure revealed in phenomaster experiments by the daily and nightly volume of O₂-consumption and CO₂-release of WT and JNK-1^{SM-KO} mice at the age of 14 weeks upon both NCD and HFD (n=8). (C) Respiratory exchange rate (RER) of WT and JNK-1^{SM-KO} mice at the age of 14 weeks upon both NCD and HFD (n=8). (D) Daily and nightly heat production measured in phenomaster experiments of WT and JNK-1^{SM-KO} mice at the age of 14 weeks upon NCD and HFD (n=8). Values are means ± SEM. ***, p ≤ 0.001.

Taken together, these data show that JNK-1^{SM-KO} mice exhibited a normal body composition and indicate that energy homeostasis is not affected by a skeletal muscle specific JNK-1 deficiency under both normal and high fat diet conditions.

3.1.4 Unaltered glucose metabolism and insulin sensitivity in JNK-1^{SM-KO} mice

Mice lack JNK-1 in the whole body display lower glucose and insulin concentrations (Hirosumi *et al.*, 2002) under obese conditions. Thus, glucose homeostasis and insulin sensitivity of JNK-1^{SM-KO} were investigated. Performing a glucose tolerance test revealed no alterations in glucose homeostasis on NCD in both genotypes (Fig. 3.8 A). However, unlike JNK-1 complete knockout mice, JNK-1^{SM-KO} mice fed a HFD developed obesity-induced hyperglycemia similar to WT mice (Fig. 3.8 B). In addition, insulin sensitivity was unaltered between WT mice and JNK-1^{SM-KO} mice feeding a NCD, indicated by an insulin tolerance test (Fig. 3.8 C). Upon HFD JNK-1^{SM-KO} mice developed obesity-

induced insulin resistance and hyperinsulinaemia, which was similar to WT mice (Fig. 3.8 D). Additionally, concentrations of serum insulin remained unchanged between WT and JNK-1^{SM-KO} mice under normal and high fat diet conditions (Fig. 3.8 E).

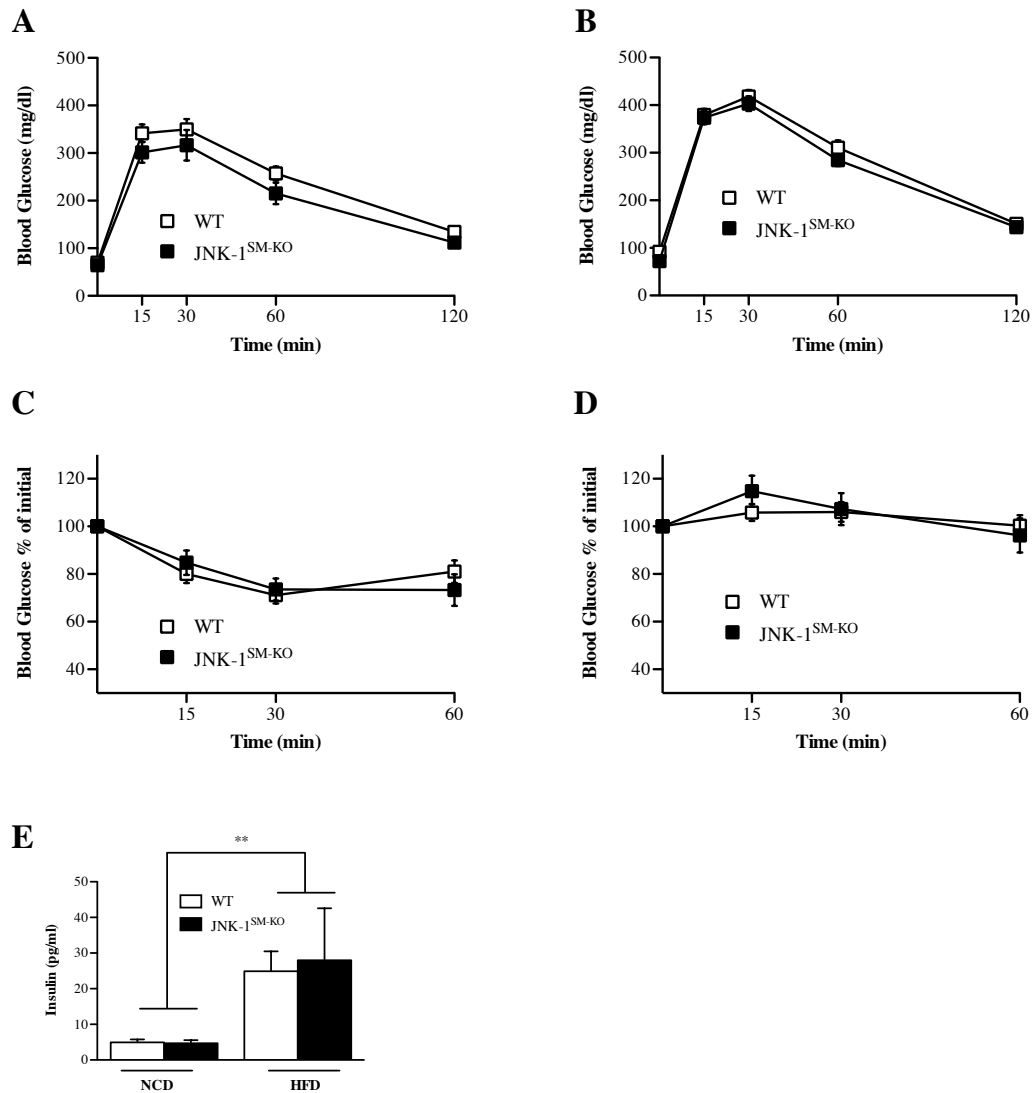


Figure 3.8: Unaltered glucose metabolism and insulin sensitivity in JNK-1^{SM-KO} mice.

(A) Glucose tolerance tests of WT and JNK-1^{SM-KO} mice fed a NCD were performed at week 11 of age (n=21). (B) Glucose tolerance tests of WT and JNK-1^{SM-KO} mice fed a HFD were performed at week 11 of age (n=21). (C) Insulin tolerance tests of WT and JNK-1^{SM-KO} mice fed a NCD were performed at week 12 of age (n=21). (D) Insulin tolerance tests of WT and JNK-1^{SM-KO} mice fed a HFD were performed at week 12 of age (n=21). (E) Serum insulin concentrations of WT and JNK-1^{SM-KO} mice at the age of 17 weeks fed a NCD or HFD were determined by ELISA (n=10). Values are means \pm SEM.**, $p \leq 0.01$.

To investigate a functional insulin signaling cascade, insulin-stimulated AKT phosphorylation was determined in these tissues of WT and JNK-1^{SM-KO} mice. Although

JNK-1 complete knockout mice lack the obesity-induced inhibitory phosphorylation of IRS-1 (Hirosumi *et al.*, 2002), no improvements in insulin-stimulated AKT phosphorylation were detectable in skeletal muscle, or liver of JNK-1^{SM-KO} mice compared to WT under both NCD and HFD (Fig. 3.9).

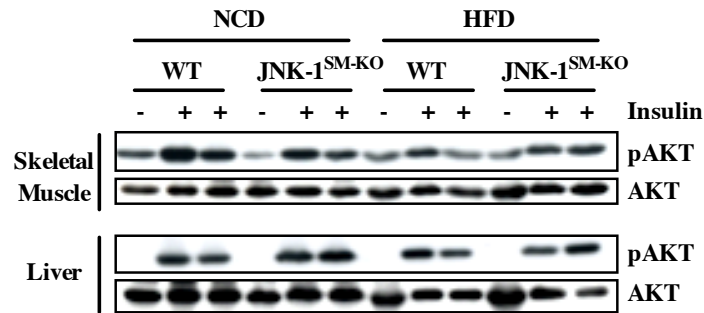


Figure 3.9: Insulin signaling in skeletal muscle and liver of JNK-1^{SM-KO} mice. Insulin-stimulated AKT phosphorylation of skeletal muscle (upper panel) and liver (lower panel) of WT and JNK-1^{SM-KO} mice fed a NCD or a HFD, in Western blot analysis using phospho-AKT and AKT (loading control) antibodies.

These data demonstrate that inactivation of JNK-1 in skeletal muscle does not protect from HFD- induced hyperglycemia and hyperinsulinemia.

Moreover, inactivation of JNK-1 in skeletal muscle does not the phenotype in terms of obesity and insulin resistance occurring in JNK-1 whole body knockout mice (Hirosumi *et al.*, 2002).

3.1.5 Exercise induces activation of JNK and IL-6 in skeletal muscle of WT mice

The lack of JNK-1 in skeletal muscle did not result in alterations for the body's energy homeostasis. In particular upon HFD-induced obesity a loss of JNK-1 in skeletal muscle did not result in improvements with regard to hyperglycemia or hyperinsulinemia.

However, an improvement of the metabolic balance can also be achieved by an increase in physical activity. Upon physical activity, skeletal muscle executes the main work in adapting the body to these conditions. Previous experiments established that during exercise the expression of the prototypical myokine IL-6 is strongly increased, albeit the precise intracellular signaling events mediating this increase are not well understood (Pedersen & Febbraio, 2008). Moreover, in 1998, for the first time an activation of JNK in the course of exercise was revealed (Boluyt *et al.*, 2003). To determine the role of skeletal muscle derived JNK-1 on the exercise-induced expression of IL-6, JNK-1^{SM-KO} mice were analyzed upon treadmill exposure.

As data are missing revealing an exercise-induced activation of JNK in mice, first phosphorylation of JNK in skeletal muscle of WT mice was determined. Upon exercise, phosphorylation of JNK was drastically increased in skeletal muscle tissue of WT mice, both after 30 minutes and 60 minutes of exercise, respectively, as demonstrated by Western blot analysis (Fig. 3.10 A). Consistently, quantification of the phosphorylation state determined a significant increase of JNK phosphorylation after exercise (Fig. 3.10 B).

These data demonstrate that JNK is activated in skeletal muscle in response to exercise.

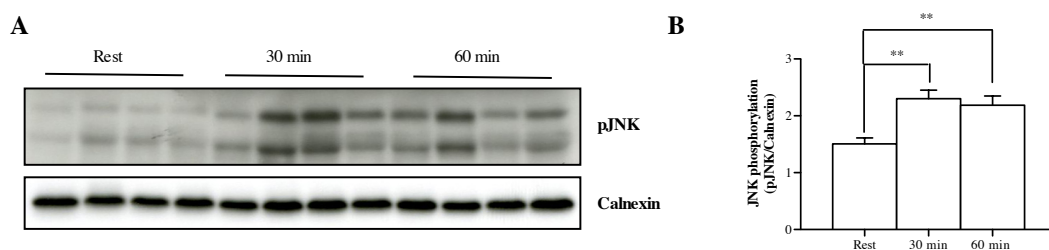


Figure 3.10: JNK is activated in skeletal muscle of WT mice upon exercise.

(A) Representative Western blot analysis of protein lysates from skeletal muscle of random fed WT mice either at rest, or running for 30 or 60 minutes, respectively, using phospho-JNK and Calnexin (loading control) antibodies. (B) Quantification of Western blot showing in (A). Quantification is indicated by the quotient of signal intensities of phospho-JNK and Calnexin antibodies (n=6). Values are means \pm SEM. **, $p \leq 0.01$; ***, $p \leq 0.001$

Next, experiments were performed to assess an exercise-induced activation of IL-6 in WT mice.

This analysis revealed a robust increase of IL-6 mRNA in skeletal muscle of WT mice after 30 minutes of exercise (Fig. 3.11). Moreover, as a consequence of an increasing anaerobic milieu during exercise the values of lactate are increased, not only in the working skeletal muscle but also in circulation (Gladden, 2004, 2008). Thus, to confirm the impact of treadmill running, lactate levels of WT mice were determined after 30 and 60 minutes of exercise. Indeed, WT mice exhibited significantly elevated levels of lactate in the circulation after 30 minutes of exercise (Fig. 3.11 B).

These data show that the exercise protocol applied in this study was sufficient to analyze exercise dependent effects in the skeletal muscle.

Taken together, JNK and IL-6 are activated in skeletal muscle of WT mice in response to physical activity. These findings are consistent with previous experiments revealing an increase of IL-6 mRNA within the skeletal muscle upon exercise (Febbraio *et al.*, 2004).

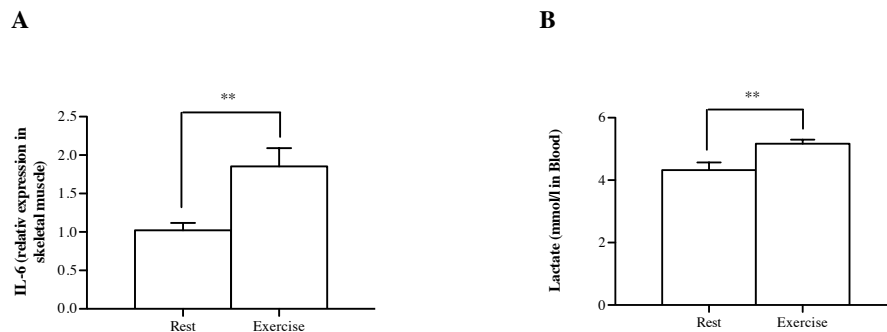


Figure 3.11: IL-6 mRNA expression is increased in skeletal muscle of WT mice upon exercise. (A) Determination of IL-6 mRNA expression in skeletal muscle of random fed WT mice either at rest or after 30 minutes of exercise by quantitative realtime PCR analysis (n=6). (B) Determination of serum lactate values of WT mice either at rest or after 30 minutes of exercise. Values are means \pm SEM. **, $p \leq 0.01$.

3.1.6 Exercise induced IL-6 mRNA increase in skeletal muscle is blunted in JNK-1^{SM-KO} mice

A large body of evidence reveal that IL-6 is activated in skeletal muscle upon exercise (data presented here, and review: (Pedersen & Febbraio, 2008)). However the underlying mechanisms for this increase in IL-6 mRNA are yet to be identified. Hence, the impact of a skeletal muscle specific inactivation of JNK-1 on the expression of IL-6 mRNA was

examined. To this end, JNK-1^{SM-KO} mice were applied in treadmill experiments.

As previously shown, investigation of IL-6 mRNA expression in skeletal muscle tissue revealed that IL-6 mRNA expression was significantly increased in WT mice running for 30 minutes compared to resting mice (Fig. 3.11 + 3.12 A). Strikingly, this increase in skeletal muscle IL-6 mRNA as a consequence to exercise was blunted in the skeletal muscle of JNK-1^{SM-KO} mice (Fig. 3.12 A).

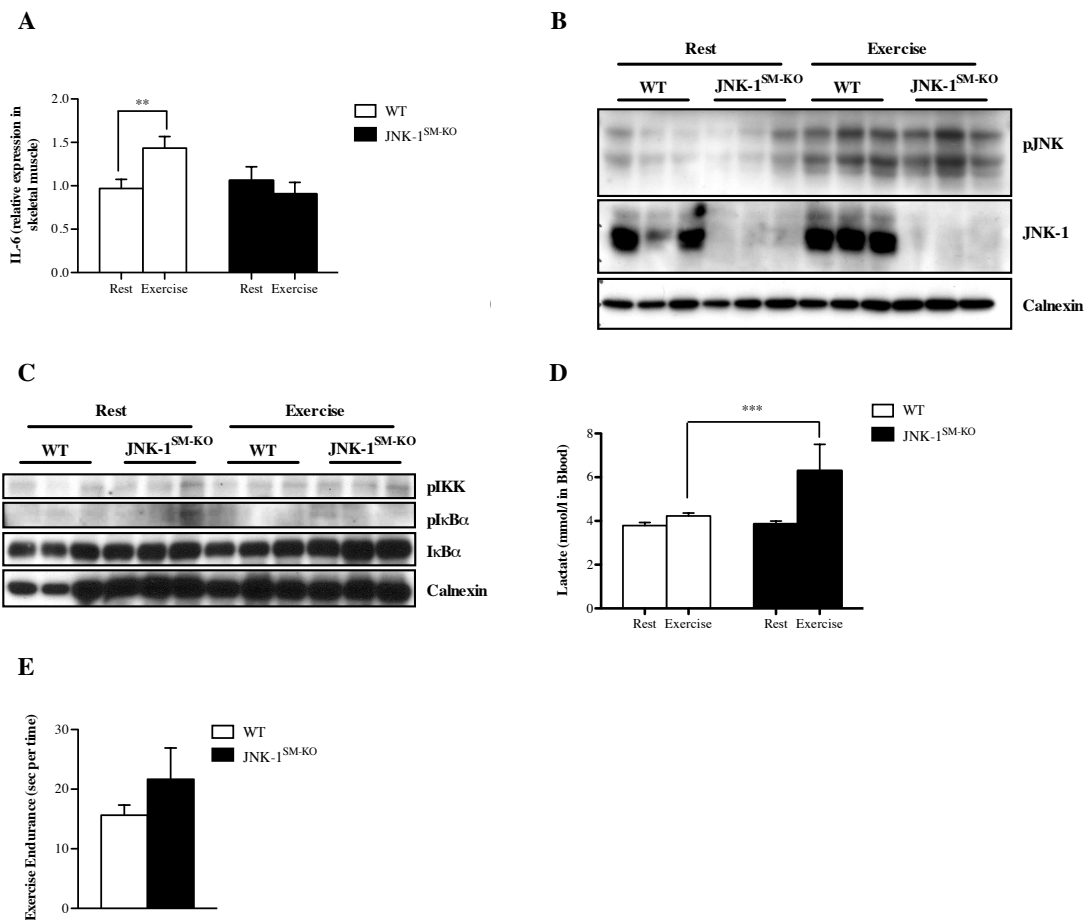


Figure 3.12: IL-6 activation upon exercise is blunted in JNK-1^{SM-KO} mice.

(A) Determination of IL-6 mRNA concentrations in skeletal muscle of WT and JNK-1^{SM-KO} mice either at rest or after 30 minutes of exercise by quantitative realtime PCR analysis (n=6). (B,C) Western blot analysis of protein lysates from skeletal muscle of WT and JNK-1^{SM-KO} mice either at rest or after 30 minutes of exercise using (B) phospho-JNK, JNK-1, and (C) phospho-IKK, phospho-IκBα, IκBα, and calnexin (loading control) antibodies. (D) Determination of serum lactate values of WT and JNK-1^{SM-KO} mice either at rest or after 30 minutes of exercise. (E) Exercise endurance of WT and JNK-1^{SM-KO} mice was determined as a quotient of running time and the number of times a mouse hit the light beam. Values are means ± SEM. **, p ≤ 0.01; ***, p ≤ 0.001.

To examine whether skeletal muscle specific JNK-1 deficiency alters JNK phosphorylation in rested and exercised skeletal muscle, Western blot analysis of protein lysates from

skeletal muscle of JNK-1^{SM-KO} mice was performed before and after exercise. This analysis revealed that consistent with previous findings JNK is phosphorylated and thus activated upon exercise. Furthermore this analysis demonstrated that the exercise induced IL-6 activation is JNK-1 dependent, since phosphorylation of total JNK in the JNK-1^{SM-KO} mice was unaltered compared to WT mice although JNK-1 protein is absent (Fig. 3.12 B), indicating a crucial role for JNK-1 in the exercise-dependent IL-6 activation.

Previously, experiments were performed demonstrating an activation of the NF κ B-pathway during exercise in rats (Ho *et al.* , 2005; Ji *et al.* , 2004). However, since exercise is believed to repress inflammation and to enhance insulin sensitivity (Pedersen & Febbraio, 2008), it seems paradoxical that the exercise-induced IL-6 activation relies on the pro-inflammatory NF κ B-pathway. Hence, studies were conducted to prove that the activation of IL-6 is independent of classical NF κ B signaling. Western blot analysis of protein lysates from skeletal muscle tissue revealed that 30 minutes of exercise exerted no effect on the activation of IKK or the inhibitory phosphorylation of I κ B α in skeletal muscle in both WT and JNK-1^{SM-KO} mice (Fig. 3.12 C), indicating that NF κ B has no role in the exercise-dependent IL-6 activation.

Supporting data from the Febbraio-group confirmed the findings presented here. Whitham *et al.* could show that JNK is activated in C2C12 cells upon electric pulse stimulation (Whitham *et al.* , 2012). Furthermore they found increased values of IL-6 mRNA and protein after this exercise stimulus. When the cells were treated at the same time with a JNK inhibitor this IL-6 response is blunted at both the mRNA and the protein level of IL-6 (Whitham *et al.* , 2012).

In addition, treated C2C12 myotubes with the exercise stimulus exhibited no activation of IKK in Western blot analysis (Whitham *et al.* , 2012). In parallel, treating the exercise stimulated cells with an IKK inhibitor had no impact on exercise induced IL-6 activation (Whitham *et al.* , 2012).

Significantly, Whitham and colleagues showed a recruitment of the JNK-1 induced transcription factor AP-1 to the IL-6 promotor, indicating a direct link between the activation of JNK and induction of IL-6 mRNA expression (Whitham *et al.* , 2012).

To reveal the significance of exercise in JNK-1^{SM-KO} mice, circulating lactate values were compared between rest and after 30 minutes of exercise in JNK-1^{SM-KO} and WT mice. This analysis revealed that JNK-1^{SM-KO} mice displayed significantly increased serum val-

ues of lactate when compared to WT mice (Fig. 3.12 C), indicating decreased exercise performance in treadmill experiments. However, exercise endurance of JNK-1^{SM-KO} mice was unaltered when compared to WT mice (Fig. 3.12 D).

Taken together, knockout of JNK-1 in skeletal muscle abolishes exercise dependent increase of IL-6 mRNA. While littermate control mice exhibited an increase in skeletal muscle IL-6 mRNA following 30 minutes of exercise on a treadmill, this effect was abrogated in JNK-1^{SM-KO} mice. This highlights a novel role for JNK-1 in the requirement for exercise-induced increases in IL-6 mRNA expression in skeletal muscle.

3.1.7 Generation of a JNK-1 gain of function mouse in skeletal muscle

Loss of function of JNK-1 in skeletal muscle did not alter mouse energy homeostasis and metabolism. However, these parameters were also addressed with a JNK-1 gain of function approach. For this, human JNK-1 was fused to a mutated version its upstream kinase MKK7 (MKK7D, (Y Wang, 1998)). This results in a constant phosphorylation of JNK-1 by MKK7 independent of inflammatory stimuli.

The cDNA of the fusion protein (JNK-1^C) was integrated into the murine ROSA26 locus. The expression of JNK-1^C was prevented by a loxP-flanked STOP-cassette. In order to induce this constant JNK-1 activation specifically in skeletal muscle, mice homozygous for JNK-1^C were crossed with mice heterozygous for the MCK-Cre transgene. This resulted in the generation of JNK-1^{SM-C} mice, which express a Cre inducible constitutively active JNK-1 protein specifically in skeletal muscle (Fig. 3.13).

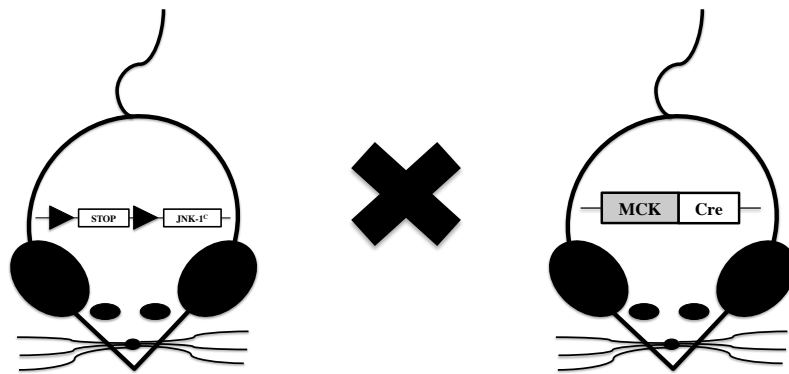


Figure 3.13: General scheme of mice with an selective constitutive activation of JNK-1 in skeletal muscle.

Mice, homozygous for a JNK-1^C allele (only one allele is depicted here) were crossed with MCK-Cre expressing mice to induce a constitutive activation of JNK-1 selectively in skeletal muscle (JNK-1^{SM-C}).

Cre-mediated recombination leads to excision of the loxP-flanked STOP-cassette resulting in expression of JNK-1^C. Expression of JNK-1^C was demonstrated by quantitative realtime PCR analysis of total RNA from skeletal muscle tissue of WT and JNK-1^{SM-C} mice. Human JNK-1 mRNA was drastically increased in skeletal muscle of JNK-1^{SM-C} mice (Fig. 3.14 A). Comparing protein expression in skeletal muscle, liver, and WAT of WT and JNK-1^{SM-C} mice revealed the muscle-specific expression of the JNK-1^C fusion protein at 90 kDa (Fig. 3.14 B). As a control, JNK-1 was expressed in all three tissues and in both, WT and JNK-1^{SM-C} mice. To test the functionality of the construct a JNK

kinase assay was performed. Increased phosphorylation of c-Jun, the downstream target of JNK, was detectable in skeletal muscle of JNK-1^{SM-C} mice indicating increased JNK activity in these animals (Fig. 3.14 C).

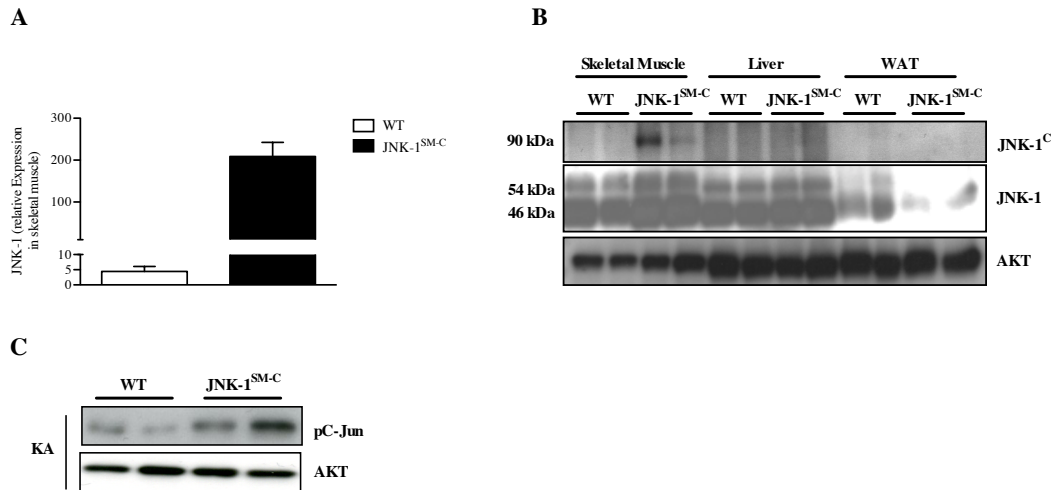


Figure 3.14: Generation of a JNK-1 gain of function approach in skeletal muscle.

(A) Determination of relative JNK-1 mRNA expression in skeletal muscle of WT and JNK-1^{SM-C} mice by quantitative realtime PCR (n=8). (B) Expression of the JNK-1^C fusion protein only in skeletal muscle of JNK-1^{SM-C} mice indicated by Western blot analysis using JNK-1 and AKT antibodies. (C) Functionality of the JNK-1^C construct in skeletal muscle of JNK-1^{SM-C} mice was revealed by increased phosphorylation of c-Jun in JNK kinase assay (KA) experiments using antibodies against phospho-c-Jun and AKT (loading control).

These data confirm a skeletal muscle specific expression of a functional constitutively active JNK-1 fusion-protein, which mimics HFD-induced inflammation even under NCD conditions.

3.1.8 Unaltered energy homeostasis in JNK-1^{SM-C} mice

A lack of JNK-1 in skeletal muscle did not alter energy and glucose homeostasis. Next, the effect of a constitutively activation of JNK-1 on these parameters should be determined. Since the increased JNK-1 activation mimics HFD- induced JNK-1 activation, energy homeostasis of JNK-1^C mice was only determined upon NCD feeding. Body weight of WT and JNK-1^{SM-C} mice was monitored from weaning until 17 weeks of age demonstrating no obvious differences between the genotypes (Fig. 3.15 A). To exclude alterations in the somatic growth axis as observed in CNS-deficient JNK-1 mice (Belgardt

et al., 2010a), naso-anal length of JNK-1^{SM-C} mice was measured. However, no differences were revealed between WT and JNK-1^{SM-C} mice (Fig. 3.15 B).

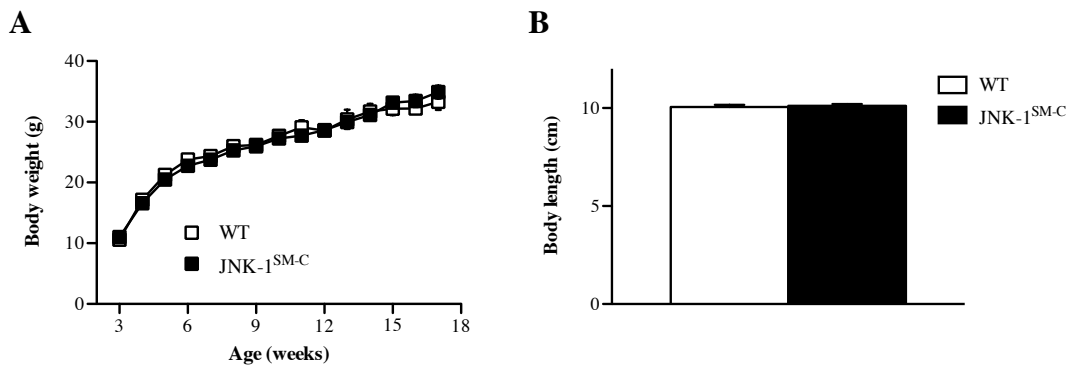


Figure 3.15: Body weight and body length of JNK-1^{SM-C} mice.

(A) The average bodyweight of WT mice was compared with JNK-1^{SM-C} mice from 3 to 17 weeks of age (n=25). **(B)** Naso-anal length of WT and JNK-1^{SM-C} mice at week 17 of age (n=25). Values are means \pm SEM.

Consistent with these findings, body fat content and weight of epigonadal fat pads were indistinguishable between WT and JNK-1^{SM-C} mice (Fig. 3.16 A + B).

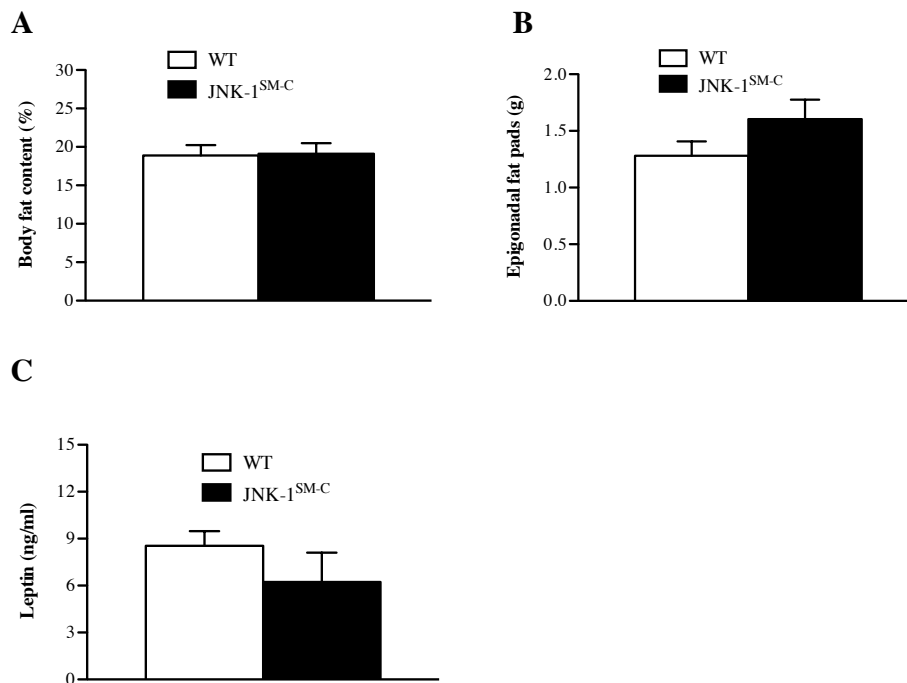


Figure 3.16: Unaltered adiposity in JNK-1^{SM-C} mice.

(A) Body fat content of WT and JNK-1^{SM-C} mice was determined by NMR at week 17 of age (n=25). **(B)** Weight of epigonadal fat pads from WT and JNK-1^{SM-C} mice in week 17 of age (n=25). **(C)** Serum leptin concentrations of WT and JNK-1^{SM-C} mice at the age of 17 weeks were determined by ELISA (n=10). Values are means \pm SEM.

In line with this experiments, unaltered serum concentrations of leptin in JNK-1^{SM-C} mice were present (Fig. 3.16 C). According to the unchanged body weight gain in JNK-1^{SM-C} mice compared to WT mice, analysis of food intake of JNK-1^{SM-C} mice revealed no differences in daily caloric uptake (Fig. 3.17 A). Moreover, parameters of energy expenditure were determined in JNK-1^{SM-C} mice. This analysis revealed unaltered oxygen consumption and carbon dioxide production in JNK-1^{SM-C} mice (Fig. 3.17 B). In line with this notion was an unchanged RER between the genotypes (Fig. 3.17 C) and also the ability to produce heat remained unchanged in JNK-1^{SM-C} mice when compared to WT animals (Fig. 3.17 D).

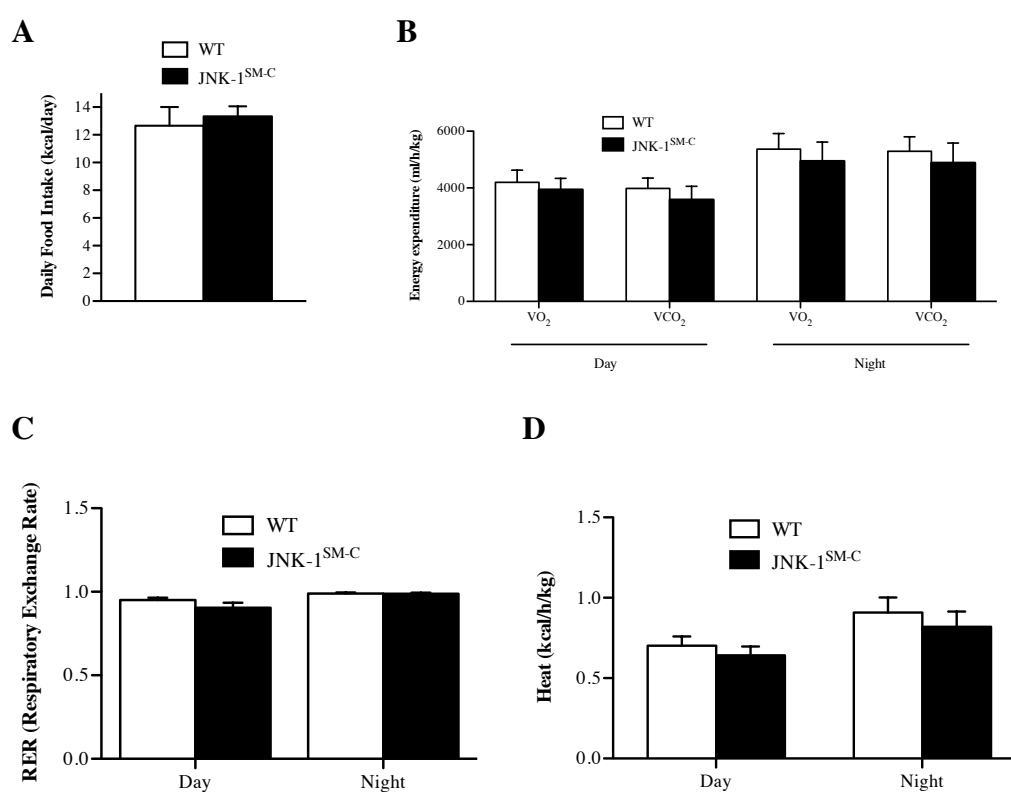


Figure 3.17: Food intake and energy expenditure of JNK-1^{SM-C} mice.

(A) Daily food intake of WT and JNK-1^{SM-C} mice at the age of 14 weeks (n=8). (B) Energy expenditure revealed in phenomaster experiments by the daily and nightly volume of O₂-consumption and CO₂-release of WT and JNK-1^{SM-C} mice at the age of 14 weeks (n=8). (C) Respiratory exchange rate (RER) of WT and JNK-1^{SM-C} mice at the age of 14 weeks (n=8). (D) Daily and nightly heat production measured in phenomaster experiments of WT and JNK-1^{SM-C} mice at the age of 14 weeks (n=8). Values are means \pm SEM.

Taken together, these data demonstrate that JNK-1^{SM-C} mice exhibited a normal body composition, and constitutively activation of JNK-1 in skeletal muscle has no effect on parameters of energy homeostasis.

3.1.9 Unaltered insulin sensitivity in JNK-1^{SM-C} mice

Obese animals lacking JNK-1 in skeletal muscle develop insulin resistance, whereas animals lacking JNK-1 in the whole body are protected against HFD- induced insulin resistance (Hirosumi *et al.*, 2002). Here, the effect of a skeletal muscle specific constitutive activation of JNK-1, on insulin sensitivity was investigated. Systemic insulin sensitivity of JNK-1^{SM-C} mice was examined by performing an insulin tolerance test, that indicated no alterations between the genotypes (Fig. 3.18 A). In addition, serum insulin concentrations remained unchanged between WT and JNK-1^{SM-C} mice (Fig. 3.18 B). Moreover, the ability of insulin to stimulate its signaling cascade was assessed in biochemical experiments in JNK-1^{SM-C} mice. These data indicated unaltered systemic insulin sensitivity as indicated by insulin-induced AKT phosphorylation (Fig. 3.18 C).

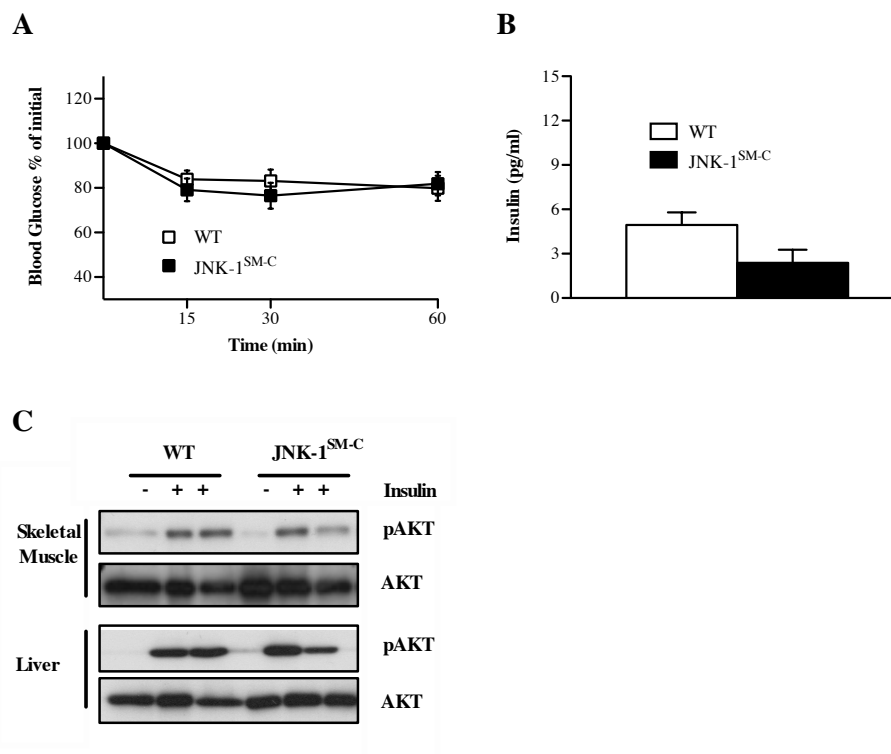


Figure 3.18: Unaltered insulin sensitivity in JNK-1^{SM-C} mice.

(A) Insulin tolerance test of WT and JNK-1^{SM-C} mice were performed at week 12 of age (n=21). (B) Serum insulin concentrations of WT and JNK-1^{SM-C} mice at the age of 17 weeks were determined by ELISA (n=10). (C) Insulin-induced AKT phosphorylation in skeletal muscle (upper panel) and liver (lower panel) of WT and JNK-1^{SM-C} mice determined in western blot analysis with antibodies against phosphorylated AKT and AKT (loading control). Values are means \pm SEM.

These findings suggest that both the local and systemic insulin signaling cascade remains unaffected by a constitutive activation of JNK-1 in skeletal muscle.

3.1.10 Hepatic glucose production of JNK-1^{SM-C} mice

The skeletal muscle is the major tissue responsible for glucose uptake, in particular during contraction (Pedersen, 2011). Thus, glucose metabolism was investigated in JNK-1^{SM-C} mice. Mice lacking JNK-1 in the whole body remain glucose tolerant even when exposed to diet-induced obesity (Hirosumi *et al.*, 2002). To investigate the effect of increased JNK-1 activation in skeletal muscle on glucose homeostasis, a glucose tolerance test was performed in WT and JNK-1^{SM-C} mice. However, constitutive activation of JNK-1 in skeletal muscle appeared to have no impact on glucose metabolism (Fig. 3.19 A), as the ability to respond to glucose challenging was unaltered in JNK-1^{SM-C} mice when compared to WT mice.

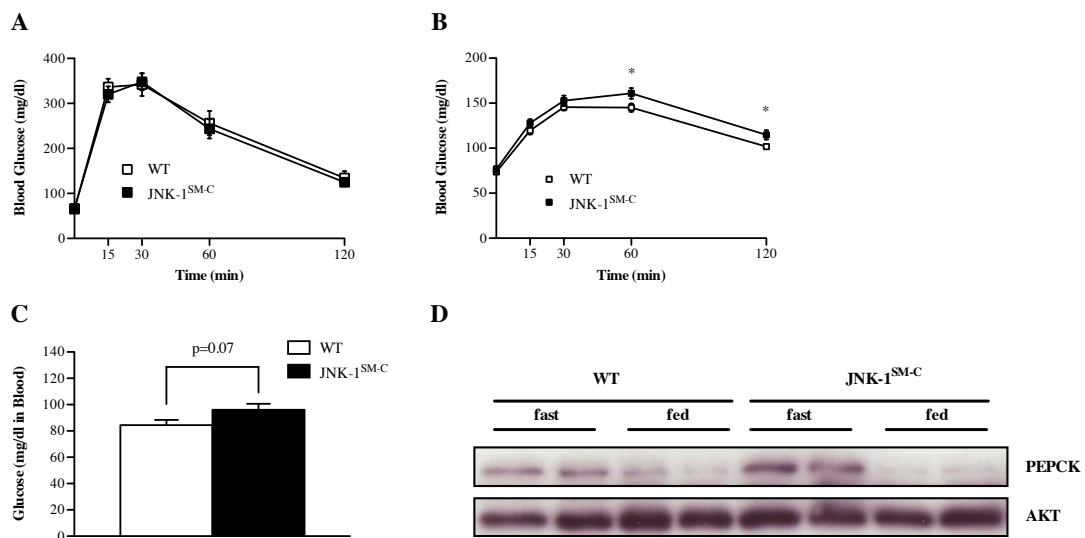


Figure 3.19: Hepatic glucose production in JNK-1^{SM-C} mice.

(A) Glucose tolerance tests of WT and JNK-1^{SM-C} mice were performed at week 11 of age (n=15). (B) Pyruvate tolerance tests of WT and JNK-1^{SM-C} mice were performed at week 13 of age (n=12). (C) Determination of serum glucose concentrations of WT and JNK-1^{SM-C} mice. (D) Western blot analysis of protein lysates from liver tissue of fasted or random fed WT and JNK-1^{SM-C} mice using PEPCK and AKT (loading control) antibodies. Values are means \pm SEM. *, $p \leq 0.05$.

During fasting periods, the liver supplies glucose to maintain stable blood glucose levels by mobilizing glucose from glycogen stores, and in a process in which pyruvate is converted into glucose (Heppner *et al.*, 2010; Unger, 1971). This *in vivo* measurement of the rate of gluconeogenesis determined significantly increased serum concentrations of glucose after 60 and 120 minutes upon a pyruvate challenge in JNK-1^{SM-C} mice indicating an increased rate of hepatic gluconeogenesis (Fig. 3.19 B). Consistent with this observation, fasted serum concentrations of glucose at week 17 of age in JNK-1^{SM-C} mice were

slightly increased when compared to WT mice (Fig. 3.19 C).

Since the rate of hepatic gluconeogenesis is dependent on the rate-limiting enzyme phosphoenolpyruvate carboxykinase (PEPCK) (Harris *et al.* , 2002), the expression of PEPCK was investigated in livers of mice which were either random fed or fasted for 16 hours. In WT mice, expression of hepatic PEPCK protein was increased upon fasting. This fasting-induced increase of PEPCK protein expression was also reflected in livers of JNK-1^{SM-C} mice. Strikingly, comparing fasted hepatic PEPCK protein of WT and JNK^{SM-C} mice revealed that PEPCK expression was elevated in mice which selectively activate JNK-1 signaling in skeletal muscle (Fig. 3.19 D), further underlining the finding of increased hepatic glucose production in JNK-1^{SM-C} mice.

As JNK-1 is constitutively activated in skeletal muscle, it remains unclear which signal implements the crosstalk between skeletal muscle and liver tissue. Moreover, it was shown that PEPCK expression can be induced by IL-6 (Banzet *et al.* , 2009). Consistently, mice with a selective deletion of JNK-1 in adipose tissue exhibit decreased concentrations of circulating IL-6 leading to a decreased hepatic glucose production under obese conditions (Sabio *et al.* , 2008). Thus, the differential expression of IL-6 in skeletal muscle and liver of WT mice was investigated. This analysis showed that skeletal muscle is the main producer of IL-6 upon fasting, and IL-6 mRNA expression in skeletal muscle was strongly increased in fasted mice when compared to IL-6 mRNA expression of random fed mice (Fig. 3.20 A). Upon 16 hours of fasting, mRNA expression in skeletal muscle was more than twofold upregulated when compared to the IL-6 mRNA expression of random fed mice, with no further increase of IL-6 mRNA expression after 24 hours of fasting (Fig. 3.20 A). Interestingly, the strength of IL-6 mRNA elevation upon fasting was attenuated in WT liver tissue, though IL-6 activation was significantly increased after 16 hours of fasting (Fig. 3.20 B).

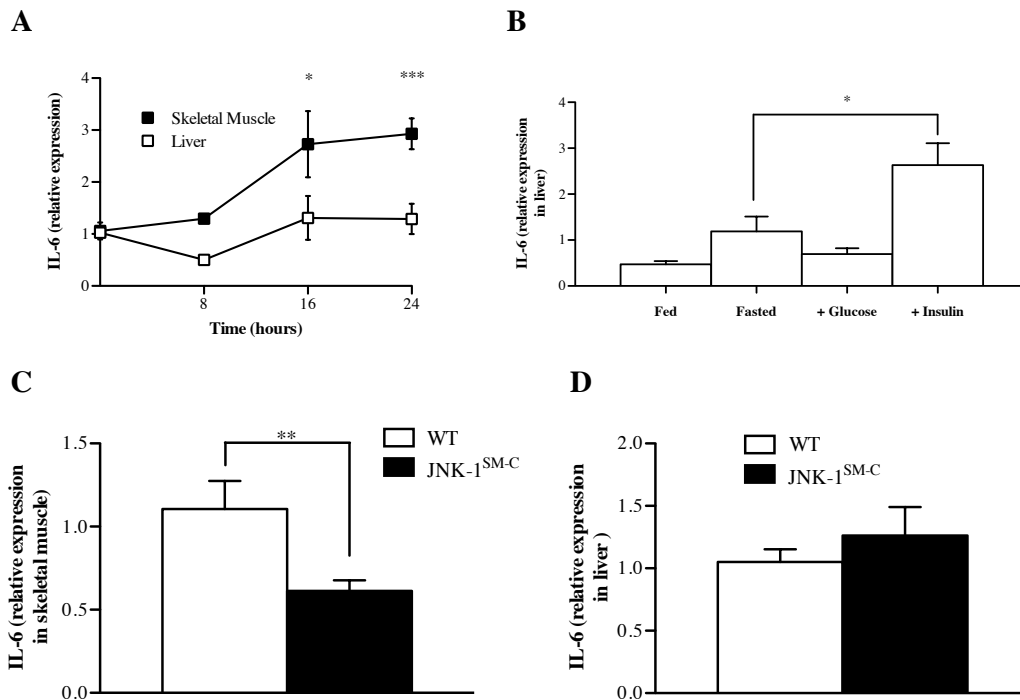


Figure 3.20: IL-6 mRNA expression is increased upon fasting.

(A) Determination of IL-6 mRNA expression in skeletal muscle and liver of WT mice by quantitative realtime PCR analysis (n=6). (B) Determination of IL-6 mRNA expression in liver by quantitative realtime PCR analysis. Mice were either random fed, fasted, fasted and injected with glucose, or fasted and injected with insulin (n=6). (C) Determination of IL-6 mRNA expression in skeletal muscle of WT and JNK-1^{SM-C} mice by quantitative realtime PCR analysis (n=6-10). (D) Determination of IL-6 mRNA expression in liver of WT and JNK-1^{SM-C} mice by quantitative realtime PCR analysis (n=6-10). Values are means \pm SEM. *, $p \leq 0.05$; **, $p \leq 0.01$; ***, $p \leq 0.001$.

To reveal a correlation between the expression of IL-6 mRNA and glucose production, mice were injected with acute doses of glucose or insulin, respectively, directly after fasting. An acute bolus of glucose after fasting, mimicking feeding, almost reduced hepatic IL-6 mRNA levels to that found in random fed mice (Fig. 3.20 B). However, an acute bolus of insulin directly after fasting further elevated the hepatic IL-6 mRNA response to threefold higher levels compared to IL-6 mRNA levels in fed mice (Fig. 3.20 B). Insulin decreases circulating glucose and ipso facto inhibits hepatic glucose production (Granner *et al.*, 1983; Mounier & Posner, 2006). Therefore, an increased IL-6 mRNA expression after acute insulin exposure suggests that IL-6 exhibits a role in inhibiting hepatic glucose production.

To test cell-type specific IL-6 mRNA expression in JNK-1^{SM-C} mice, skeletal muscle and liver were analyzed. While JNK-1^{SM-C} mice comprised an elevated hepatic glucose production, the mRNA expression of IL-6 in skeletal muscle was significantly reduced in

fasted animals when compared to IL-6 mRNA expression in WT mice (Fig. 3.20 C).

To clarify the role of IL-6 in the livers of JNK-1^{SM-C} mice, hepatic IL-6 mRNA expression was examined. This analysis revealed unaltered IL-6 mRNA expression in livers of fasted JNK-1^{SM-C} mice when compared to WT mice (Fig. 3.20 D).

IL-6 was predicted to suppress hepatic glucose production, partly by inhibition of PEPCK expression (Inoue *et al.* , 2006). As hepatic IL-6 mRNA expression was unaltered between the genotypes, other metabolites may be responsible for the increase in hepatic glucose production observed in JNK-1^{SM-C} mice.

Taken together, mice constitutively activating JNK-1 in skeletal muscle displayed an elevated hepatic glucose production. However, the factors which transmit the crosstalk between skeletal muscle and liver and are therefore responsible for this increase in gluconeogenesis remain unknown.

3.1.11 Expression pattern of the JNK isoforms in tissues of WT mice

The JNK protein kinase family consists of three isoforms, JNK-1, JNK-2, and JNK-3, with various splicing variants (Davis, 2000).

As no alterations in the development of obesity-associated insulin resistance in mice lacking JNK-1 in skeletal muscle were found, compensatory effects by other JNK isoforms cannot be excluded.

To determine the cell-type specific expression of all three JNK isoforms quantitative real-time PCR analysis was performed from total RNA of numerous tissues obtained from 8 weeks old WT mice. In this analysis the value of JNK-1 expression was set to 1 and values obtained for JNK-2 and JNK-3 expression were correlated to that. Strikingly, JNK-1 always showed the lowest expression level compared to JNK-2, whereas JNK-3 was only expressed in brain, heart, testis, and pancreas though to a lower extent (Fig. 3.21).

Indeed, JNK-1 and JNK-2 were expressed in all tissues investigated. Interestingly, liver and skeletal muscle tissue exhibited relatively high mRNA expressions of JNK-2 (Fig. 3.21). JNK-1 and JNK-2 perform similar functions as the activation of the transcription factor AP-1 via phosphorylation of its subunit c-Jun (Weston & Davis, 2007), compensatory activities of JNK-2 when JNK-1 is missing can not be ruled out in the experiments presented here.

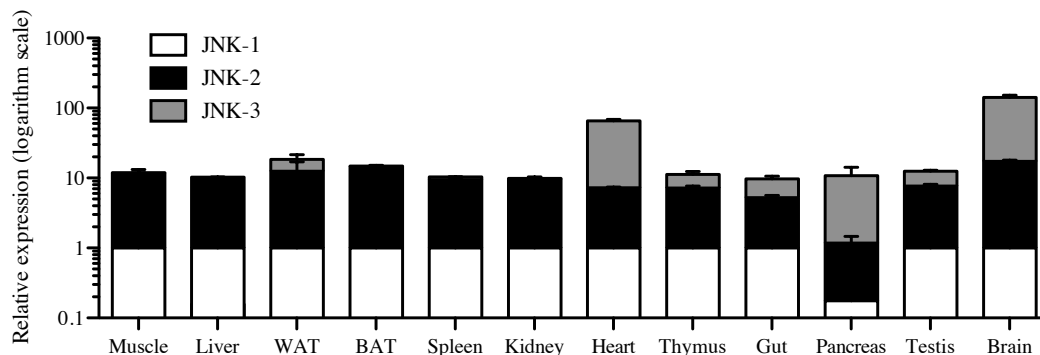


Figure 3.21: Expression pattern of JNK isoforms in tissues of WT mice.

Determination of relative JNK-1, JNK-2, and JNK-3 mRNA expression in indicated organs of 8 weeks old WT mice by quantitative realtime PCR analysis (n=6). Values for JNK-1 expression were set to 1, with exception for pancreatic tissue in which JNK-2 expression was set to 1. Values are means \pm SEM.

Thus, it might be necessary to investigate parameters of energy homeostasis in mice lacking all JNK isoforms in the respective tissues.

3.1.12 Generation of a loxP-flanked JNK-2 allele in mice

Analysis of mice lacking all three JNK isoforms is inevitable, since compensatory activities of other JNK isoforms are feasible. A conditional JNK-3 knockout mouse has already been successfully generated (ref Martin Pal, DA). Here, conditional JNK-2 knockout mice were generated by gene targeting.

For the conditional inactivation of JNK-2, the JNK-2 targeting vector was introduced into the murine genome. Upon homologous recombination into the genome of murine embryonic stem cells, the vector introduces a selection cassette into intron 2 of the JNK-2 gene and flanks exon 3 of the murine JNK-2 gene by two loxP sites (Fig. 3.22 A). The JNK-2 targeting vector also exhibits a FRT-flanked neomycine resistance (neo^R) cassette, which is essential for the positive selection of ES cell clones. After transfection of the pluripotent embryonic stem cells, the neo^R gene enables selection of those ES cell clones, which have stably integrated the JNK-2 construct into their genome. It is essential to excise the neo^R -cassette after establishing of the conditional JNK-2 allele, since the selection gene is transcriptionally active and its expression could interfere with transcription of the JNK-2 gene. Upon Flp-mediated recombination at the FRT sites, the neo^R cassette is excised. Moreover, the JNK-2 targeting vector comprises the diphtheria toxin A gene as negative selection marker. Homologous recombination between the JNK-2 targeting vector and the endogenous JNK-2 allele is mediated by 3.4 kb and 4.6 kb homologous regions on both sides of the loxP-flanked exon 3 of the JNK-2 gene (Fig. 3.22 A).

Loss of exon 3 upon Cre-mediated recombination, and thus, splicing from exon 2 to exon 4 leads to a frameshift which produces a premature STOP-codon within exon 4 leading to a non-functional JNK-2 protein. As a result, JNK-2 is conditionally inactivated in Cre expressing cells.

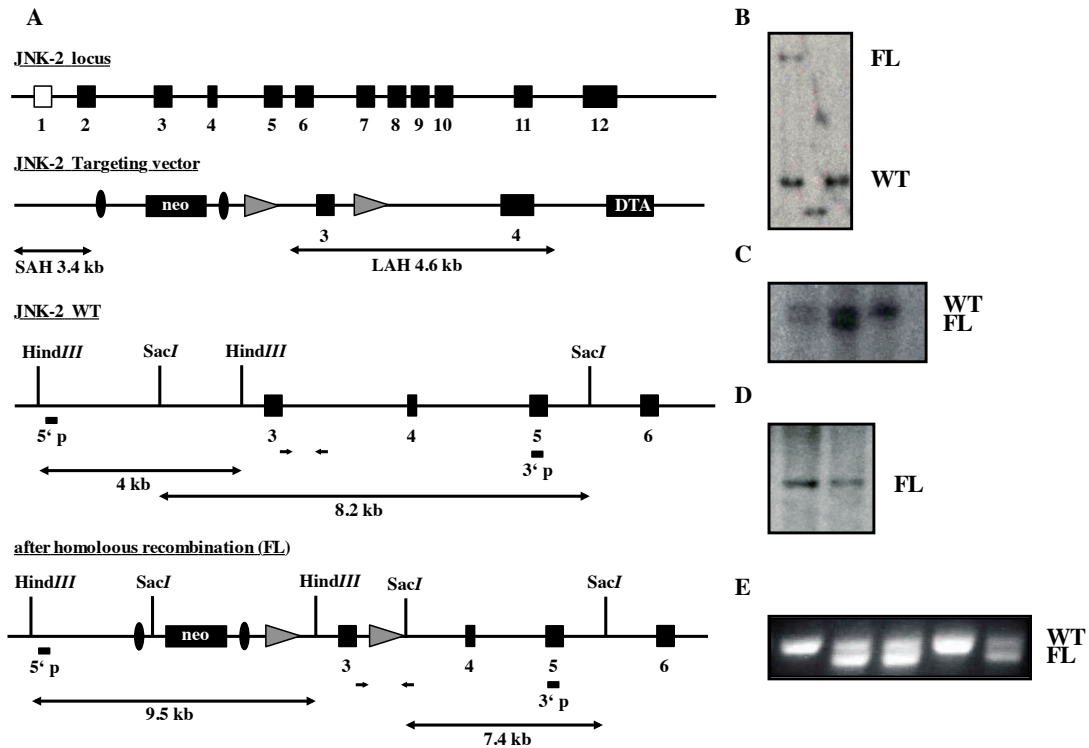


Figure 3.22: Generation of mice with a loxP-flanked allele of the murine JNK-2 gene.

(A) Targeting strategy to generate a conditional JNK-2 allele. The JNK-2 targeting vector exhibits a FRT-flanked (black ovals) neomycin resistance (*neo*) gene and a loxP-flanked (grey triangles) exon 3, and the gene for diphtheria toxin A (DTA), essential for negative selection. 5' short and 3' long arms of homology are indicated. Homologous recombination between the targeting vector and the endogenous JNK-2 allele leads to a homologous recombinant, which exhibits a loxP-flanked exon 3 of the JNK-2 gene. For Southern blot analysis, *HindIII* digest of WT DNA produces a 4 kb fragment using the 5' probe, *SacI* digest of WT DNA results in a 8.2 kb fragment using the 3' probe. *HindIII* digest after homologous recombination results in 9.5 kb fragment using the 5' probe, *SacI* digest produces a 7.4 kb DNA fragment using the 3' probe in Southern blot analysis. (B,C) Identification of homologous recombinants of a conditional JNK-2 allele using the (B) 5' probe after *HindIII* digest and using the (C) 3' probe after *SacI* digest in Southern blot analysis. (D) Confirmation of single integrated homologous recombined JNK-2 ES cell clones using the *neo^R*-probe after *HindIII* digest in Southern blot analysis. (E) Germline transmission for the conditional JNK-2 allele revealed by PCR analysis with the in (A) indicated primers (black arrows).

The incorporation of the JNK-2 targeting vector DNA into the ES cell's genome was determined by Southern Blot analysis. After *HindIII* digest, hybridization with genomic DNA on the membrane led to hybridization signals of 4 kb for the WT allele and of 9.5 kb for the targeted allele using the 5' probe (Fig. 3.22 B). In turn, hybridization of the 3' probe yielded a 8.2 kb long fragment for the WT JNK-2 allele when digested with *SacI*, whereas after successful homologous recombination, hybridization with the 3' JNK-2 probe resulted in a 7.4 kb fragment for the targeted allele (FL) (Fig. 3.22 C). Moreover, hybridization with a radioactive labeled probe for the neomycin resistance cassette, *neo^R*

upon *HindIII* digest, produces a single band at 9.5 kb (Fig.3.22 D), revealing the single integration of the construct into the endogenous JNK-2 locus.

To generate those conditional JNK-2 ES cell clones, 40 μ g of linearised JNK-2 targeting vector were electroporated in Bruce4 ES cells (F Köntgen, 1993), and 23 ES cell clones were identified displaying both, the WT allele as well as the targeted JNK-2 allele. These positive clones were expanded and clones F1 and H6 were injected into CB-20 blastocytes and subsequently implanted into the uterus of pseudo-pregnant foster-mice. 5 chimeras were born with an chimerism higher than 50 % for the ES cell clone F1. These chimeric mice were backcrossed with C57BL/6 mice. Germline transmission of the targeted JNK-2 allele was proven by PCR analysis, which resulted in a 363 bp long DNA fragment for the WT allele and a 335 bp long DNA fragment for the targeted JNK-2 allele when using primers P1 and P2 (Fig. 3.22 E). Mice, positive for the targeted JNK-2 allele were crossed with Flp-Deleter mice (Rodríguez *et al.* , 2000). Flp-mediated recombination led to excision of the neo^R-cassette, which otherwise could interfere with JNK-2 gene expression.

Taken together, these data demonstrate the generation of mice with a conditional JNK-2 allele. Through the generation of the conditional JNK-2 allele, it is possible to exclude compensatory activities between JNK-1 and JNK-2 (and JNK-3). The newly generated JNK-2^{FL} mice were intercrossed with JNK-1^{FL} mice to create conditional double knock-outs of JNK-1 and JNK-2 in the main metabolic target tissues such as brain, liver, skeletal muscle, and WAT. However, since the JNK kinases are also activated during the UPR it is of particular interest to investigate their role in the course of ER stress.

3.2 Central and peripheral induction of ER stress

Obesity increases the demand of cells to produce and mature proteins thereby exposing the endoplasmic reticulum (ER) to a bulk of stress. To cope that high load of stress, the ER initiates the unfolded protein response (UPR) (Ozcan *et al.* , 2004).

A main pathway of the UPR comprises the transmembrane-kinase inositol requiring enzyme 1 (IRE1) and its target X-box binding protein 1 (XBP1). ER stress activates the endoribonuclease activity of IRE1, which subsequently processes mRNA of the XBP1 to produce the active form of XBP1 (XBP1s). XBP1s then triggers a transcriptional cascade to induce chaperones and proteins.

To unravel central and peripheral mechanisms of ER stress, mice were generated carrying an allele for the murine XBP1s (mXBP1s) in their ROSA26 locus.

3.2.1 Targeted insertion of mXBP1s into the murine ROSA26 locus

To introduce the gene for mXBP1s into the murine genome the advantages of the ROSA26 locus were used. The ROSA26 locus was identified in 1991 by Friedrich and Soriano, and is ubiquitously expressed, while its transcripts remain without functional relevance. Due to its easy accessibility by homologous recombination it is widely used to introduce transgenes into the murine genome (Belgardt *et al.* , 2008; Friedrich & Soriano, 1991; Mao *et al.* , 1999; Possemato *et al.* , 2002; Soriano, 1999). In order to integrate the cDNA of mXBP1s into the locus, a targeting vector was created, containing the strong chicken beta-actin promotor (CAGS), a loxP-flanked neo^R/STOP- cassette, cDNA of mXBP1s, and a FRT-flanked internal ribosome entry site (IRES)/eGFP- cassette (SERCA vector) (Fig. 3.23 A) (Belgardt *et al.* , 2008).

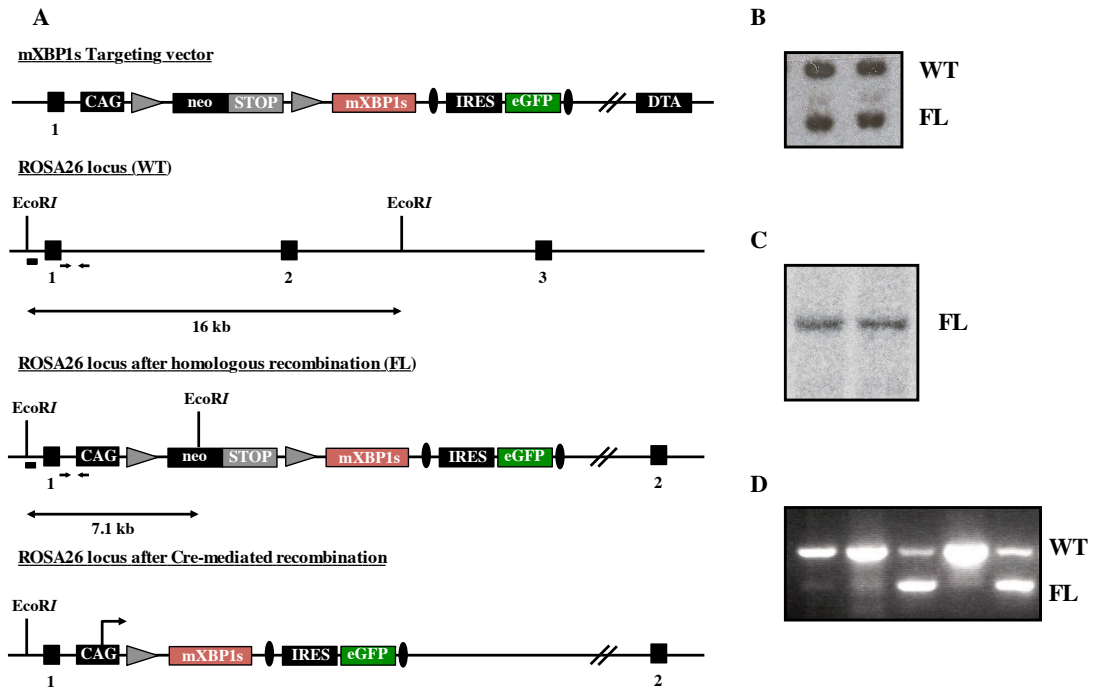


Figure 3.23: Generation of mice with targeted insertion of mXBP1s into the ROSA26 locus.

(A) Targeting strategy for insertion of mXBP1s into the murine ROSA26 locus. Targeting vector containing the strong chicken beta-actin (CAG) promoter, loxP-flanked (grey triangles) *neo*^R/STOP-cassette, mXBP-1 cDNA (colored red), FRT-flanked (black ovals) IRES/eGFP-cassette, and the gene for diphtheria toxin A (DTA) essential for negative selection. Homologous recombination between the mXBP1 targeting vector and the WT ROSA26 locus leads to integration of the mXBP1 targeting vector into the genome. Southern blot analysis using ROSA26 probe leads to DNA fragments of 16 kb for the wild type allele and 7.1 kb for the targeted allele upon *EcoRI* digest. (B) Identification of homologous recombined ES cell clones for the insertion of mXBP1s into the ROSA26 locus by using the ROSA26-probe after *EcoRI* digest in Southern blot analysis. (C) Confirmation of single integrated homologous recombined mXBP1s ES cell clones using the *neo*^R-probe after *EcoRI* digest in Southern blot analysis. (D) Germline transmission for the inserted mXBP1s allele revealed by PCR analysis with the in (A) indicated primers.

The incorporation of the targeting vector DNA into the genome after transfection in ES cells was determined by Southern blot analysis of genomic DNA from the isolated ES cell clones. For this, 10^7 Bruce4-ES cells were transfected with 40 μ g linearized mXBP1s targeting vector and subsequently selected with G418 containing medium. Eight days after transfection 96 colonies were isolated as single clones and screened via Southern blot analysis. Hybridization of the radioactively labeled ROSA26 probe (Mao *et al.*, 1999) with the *EcoRI* digested ES cell clone DNA resulted in a 16 kb long DNA fragment for the endogenous WT ROSA26 allele. After successful recombination of the mXBP1s targeting vector DNA into the ES cell's genome, hybridization with the ROSA26 probe led to an additional fragment of 7.1 kb in size with the same signal intensity (Fig. 3.23 B). 44 positive clones, carrying both the WT and the mXBP1s allele were identified. A radioactive

labeled neo^R probe was used to check for single integration of the construct by recognizing the neomycine resistance cassette. Hybridization with this radioactively labeled neo^R probe results in a single band at 7.1 kb (Fig. 3.23 C).

Among these 44 positive clones, clone A10 was injected into blastocytes and implanted into the uterus of pseudo-pregnant foster-mice. Chimeras with the highest degree of chimerism were chosen for backcross with C57BL/6 mice. Germline transmission of black offspring was revealed by PCR analysis of genomic tail DNA. For this, primers were used which bind to sequences within the CAGS-promotor and the ROSA26 locus. Using these primers resulted in a 570 bp DNA fragment for the WT allele whereas a 380 bp long fragment is amplified when the ROSA26 locus was successfully targeted. Indeed from the first offspring 2 littermates carried the additional 380 bp band that were subsequently used to establish the ROSA-mXBP1s mouse line (Fig. 3.23 D).

Taken together, transgenic mice, which exhibit a Cre inducible mXBP1s allele, were generated. These generated ROSA-mXBP1s mice will help to gain insights into the mechanisms of the development of ER stress. As brain and liver represent major metabolic targets for obesity-induced ER stress (Ozcan *et al.* , 2004), the newly generated ROSA-mXBP1s mice were used to assess the impact of brain- or liver specific induction of ER stress on mouse physiology.

3.2.2 Hippocampal expression of mXBP1s results in increased expression of central and hepatic ER stress markers

The brain is a central regulator of energy homeostasis and ER stress in the brain is increased during the course of metabolic disorders (Ozcan *et al.* , 2009; Zhang *et al.* , 2008). To elucidate whether brain-derived ER stress also transmits to peripheral organs, the newly generated ROSA-mXBP1s mice were crossed with two different Cre mouse lines, which express the Cre recombinase either under the control of the promotor for the α -subunit of calcium- calmodulin dependent protein kinase II (CAMKII-Cre, (Casanova *et al.* , 2001)), or under the control of the albumin promotor constituted with the α -fetoprotein enhancer (ALFP-Cre, (Kellendonk *et al.* , 2000)) (Fig. 3.24). While expression of the CAMKII-Cre in mice starts shortly after birth and reaches it maximum at 6 to 8 weeks of age (Casanova *et al.* , 2001), expression of the albumin gene starts early dur-

ing embryogenesis (Kellendonk *et al.*, 2000). CAMKII-Cre-mediated recombination of the loxP-flanked neo^R/STOP- cassette should result in mXBP1s expression in the brain (mXBP1s^{CAMKII}). Strongest expression of the CAMKII-Cre was observed in hippocampus (Casanova *et al.*, 2001), therefore experiments presented here concentrated on Cre-mediated recombination in the hippocampus. Recombination by the ALFP-Cre is only occurring in liver parenchymal cells (Kellendonk *et al.*, 2000) (mXBP1s^{ALFP}).

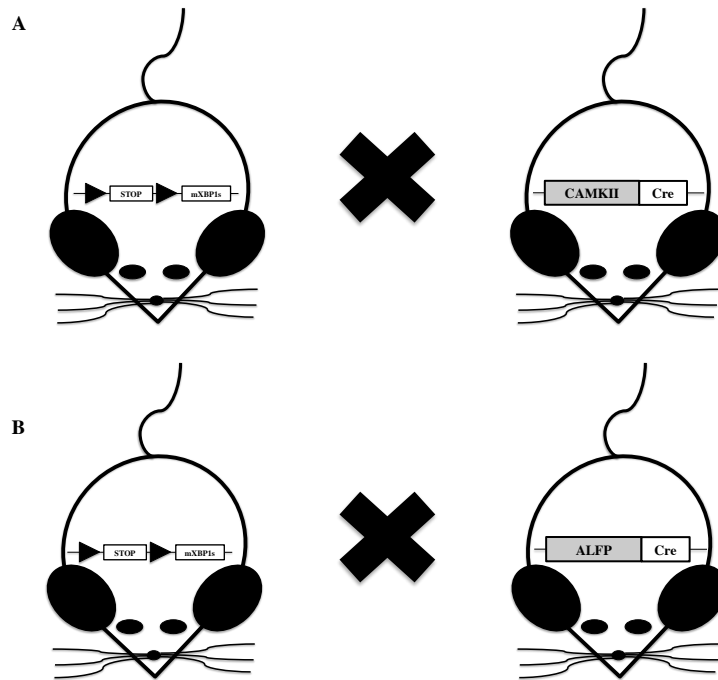


Figure 3.24: General scheme of mice with a selective overexpression of mXBP1s in hippocampus (mXBP1s^{CamKII}) and liver (mXBP1s^{Alfp}).

(A) Mice, harbouring the mXBP1s allele were crossed with mice expressing Cre from the promoter of CAMKII- α to induce mXBP1s overexpression in the brain (mXBP1s^{CamKII}) (B) Mice, harbouring the mXBP1s allele were crossed with mice expressing Cre from the ALFP promoter to induce mXBP1s overexpression selectively in hepatocytes (mXBP1s^{Alfp}).

While mice carrying both the ROSA-mXBP1s allele as well as the respective Cre allele (mXBP1s^{CamKII}, mXBP1s^{Alfp}) were used for analysis, mice carrying only the mXBP1s allele served as wild type control animals (WT). First, the functionality of the newly generated mXBP1s mouse was tested. To this end, total RNA isolated from the hippocampus of WT mice, mXBP1s^{CamKII} mice, and mXBP1s^{Alfp} mice was isolated and quantitative realtime analysis was performed. Hippocampi of mXBP1s^{CamKII} mice exhibited significantly increased mRNA expression of XBP1s and XBP1u in mXBP1s^{CamKII} mice when compared to WT or mXBP1s^{Alfp} mice, revealing that the mXBP1s construct is overexpressed from the ROSA26 locus in the hippocampus of mXBP1s^{CamKII} mice (Fig. 3.25 A +

B). However, also a significant increase in XBP1u mRNA in hippocampus of mXBP1s^{Alfp} mice was observed.

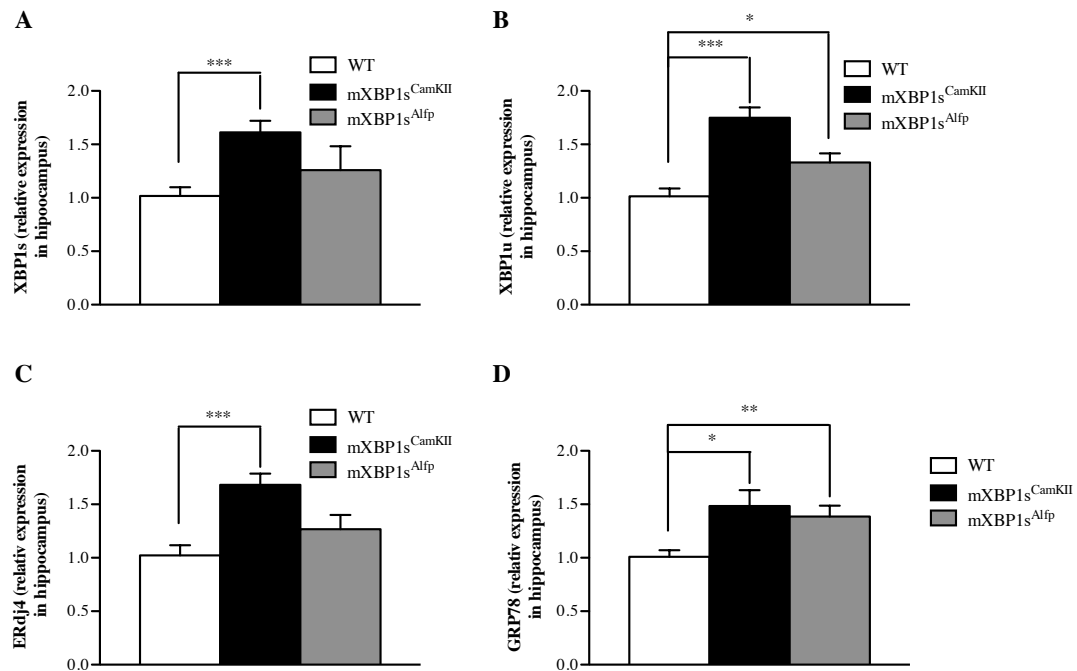


Figure 3.25: XBP1s is overexpressed in hippocampi of mXBP1s^{CamKII} mice. Determination of XBP-1s (A), and XBP-1u (B), and ERdj4 (C), and GRP78 (D) mRNA concentrations in hippocampus of WT, mXBP1s^{CamKII}, and mXBP1s^{Alfp} mice by quantitative realtime PCR analysis (n=5-8). Values are means \pm SEM. *, $p \leq 0.05$; **, $p \leq 0.01$; ***, $p \leq 0.001$

Consistent with elevated levels of XBP-1 mRNA was also a significant increased mRNA expression of the XBP-1 target gene ER-BiP co-factor, ERDJ4, in hippocampus of mXBP1s^{CamKII} mice, whereas the hippocampal expression of ERDJ4 in mXBP1s^{Alfp} remained unaltered (Fig. 3.25 C). Moreover, increased markers of ER stress in hippocampi of mXBP1s^{CamKII} mice could also mediated by the PERK-eIF2 α pathway, as indicated by significant elevated mRNA expression of the molecular chaperone GRP78 in mXBP1s^{CamKII} and mXBP1s^{Alfp} mice (Fig. 3.25 D).

Similar results were observed in livers of mXBP1s^{Alfp} mice when crossing ROSA-mXBP1s mice to ALFP-Cre mice. Indeed, mXBP1s^{Alfp} mice exhibited a significant increased expression of hepatic XBP1s and XBP1u mRNA (Fig. 3.26 A + B). Consistently, this increase was confirmed on protein level by Western blot analysis. Expression of

XBP1s protein (50 kDa) was highly elevated in the liver of mXBP1s^{Alfp} mice, when compared to hepatic XBP1s protein expression in WT or mXBP1s^{CamKII} mice. Hepatic XBP1s expression of the latter was slightly decreased (Fig. 3.26 B + C). Consistent with elevated XBP1 levels in the liver of mXBP1s^{Alfp} mice, also the XBP1 target gene ERdj4 showed a significant increased mRNA expression, whereas ERdj4 expression in the liver of mXBP1s^{CamKII} mice remained unaltered (Fig. 3.26 D).

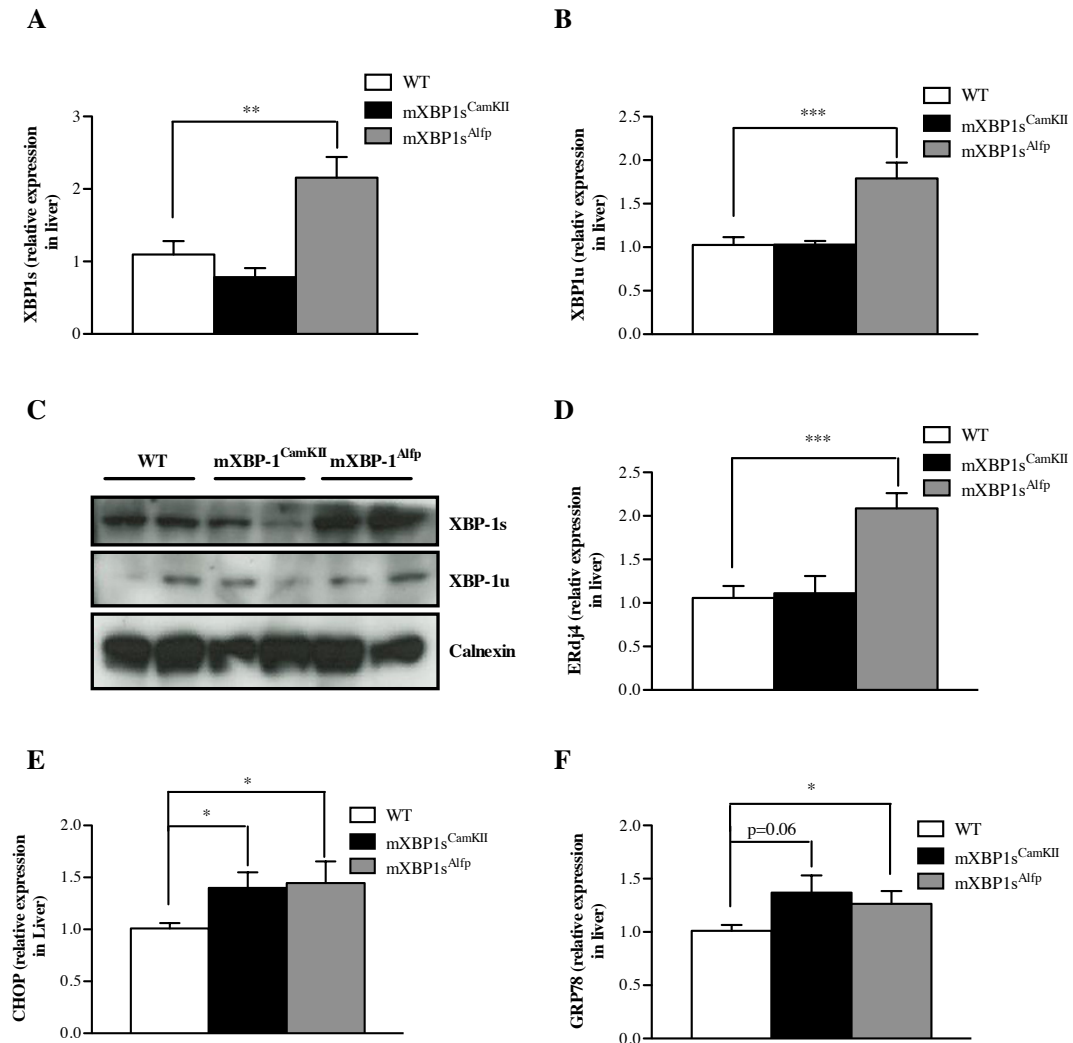


Figure 3.26: XBP1s is overexpressed in livers of mXBP1s^{Alfp} mice.

Determination of XBP-1s (A), and XBP-1u (B), ERdj4 (D), CHOP (E), GRP-78 (F) mRNA concentrations in liver tissue of WT, mXBP1s^{CamKII}, and mXBP1s^{Alfp} mice by quantitative real-time PCR analysis (n=5-8). (C) Western Blot analysis of protein lysates from liver tissue of WT, mXBP1s^{CamKII}, and mXBP1s^{Alfp} mice using XBP1 and Calnexin (loading control) antibodies. Values are means \pm SEM. **, p \leq 0.01; ***, p \leq 0.001.

Taken together, these data demonstrate, that mXBP1s is selectively overexpressed in either hippocampal regions or hepatocytes in mXBP1s^{CamKII} and mXBP1s^{Alfp} mice, respec-

tively. Moreover, the expression of mXBP1s leads to the induction of ER stress in the respective tissues.

To elucidate whether genetically induced ER stress through mXBP1s expression in hippocampal neurons leads to ER stress in peripheral tissues, ER stress markers in skeletal muscle and liver were determined. In skeletal muscle, the expression of the ER stress markers XBP1, CHOP, GRP78, and ATF6 (not shown) were unaltered in mXBP1s^{CamKII} and mXBP1s^{Alfp} mice when compared to WT mice (Fig. 3.27). Surprisingly, expression of transcriptionally active XBP1s in the brain of mXBP1s^{CamKII} mice resulted in significant activation of hepatic C/EBP homologous protein (CHOP) (Fig. 3.26 E), which triggers apoptotic events in UPR responses (Hotamisligil, 2010). Additionally, increased mRNA expression of the molecular chaperone GRP78 was observed (Fig. 3.26 F), although the values for GRP78 in the livers of mXBP1s^{CamKII} mice did not reach statistical significance when compared to WT mice.

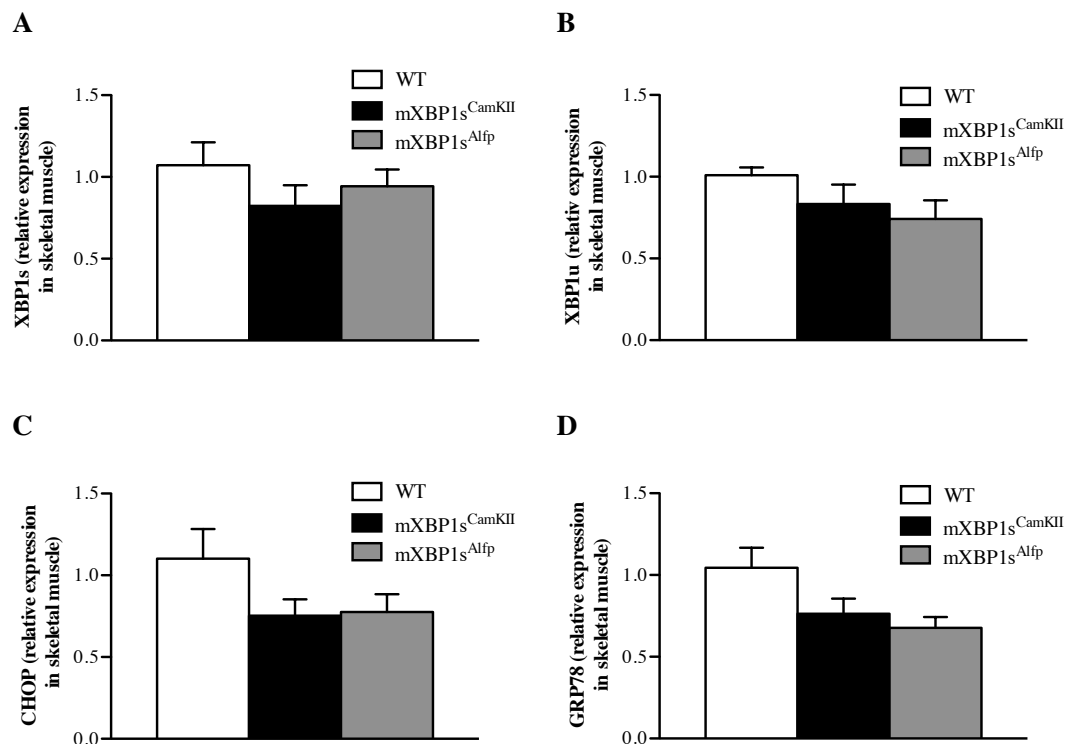


Figure 3.27: Expression of ER stress markers in skeletal muscle of mXBP1s^{CamKII} and mXBP1s^{Alfp} mice.

(A-D) Determination of XBP-1s (A), and XBP-1u (B), and CHOP (C), and GRP78 (D) mRNA concentrations in skeletal muscle of WT, mXBP1s^{CamKII}, and mXBP1s^{Alfp} mice by quantitative real-time PCR analysis (n=5-8). Values are means \pm SEM.

Taken together, these data demonstrate that central induction of ER stress by overexpression of the transcriptionally active mXBP1s might contribute to peripheral ER stress in liver tissue as determined by quantitative realtime PCR analysis.

In this thesis, ER stress was assessed in brain and liver, however it is also of intriguing interest to determine the role of obesity-induced ER stress in the adipose tissue.

3.3 Characterization of a novel adipose tissue specific Cre recombinase mouse line

The adipose tissue plays a key role in metabolism. Besides its function as an endocrine organ releasing adipokines, it also stores excessive lipids and thereby constitutes the origin of obesity (Ferris & Crowther, 2011). Thus, mouse knockout models as well as gain of function approaches using the Cre/loxP- system are crucial to gain novel insights into the mechanism of adipose tissue metabolism.

In order to generate a Cre mouse line, that is selectively active in adipose tissue derived cells, the expression of Cre has to be placed under the control of an adipose tissue specific promotor. The promotor sequences of the fatty acid binding protein 4 (FABP4), also termed adipocyte protein 2 (AP2), have been identified (Ross *et al.* , 1990), and, since it is mainly expressed in differentiated adipocytes and functions as a fatty acid chaperone (Hunt *et al.* , 1986), it is an appropriate candidate for the purpose to generate a novel adipose tissue specific Cre mouse strain.

Here, a transgenic mouse line which express Cre specifically in FABP4-expressing cells was generated by targeted knock-in of the cDNA for Cre recombinase into the endogenous FABP4 locus and by applying the properties of the virus-derived 2A-peptide. The 2A-peptide was initially discovered in the foot-and-mouth disease virus and exhibits proteolytic activity (de Felipe, 2004). In this thesis it was used to preserve the endogenous gene expression, through its ability to cleave itself after translation.

To this end, a fusion protein of FABP4, 2A-peptide, and Cre was generated by replacing the endogenous STOP-codon of FABP4 for the 2A- peptide and Cre sequences (Hees, n.d.), which leads to expression of FABP4 and Cre in a 1:1 stoichiometry from one mRNA molecule after C-terminal cleavage of the viral 2A-peptide chain (Fig. 3.28).

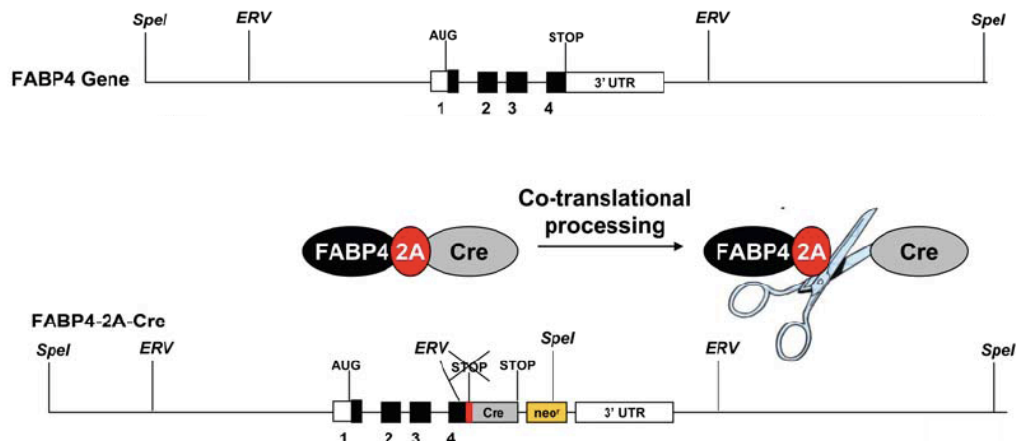


Figure 3.28: The 2A- technology allows equivalent expression of FABP4 and Cre.

The cDNA of 2A-peptide and Cre was inserted into the FABP4 gene by replacing the endogenous STOP-codon in exon 4. A neo^R-cassette was inserted for negative selection of ES cell clones. Co-translational processing by the 2A-peptide allows expression of both, FABP4 and Cre. (adapted from (Hees, n.d.))

To characterize this novel Cre mouse line, FABP4-2A-Cre mice were crossed with 2 established independent mouse models containing loxP-flanked target sequences. In a first approach FABP4-2A-Cre mice were crossed with mice expressing a dominant-negative form of FOXO1 upon Cre-mediated recombination (FOXODN, (Belgardt *et al.*, 2008)). Secondly, FABP4-2A-Cre mice were crossed with mice exhibiting a loxP-flanked allele of IL-6R α gene (IL-6R α ^{FL}, (Wunderlich *et al.*, 2010)).

3.3.1 FABP-4-2A-Cre-mediated recombination in FOXODN^{FABP4} mice

To characterize the newly generated FABP4-2A-Cre mice, animals were crossed with ROSA-FOXODN mice (Belgardt *et al.*, 2008) to obtain FOXODN^{FABP4} mice (Fig. 3.29). Cre-mediated recombination of the loxP-flanked neo^R/STOP-cassette leads to the compound expression of FOXODN and eGFP that can be visualized by FACS or immunohistochemistry analysis.

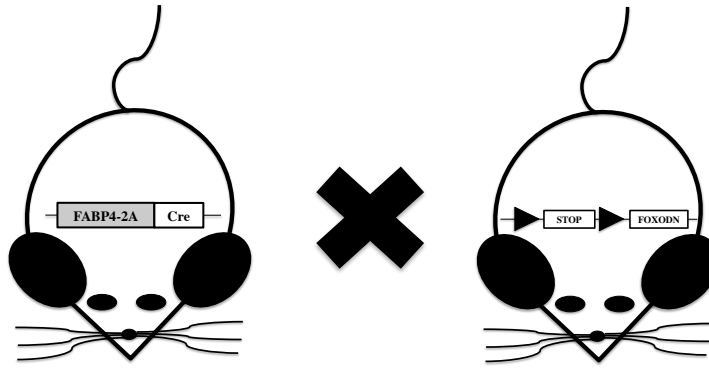


Figure 3.29: Schematic view of crossing FABP4-2A-Cre mice to FOXODN mice to obtain FOXODN^{FABP4} mice.

Mice, heterozygous for FABP4-2A-Cre were crossed with mice homozygously expressing a targeted FOXODN allele, which resulted in the generation of FOXODN^{FABP4} mice.

Moreover, the targeted insertion of the FOXODN construct into the ROSA26 locus allows for examining the FABP4-2A-Cre-mediated excision efficiency by Southern blot analysis (Fig. 3.30 A). For this, hybridization of EcoRV digested genomic DNA with the ROSA26-probe leads to DNA fragments of 11.5 kb for the WT allele, 11.1 kb for the targeted allele (FL), and of 8.8 kb (Δ) when the allele is deleted by Cre-mediated recombination.

To examine FABP4-2A-Cre-mediated recombination of the loxP-flanked neo^R/STOP-cassette by the FABP4-2A-Cre, Southern blot analysis using genomic DNA isolated from numerous organs was performed. Deletion of the loxP-flanked STOP-cassette was detected in adipocytes, WAT, and BAT of FOXODN^{FABP4} mice but not in WT mice (Fig. 3.30 B). In order to investigate the specificity of FABP4-2A-Cre, skeletal muscle, brain and WAT were also monitored. Strikingly, recombination of the loxP-flanked allele was only present in WAT of FOXODN^{FABP4} mice (Fig. 3.30 C), but not in skeletal muscle and brain of these mice (Fig. 3.30 C).

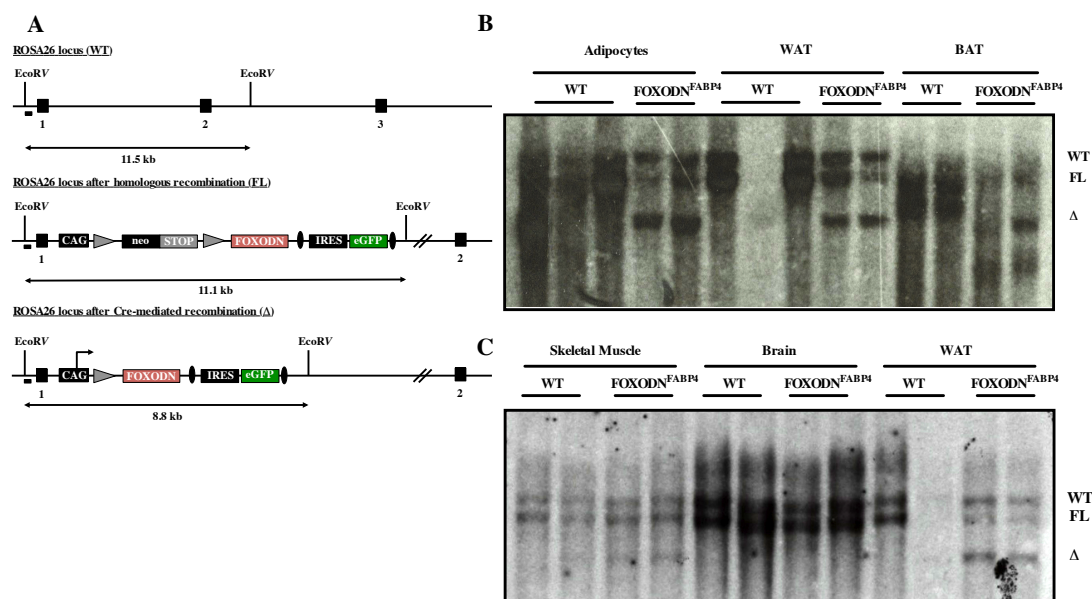


Figure 3.30: FABP4-2A-Cre-mediated recombination in FOXODN^{FABP4}-Cre mice.

(A) Strategy to detect Cre-mediated recombination in FOXODN^{FABP4} mice. Hybridization of EcoRV digested genomic DNA with the ROSA26 probe results in DNA fragments of 11.5 kb (WT), 11.1 kb (FL), and 8.8 kb (Δ). (B) Southern Blot analysis of genomic DNA isolated from adipocytes, WAT, and BAT of WT and FOXODN^{FABP4} mice using the in (A) mentioned strategy. (C) Southern Blot analysis of genomic DNA isolated from liver, skeletal muscle, brain, and WAT of WT and FOXODN^{FABP4} mice resulted in the in (A) mentioned DNA fragments.

Next, FABP4-2A-Cre-mediated recombination was further investigated by the extent of eGFP expression using immunohistochemistry analysis. Since eGFP is expressed upon Cre-mediated recombination, eGFP detection is an appropriate indicator for Cre activity. This analysis revealed a specific deletion of the loxP-flanked neo^R/STOP-cassette and thereby eGFP expression in WAT of FOXODN^{FABP4} mice but not in WAT of WT mice (Fig. 3.31 A, upper panels). Similarly, investigating eGFP expression in BAT revealed IRES driven eGFP expression in BAT of FOXODN^{FABP4} mice but not in BAT of WT mice (Fig. 3.31 A, lower panels).

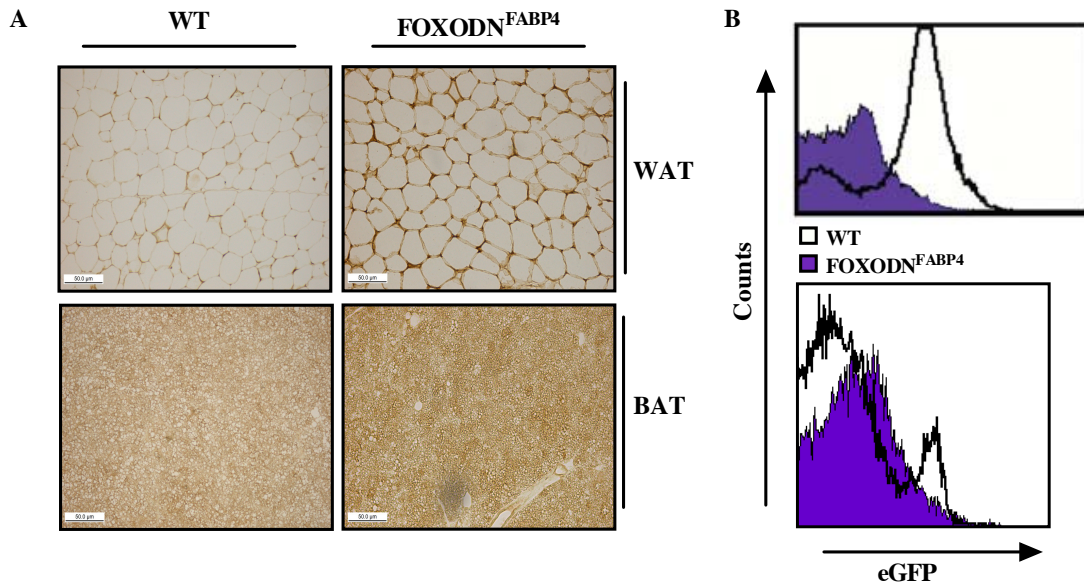


Figure 3.31: GFP expression in adipose tissue and macrophages of FOXODN^{FABP4} mice. (A) Immunohistochemistry analysis using anti-GFP antibodies was performed with WAT and BAT from WT and FOXODN^{FABP4} mice. (B) FACS analysis to reveal GFP fluorescence was performed with primary peritoneal macrophages (upper panel) and Kupffer Cells (lower panel) from WT and FOXODN^{FABP4} mice.

The recombination event in FOXODN^{FABP4} mice was additionally investigated in primary peritoneal macrophages and liver resident Kupffer cells, since the expression of FABP4 is not restricted to adipose tissue alone (Makowski *et al.*, 2001). FACS analysis revealed a 95 % deletion of the loxP- flanked STOP-cassette in primary peritoneal macrophages of FOXODN^{FABP4} mice, indicated by GFP fluorescence (Fig. 3.31 B, upper panel). Consistent with an almost complete recombination in peritoneal macrophages, also in Kupffer cells of FOXODN^{FABP4} mice, GFP fluorescence was detectable. However, the recombination efficiency, indicated by the amount of GFP fluorescence, was verified in only 15 % of the Kupffer cells in FOXODN^{FABP4} mice (Fig. 3.31 B, lower panel). Taken together, a transgenic mouse was characterized expressing the Cre recombinase under the control of the FABP4 promoter. It was shown that the FABP4-2A-Cre is functional and its activity reflects the expression pattern of FABP4.

3.3.2 FABP4-2A-Cre-mediated recombination in $IL-6R\alpha^{FABP4}$ mice

Recombination by the newly generated FABP4-2A-Cre mouse and its specificity was demonstrated using the FOXODN mouse mutant.

To confirm these findings, recombination of FABP4-2A-Cre mice was also investigated in a different control mouse line. JNK-1 was shown to be required for exercise-induced IL-6 activation. Here, Cre-mediated recombination would selectively inactivate one allele of the $IL-6R\alpha$ gene. To this end, FABP4-2A-Cre mice were crossed with mice exhibiting loxP-flanked alleles of the $IL-6R\alpha$ gene ($IL-6R\alpha^{FL/FL}$, (Wunderlich *et al.*, 2010)) to obtain $IL-6R\alpha^{FABP4}$ mice (Fig. 3.32).

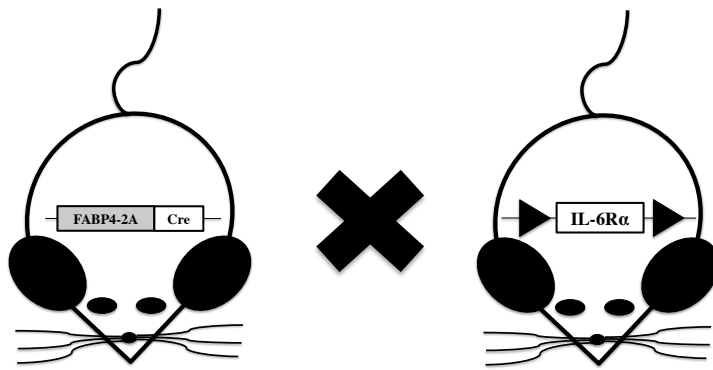


Figure 3.32: Schematic view of crossing FABP4-2A-Cre mice to $IL-6R\alpha^{FL/FL}$ mice to obtain $IL-6R\alpha^{FABP4}$ mice.

Mice, heterozygous for FABP4-2A-Cre were crossed with mice homozygous for a loxP-flanked $IL-6R\alpha$ gene, which served as a control to test the functionality of the newly generated FABP4-2A-Cre.

Efficient deletion of the loxP-flanked exons 2 and 3 and thereby the activity of the newly generated Cre was proven in Southern blot analysis. Hybridization of *Bgl*I digested genomic DNA with the $IL-6R$ probe leads to DNA fragments of 11.5 kb for the WT allele, 11.1 kb for the targeted allele (FL) and of 6.3 kb for the deleted allele by Cre-mediated recombination (Fig. 3.33 A).

FABP4-2A-Cre-mediated recombination was observed in WAT and BAT of $IL-6R\alpha^{FABP4}$ mice but not in WT mice (Fig. 3.33 B). In addition, Cre-mediated recombination was not detected in liver, skeletal muscle, spleen, and brain of WT mice. However, in $IL-6R\alpha^{FABP4}$ mice, deletion of the loxP-flanked STOP-cassette was also observed in liver, skeletal muscle, spleen, and brain, indicating that the activity of FABP4-2A-Cre in $IL-6R\alpha^{FABP4}$ mice is not restricted to adipose tissue (Fig. 3.33 B).

As the Cre was inherited by the mother in case of $\text{FOXODN}^{\text{FABP4}}$, but was inherited by the father in $\text{IL-6R}\alpha^{\text{FABP4}}$ mice, it is possible that recombination by FABP4-2A-Cre underlies gender-specific effects as it was shown for Keratin-14 Cre mice, in which loxP-flanked sequences were completely deleted in all tissues when the Cre allele was inherited by the mother (Hafner *et al.*, 2004).

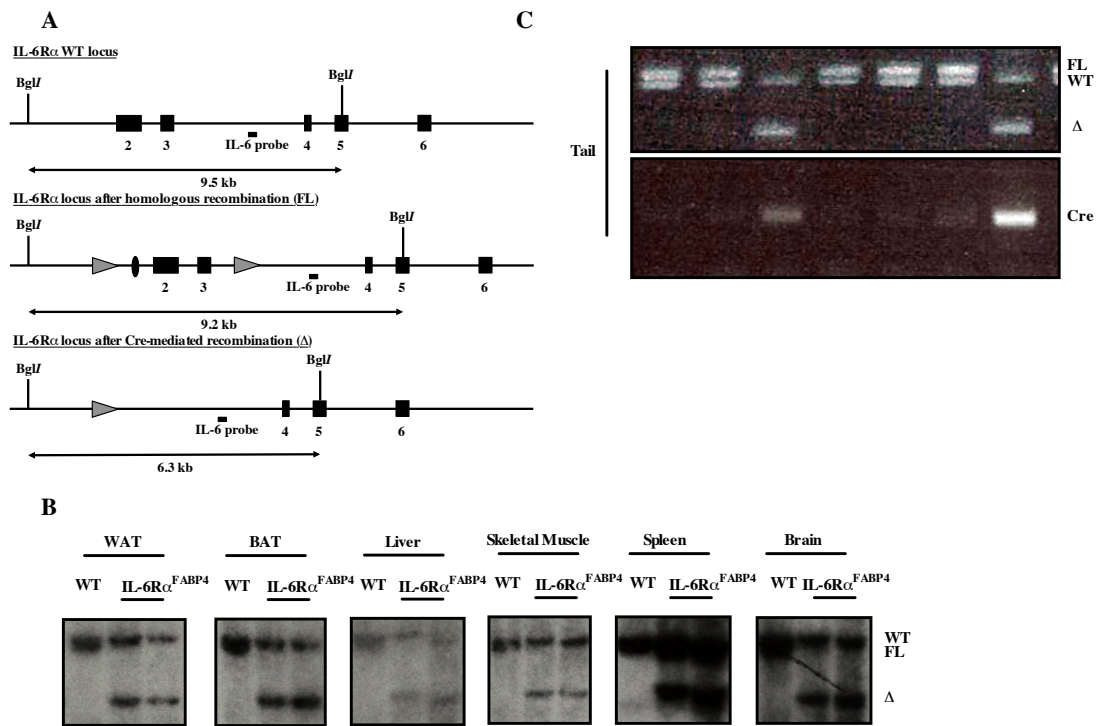


Figure 3.33: FABP4-2A-Cre-mediated recombination in $\text{IL-6R}\alpha^{\text{FABP4}}$ mice.

(A) Strategy to detect Cre-mediated recombination in $\text{IL-6R}\alpha^{\text{FABP4}}$ mice. Hybridization of BglI digested genomic DNA with the IL6R probe results in DNA fragments of 11.5 kb (WT), 11.1 kb (FL), and 6.3 kb (Δ). (B) Southern Blot analysis of genomic DNA isolated from WAT, BAT, liver, skeletal muscle, spleen, brain, and tail of WT and $\text{IL-6R}\alpha^{\text{FABP4}}$ mice using the in (A) mentioned strategy. Mice are male and female, Cre recombinase was inherited by the father. Note that the fragment size for WT and FL alleles is almost similar. (C) PCR analysis of genomic DNA isolated from tail of WT and $\text{IL-6R}\alpha^{\text{FABP4}}$ mice using primers to detect recombined alleles of the $\text{IL-6R}\alpha$ gene and the appearance of Cre, respectively. PCR analysis lead to DNA fragments of 630 bp (WT), 600 bp (targeted allele, FL), and 450 bp (deleted allele, Δ). Mice are male and female, Cre recombinase was inherited by the mother.

To unravel such gender-specific effects, $\text{IL-6R}\alpha^{\text{FABP4}}$ mice were generated, in which the FABP-4-2A-Cre was inherited by the mother. However, PCR analysis from genomic tail DNA revealed that FABP4-2A-Cre activity leads to deletion of the exons 2 and 3 of the $\text{IL-6R}\alpha$ gene in tail tissue (Fig. 3.33 C). The $\text{IL-6R}\alpha$ deletion band is only detectable in those mice, co-expressing the gene for the FABP4-2A-Cre (Fig. 3.33 C). This indicates that FABP4-2A-Cre activity leads to recombination of the $\text{IL-6R}\alpha$ gene in all tissues and

confirms the results obtained from Southern Blot analysis.

Taken together, a transgenic mouse line was characterized expressing the Cre recombinase under the control of the FABP4 promoter. Furthermore, the expression of Cre is similar to endogenous gene expression of FABP4. Thus, the newly generated FABP4-2A-Cre is a useful addition to the pool of tools for genetic loss or gain of function studies in myeloid cells and adipose tissue and selectively in adipose tissue after replacing bone marrow derived cells by WT myeloid cells. However, caution is needed when investigating FABP4-2A-Cre-mediated recombination in specific loci, such as the *IL-6R α* gene.

4 Discussion

Body weight gain and on a longer time scale obesity result from positively shifting the equilibrium between energy consumption and energy expenditure. Strikingly, obesity presents the basis for the development of several metabolic disorders, including insulin resistance and type 2 diabetes, and in cooperation with physical inactivity obesity is one of the main causes for premature death.

To develop therapeutical strategies to combat the obesity pandemic it is crucial to gain mechanistical insights into the molecular regulation of energy homeostasis and its underlying signaling pathways.

The finding that obesity is accompanied with an increased inflammatory tone (Hotamisligil *et al.* , 1993) has set the ground to unravel the signaling pathways contributing to the development of obesity-associated insulin resistance. The stress-sensitive kinase JNK was shown to negatively interfere with insulin signaling via inhibitory serine phosphorylation of IRS, and thereby blocking downstream insulin signaling (Aguirre *et al.* , 2000). Moreover, obesity-induced ER stress contributes to the activation of JNK, an effect which is aggravated by the release of pro-inflammatory cytokines, such as TNF- α or IL-6 into the circulation.

To directly address the role of skeletal muscle-derived JNK-1 in the regulation of insulin signaling, JNK-1 was conditionally ablated in the skeletal muscle and animals were analyzed in terms of energy and glucose homeostasis.

4.1 Role of skeletal muscle specific JNK-1 in metabolic regulation

4.1.1 Inactivation of the JNK-1 gene specifically in skeletal muscle

The JNK protein family comprises three members, namely JNK-1, JNK-2, and JNK-3 (Davis, 2000). While the metabolic role of JNK-2 and JNK-3 remain to be elucidated, the JNK-1 protein isoform was found to possess a central role in the regulation of obesity-associated insulin resistance (Hirosumi *et al.* , 2002). Previous experiments revealed that

conventional JNK-1 knockout mice (JNK-1 Δ) exhibit decreased body weight gain in diet-induced obesity and concomitantly display strongly improved glucose tolerance and insulin sensitivity. However due to the nature of the JNK-1 construct used in this study, the authors were unable to address the metabolic tissue in which the activity of JNK-1 is contributing to the development of obesity-associated insulin resistance.

Here, mice were generated with a conditional inactivation of the JNK-1 gene in skeletal muscle (JNK-1^{SM-KO} mice). A conditional disruption of loxP-flanked allele in the skeletal muscle was first described in 1998 by using a mouse line expressing the Cre recombinase from the promoter of muscle creatine kinase (MCK) (Brüning *et al.*, 1998). The expression of MCK is restricted to skeletal muscle and heart and the maximum of expression is achieved ten days after birth (Brüning *et al.*, 1998). MCK-Cre-mediated recombination of the loxP-flanked exon 2 of the JNK-1 gene results in the total absence of JNK-1 protein in skeletal muscle of JNK-1^{SM-KO} mice, whereas JNK-1 expression in the liver of JNK-1^{SM-KO} mice was comparable to WT mice. Moreover, JNK-1^{SM-KO} mice were vital and displayed no apparent abnormalities compared to WT mice. Taken together, mice with a skeletal muscle specific deficiency of JNK-1 represent a reliable model to analyze the role of JNK-1 in this tissue *in vivo*.

4.1.2 Role of skeletal muscle specific JNK-1 in the regulation of energy and glucose homeostasis

Obesity leads to JNK activation in numerous metabolic tissues (Hirosumi *et al.*, 2002). Importantly, JNK activity increased in skeletal muscle of WT mice after 17 weeks of HFD-feeding that furthermore resulted in obesity and increased adiposity of WT mice, which was accompanied by increased circulating levels of leptin, insulin, and glucose. These data revealed that feeding a HFD is an appropriate model to study the development of obesity.

However, a skeletal muscle specific JNK-1 deficiency did not ameliorate the degree of adiposity. Since JNK-1^{SM-KO} mice displayed no alterations in body composition when compared to WT mice, also the rate of energy expenditure, indicated by O₂ consumption and CO₂ production, remained unaltered between the genotypes.

Taken together, these data demonstrate that the protective effects observed in JNK-1 Δ mice (Hirosumi *et al.*, 2002), not originate from the activity of JNK-1 in skeletal muscle,

and that JNK-1 activity in other metabolic tissues than skeletal muscle accounts for these improvements.

However, Sabio and colleagues proposed skeletal muscle derived JNK-1 to contribute to the systemic insulin resistance observed in WT mice upon HFD feeding (Sabio *et al.* , 2010), an effect which was further supported by the finding of an enhanced insulin-stimulated glucose uptake in skeletal muscle upon HFD in these mice when compared to WT mice (Sabio *et al.* , 2010).

In contrast, the data presented in this thesis could not confirm the described role of skeletal muscle derived JNK-1 to contribute to local and systemic insulin resistance. Feeding a HFD resulted in the development of insulin resistance in both, WT and JNK-1^{SM-KO} mice, and the absence of JNK-1 in skeletal muscle in the present work did not result in improved insulin signaling. Furthermore JNK-1^{SM-KO} mice did not show alterations in glucose homeostasis.

Taken together, the data of the present thesis demonstrate that lacking JNK-1 in skeletal muscle does not contribute to enhanced insulin sensitivity or an improved glucose homeostasis as observed in conventional JNK-1 knockout mice (Hirosumi *et al.* , 2002).

The controversial outcome of this study and the study of Sabio and colleagues cannot be explained. Sabio and colleagues assumed that an increased inflammation status of the adipose tissue in mice lacking JNK-1 in skeletal muscle could additionally contribute to the systemic insulin resistance in those mice (Sabio *et al.* , 2010).

However, the differences in data presented here to the previously described role for skeletal muscle specific JNK-1 by Sabio and colleagues are only minor, and also in the latter study skeletal muscle derived JNK-1 did not contribute to the development of obesity (Sabio *et al.* , 2010).

Moreover, analysis of mice lacking JNK-1 in the liver or in the adipose tissue revealed that JNK-1 in none of those tissues contributed to the development of obesity-associated insulin resistance (Sabio *et al.* , 2008, 2009) that was improved in mice with complete JNK-1-deficiency (Hirosumi *et al.* , 2002). JNK-1 in adipose tissue is associated with the development of hepatic insulin resistance (Sabio *et al.* , 2008) that was not reflected in mice lacking JNK-1 in the liver as these mice show the same status of insulin sensitivity as WT mice (Sabio *et al.* , 2009). Interestingly, mice with an ablation of JNK-1 signaling in the adipose tissue showed reduced circulation levels of the pro-inflammatory cytokine

IL-6, and hence a reduction in SOCS3-mediated hepatic insulin resistance in diet induced obesity (Sabio *et al.* , 2008). Though this finding revealed a crosstalk between adipose tissue-derived JNK-1 and hepatic insulin sensitivity through JNK-1 mediated increases of systemic IL-6, the adipose tissue cannot be the tissue that is affected by JNK-1 deficiency to result in resistance to diet induced obesity.

Interestingly, a central inactivation of JNK-1 using the Nestin-Cre line results in a decreased body weight gain in both NCD and HFD (Belgardt *et al.* , 2010a), an effect which is comparable occurring in mice with a whole body ablation of JNK-1 (Hirosumi *et al.* , 2002). However, absence of JNK-1 in Nestin-expressing cells does not lead to alterations in levels of adiposity, but reduced length was observed in these mice. This indicates that the observed reduction in body weight gain in those mice might result from a decrease in naso-anal length, which develops as a consequence of a decreased activation of the somatotrophic axis, as revealed by decreased circulating levels of the pituitary derived growth hormone and insulin-like growth factor (IGF)-1 (Belgardt *et al.* , 2010a).

However, CNS-specific JNK-1 inactivation also ameliorated diet induced development of insulin resistance. Nevertheless, improvements in insulin sensitivity and glucose tolerance in CNS-deficient JNK-1 mice might be a secondary consequence due to disorders in the growth axis, and, hence a failure to develop obesity (Belgardt *et al.* , 2010a). While these data demonstrate a crucial role for neuron-derived JNK-1 in obesity-associated pathologies, the exact neuron population mediating this effect has not been defined yet. Taken together, this thesis (JNK-1^{SM-KO} mice) and studies in mice with a selective deletion of JNK-1 in adipose tissue (Sabio *et al.* , 2008), liver (Sabio *et al.* , 2009), or CNS (Belgardt *et al.* , 2010a) could not fully clarify the molecular and tissue specific mechanisms leading to the decreased adiposity observed in whole body JNK-1 knockout mice (Hirosumi *et al.* , 2002).

4.1.3 Role of skeletal muscle specific JNK-1 in the regulation of exercise-induced IL-6 activation

Exercise was shown to activate JNK in skeletal muscle of humans and rats (Boluyt *et al.* , 2003; Goodyear *et al.* , 1996). However, data for a skeletal muscle specific increase of JNK activation in mice are still missing.

Here, a significantly increased JNK phosphorylation in skeletal muscle of WT mice was

observed after 30 and 60 minutes of treadmill running representing a bout of exercise. Hereto, increased ROS levels due to an elevated oxidative phosphorylation in mitochondria might be a contributing factor (Davies *et al.* , 1982). In fact, it has been demonstrated that ROS are able to activate the JNK pathway (Bouloumie *et al.* , 1999).

In line with previous findings, indicating muscle tissue as an endocrine organ releasing myokines into the circulation (Pedersen & Febbraio, 2008), the results of this thesis demonstrated increased levels of IL-6 mRNA within the skeletal muscle after 30 minutes of exercise. Crucially, the production of IL-6 by the skeletal muscle during exercise fulfills beneficial effects to satisfy the needs of the working muscle, either intrinsically to enhance glucose uptake and fat oxidation, or systemically to promote hepatic glycogenolysis and lipolysis (Kelly *et al.* , 2009).

However, the signaling pathways within the skeletal muscle that increase IL-6 upon exercise stimulation are not understood (Pedersen, 2011). Previously, it has been reported that the mechanical load upon contraction leads to increased calcium concentrations within the skeletal muscle, and thus to activation of the calcium-sensitive kinase Calcineurin leading to increased activity of the transcription factor NFAT (Dolmetsch *et al.* , 1998). However, experiments in human muscle biopsies after 60 minutes of concentric exercise revealed no effect on the nuclear abundance of NFAT but IL-6 mRNA levels were increased (Chan *et al.*, 2004). Moreover, as a result of low glycogen concentrations, the skeletal muscle elevated IL-6 mRNA expression, through a MAP kinase p38 including mechanism (Chan *et al.* , 2004). However, IL-6 expression is quick and starts with the beginning of exercise (Pedersen & Febbraio, 2008). Thus, other signaling pathways might be responsible for the exercise-dependent increase of IL-6 expression in skeletal muscle. In immune cells, IL-6 is a classical target gene of the transcription factor family NF κ B (Jimi & Ghosh, 2005). However, in collaboration with the Febbraio group, this thesis presents evidence that the observed increase in IL-6 mRNA in skeletal muscle of mice occurs independently of NF κ B-regulated transcriptional control (Whitham *et al.* , 2012). To ascertain a role for skeletal muscle derived JNK-1 in the exercise dependent regulation of IL-6, exercise dependent changes were determined in JNK-1^{SM-KO} mice. First, exercise-dependent changes in the phosphorylation state of IKK β or the inhibitor I κ B were not observed in both, WT and JNK-1^{SM-KO} mice. Second, Whitham and colleagues mimicked exercise in C2C12 myotubes by applying electronic pulse stimulation (Whitham *et al.* ,

2012). However, upon exercise stimulation C212 myotubes did not show alterations in the activation of NF κ B but IL-6 levels were highly increased (Whitham *et al.* , 2012).

It was reported previously that mice lacking JNK-1 in the adipose tissue displayed decreased levels of IL-6 mRNA within the adipose tissue that translated to reduced IL-6 levels in circulation (Sabio *et al.* , 2008). Here, JNK-1^{SM-KO} mice exhibited IL-6 levels comparable to that in WT mice under resting conditions. However, when exposed to exercise, WT mice showed a marked increase of IL-6 mRNA expression in the skeletal muscle that was blunted in skeletal muscle of JNK-1^{SM-KO} mice, indicating a crucial role JNK-1 in the regulation of the exercise-dependent activation of IL-6. Together with the finding that JNK is activated upon exercise, it is tempting that JNK-1 mediated AP1 activation induces IL-6 in the exercised muscle (Fig. 4.1).

The data presented here are consistent with previous findings, revealing an association between JNK phosphorylation and IL-6 expression in myotubes treated with LPS (Frost *et al.* , 2003). Moreover, unchanged total JNK phosphorylation upon exercise in skeletal muscle specific JNK-1 deficient mice revealed that the insufficiency to produce IL-6 mRNA in skeletal muscle of JNK-1^{SM-KO} mice is dependent on the JNK-1 protein isoform. Additionally, exercise stimulation in myotubes led to a marked increase in JNK activity, also indicated by increased activity of AP-1 on the IL-6 promotor, and inhibition of JNK signaling abrogated the effect of an exercise-dependent increase of IL-6 (Whitham *et al.* , 2012).

Taken together, these data demonstrate that JNK-1 activity in skeletal muscle is essential to induce exercise-dependent increases of IL-6. Besides the finding that JNK-1 in skeletal muscle does not contribute to insulin resistance, the requirement of JNK-1 in the exercise-dependent induction of IL-6 indicates a beneficial role of JNK-1 in skeletal muscle.

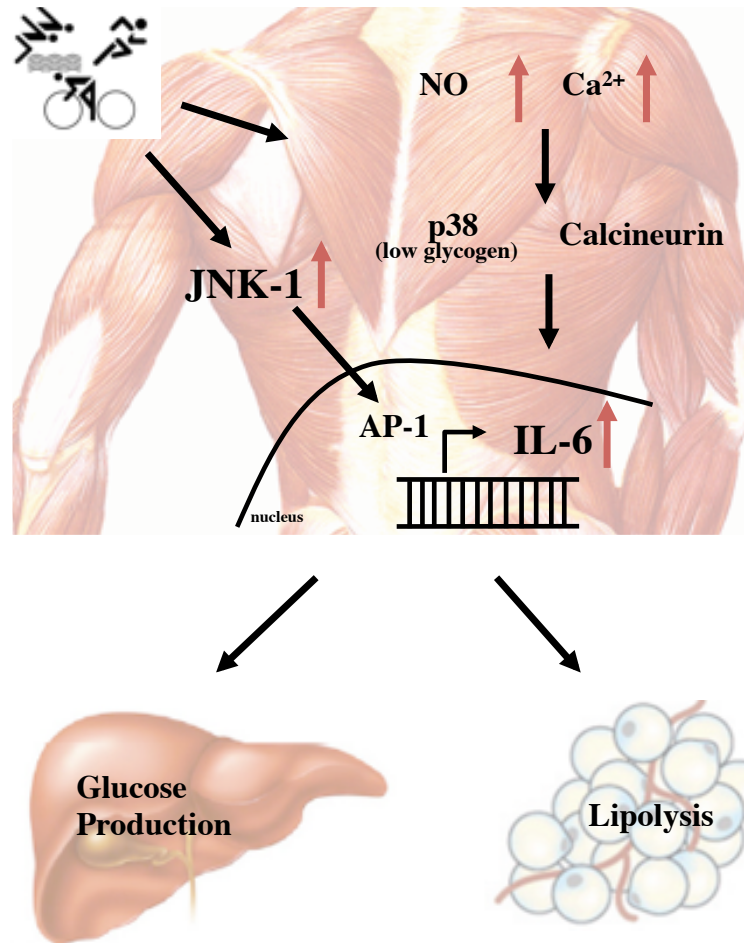


Figure 4.1: JNK-1 is required for exercise induced IL-6 activation in skeletal muscle.

Physical exercise leads to activation of IL-6 most probably by activation of the JNK-1 signaling pathway. Exercise induces the activation of JNK-1, which activates its transcription factor AP-1. AP-1 binds to responsive elements on the IL-6 promoter leading to increase of IL-6 mRNA and its activation. Exercise-dependent increases in the amount of nitric oxide and calcium within the muscle cells may only be secondary for IL-6 induction and JNK-1 is the main pathway leading to exercise dependent IL-6 activation. (adapted from (Belgardt *et al.*, 2010b))

4.1.4 Constitutive JNK activation in skeletal muscle

The above described data were obtained from mice lacking JNK-1 specifically in skeletal muscle. However, as a gain of function approach, parameters of energy and glucose homeostasis were also addressed in mice constitutively activating JNK-1 in skeletal muscle (JNK-1^{SM-C}). In order to generate such mice, a fusion protein of JNK-1 and a mutated version of its upstream kinase MKK7 (MKK7D) was created (Y Wang, 1998). This fusion brings MKK7 and JNK-1 in close proximity that results in constitutive phosphorylation of JNK-1 by MKK7 independently of any stimuli. The fusion protein of 90 kDa was specifically expressed in the skeletal muscle of JNK-1^{SM-C} mice by crossing MCK-cre mice

with ROSA26-JNK-1^C mice. The functionality of that construct was verified by enhanced phosphorylation of the JNK-1 downstream target c-Jun specifically in skeletal muscle. Therefore, this model of JNK-1 activation is suited to analyze the effects of a HFD-induced JNK-1 activation specifically in skeletal muscle even without exposing those mice to HFD.

Parameters of energy homeostasis were assessed upon feeding a NCD in both, WT and JNK-1^{SM-C} mice. However, JNK-1^{SM-C} mice gained body weight similarly as WT mice. Moreover, naso-anal length as well as adiposity levels were unchanged between the genotypes. These data demonstrate that a constitutive activation of JNK-1 in skeletal muscle leaves bodyweight gain and adiposity unaltered.

To assess putative differences in glucose homeostasis between WT and JNK-1^{SM-C} mice, a glucose or a pyruvate challenge was applied, respectively. While an acute bolus of glucose did not alter serum glucose levels during the GTT in JNK-1^{SM-C} mice, injecting pyruvate resulted in increased serum glucose concentrations in JNK-1^{SM-C} mice when compared to WT mice. During fasting, pyruvate is metabolized back to glucose in the liver to maintain stable serum glucose levels. Thus, this indicates an enhanced hepatic glucose production in JNK-1^{SM-C} mice, a finding which is supported by an increased expression of the gluconeogenesis rate-limiting enzyme PEPCK in the liver of JNK-1^{SM-C} mice.

Previous observations demonstrated that hepatic glucose production is regulated by IL-6 and insulin (Belgardt *et al.*, 2010a; Wunderlich *et al.*, 2010). For instance, mice lacking the IL-6R α gene in hepatocytes display not only systemic and hepatic insulin resistance, but also altered expression of key-enzymes of hepatic glucose production such as glucose-6-phosphatase and glucokinase (Wunderlich *et al.*, 2010). Moreover, recent experiments revealed a CNS-specific role of insulin in the regulation of hepatic IL-6 expression that resulted in alterations of hepatic glucose production (Belgardt *et al.*, 2010a). Experiments with obese mice lacking JNK-1 in the CNS revealed a reduced hepatic glucose production and a protection from hepatic obesity-induced insulin resistance as a result of decreased circulating IL-6 (Belgardt *et al.*, 2010a). Moreover the insulin sensitive neuronal cell type that regulates hepatic IL-6 expression was identified as agouti-related peptide (AgRP)-expressing neurons (Könner *et al.*, 2007). In this study, mice lacking the insulin receptor specifically in AgRP neurons displayed reduced insulin-stimulated hepatic IL-

6 expression and increased hepatic glucose production in euglycemic-hyperinsulinemic clamp analysis when compared to WT mice (Könner *et al.* , 2007). Furthermore, it was shown that IL-6 directly activates the expression of PEPCK in the liver (Banzet *et al.* , 2009). Thus, IL-6 regulates hepatic glucose production and could be a cause of enhanced pyruvate conversion to glucose in JNK-1^{SM-C} mice.

To directly address expression of IL-6 in JNK-1^{SM-C} mice, IL-6 mRNA expression was investigated in both, skeletal muscle and liver. While fasted IL-6 mRNA expression in skeletal muscle was decreased in JNK-1^{SM-C} mice when compared to WT mice, IL-6 mRNA expression in liver was unaltered between the genotypes.

Thus, in the model of JNK-1 activation in skeletal muscle presented here, IL-6 is not responsible for the elevated hepatic glucose production observed in JNK-1^{SM-C} mice. The muscle specific factor which is responsible for the impaired hepatic glucose production in JNK-1^{SM-C} mice that links skeletal muscle and liver metabolism, remains unknown and still has to be identified.

4.1.5 Successful generation of a conditional JNK-2 allele in mice

Previously it was demonstrated that the JNK-1 isoform rather than JNK-2 and JNK3 plays a critical role in the development of obesity induced insulin resistance (Hirosumi *et al.* , 2002). However, compensatory effects of the two other JNK isoforms in JNK-1 knockout mice cannot be fully excluded. In line with this notion, JNK-2 is able to phosphorylate the same transcription factors as JNK-1 and both isoforms are co-expressed in every tissue whereas JNK-3 expression is mainly detectable in the brain and heart. Thus, synergistic and compensatory activities between the JNK-1 and JNK-2 isoforms cannot be excluded. To dissect the defined actions of JNK-1 and JNK-2 in metabolic tissues, a conditional JNK-2 allele had to be generated. Therefore, a targeting vector containing a loxP flanked exon 3 of the JNK-2 gene was obtained from the European Conditional Mouse Mutagenesis Program (Eucomm) and introduced into the genome of murine embryonic stem cells by gene targeting. Southern blot analysis revealed 23 homologous recombined ES cell which corresponds to a recombination efficiency of 12 %. Properly targeted ES cell clones were used to generate chimeric mice and JNK-2 chimeras were crossed with Flp-deleter mice (Rodríguez *et al.* , 2000) to achieve germline transmission of the JNK-2 allele together with the excision of the FRT-flanked neo^R-cassette, that could influence JNK-2 expression.

To yield homozygous JNK-2^{FL/FL} mice, the germline transmitted offspring was intercrossed. Moreover, JNK-2^{FL/+} mice were crossed to JNK-1^{FL/FL} mice in order to generate a mouse line which exhibits both conditional alleles for JNK-1 and JNK-2.

In order to analyze the specific inactivation of JNK-2, or a combined loss of JNK-1 and JNK-2, these mice can now be crossed with mice expressing Cre in a specific tissue or cell type (Kühn *et al.*, 1995). The conventional combined loss of JNK-1 and JNK-2 was shown to result in embryonic lethality, further supporting the importance of a conditional JNK-2 allele (Sabapathy *et al.*, 1999).

Taken together, a conditional JNK-2 allele was successfully generated and the newly created JNK-2^{FL} mice can be used to further investigate JNK signaling in the control of energy and glucose homeostasis in tissues that express the Cre recombinase.

4.2 Conditional overexpression of mXBP1s protein in brain and liver

Obesity is associated with elevated levels of ER stress, which leads to the activation of the UPR (Hotamisligil, 2010). A main pathway of the UPR is the IRE1/XBP1 pathway. Upon activation of IRE1 the endoribonuclease activity cleaves inactive XBP1u mRNA to yield transcriptionally active XBP1s mRNA, which results in the protein expression of the XBP1s transcription factor. XBP1s translocates into the nucleus and induces target gene expression of chaperones to compensate the amount of stress on the ER (Glimcher, 2010). To mimic ER stress genetically, mice were generated that contain the active form XBP1s in the ROSA26 locus whose expression is prevented by a loxP-flanked STOP cassette. For this, the SERCA vector containing mXBP1s was generated (Klisch, 2006) and introduced into the genome of murine ES cells. 24 homologous recombined clones were detected by Southern blot analysis, which corresponds to a recombination efficiency of 25 %. Correctly targeted clones were used to generate the ROSA-mXBP1s mouse line.

Subsequently, mXBP1s germline transmitted ROSA-mXBP1s mice were crossed to CAMKII-Cre (Casanova *et al.*, 2001) (mXBP1s^{CamKII}), and ALFP-Cre (Kellendonk *et al.*, 2000) mice (mXBP1s^{Alfp}), respectively. CAMKII is expressed in all brain regions, however the most reliable expression was observed in the hippocampus (Casanova *et al.*, 2001). Therefore, expression analysis of mXBP1s^{CamKII} mice was conducted in the hippocampus revealing

increased XBP1s mRNA expression accompanied with enhanced mRNA expression of the XBP1s downstream target ERdj4 in the hippocampus of mXBP1s^{CamKII} mice. Moreover, the functionality of mXBP1s^{CamKII} mice was also revealed by enhanced mRNA expression of the ER chaperone GRP78.

Surprisingly, however, hepatic CHOP mRNA expression in mXBP1s^{CamKII} mice was significantly increased similarly as in mXBP1s^{Alfp} mice indicating a crosstalk between the CNS and the liver in ER stress induced gene expression, while ER stress markers in skeletal muscle were unaffected in mXBP1s^{CamKII} mice.

Moreover, hepatic GRP78 mRNA expression was also increased in mXBP1s^{CamKII} mice, though the values did not reach statistical significance. In line with this experiment, gene expression analysis in liver of mXBP1s^{Alfp} mice revealed increased mRNA and protein expression of XBP1s that not only increased mRNA expression of its downstream target ERdj4 but also of CHOP, GRP78, and ATF6 that were significantly upregulated in the livers of mXBP1s^{Alfp} mice.

Thus, these data not only demonstrate that mXBP1s mice are a valuable tool to characterize the consequences of ER stress induced gene expression, but also hint to a possible crosstalk between central and hepatic ER stress. The mechanism how such crosstalk could function is unclear, however could involve a soluble factor that is induced through central ER stress that subsequently acts systemically especially on the liver. Moreover, sympathetic or parasympathetic efference could also account for the observed phenomenon that might regulate liver innervation through the induction of central ER stress. However at this point of analysis, the aforementioned mechanisms still have to be experimentally addressed and are therefore speculative.

In collaboration with the Dillin laboratory, the consequences of central ER stress induced crosstalk to liver ER stress in mXBP1s^{CamKII} mice will be addressed in future studies. These collaborators generated precedent data in *Caenorhabditis elegans* revealing that neuronal ER stress induced ER stress in the worms gut (A. Dillin and J. Brüning, personal communications).

Thus, to reveal whether this mechanism also is present in mammals, the mXBP1s^{CamKII} mice should be useful to clarify this notion though it might be possible that the neuronal population that is responsible for the crosstalk between brain and liver may not be affected in those mice. CamKII Cre mice excise loxP-flanked target sequences mainly in neurons

of the hippocampus but also in parts of the cortex but nevertheless not in all neurons. A possible other useful Cre line to address this issue might be the Nestin-Cre mouse that expresses the Cre recombinase in neuronal precursors and thus in all neurons. Further analysis by the Dillin laboratory will reveal the phenotypical consequences of neuronal ER stress on mouse physiology and clarify the mechanisms that are used to transmit ER stress between brain and liver. In line with this notion, the hepatic ablation of XBP1 results in improved insulin sensitivity accompanied by improved suppression of hepatic glucose production (Jurczak *et al.*, 2012). However, brain-deficient XBP1 mice exhibit increased levels of ER stress and their analysis revealed a link between the induction of ER stress and leptin resistance, a finding which is accompanied by increased food intake and body weight gain in these mice (Ozcan *et al.*, 2009). Moreover, a beneficial and protective effect for ER stress was indicated by its exercise-induced activation in the brain, resulting in amelioration of neurodegenerative disorders (Kim *et al.*, 2010).

Taken together, the newly developed ROSA-mXBP1s mice comprise an appropriate tool to investigate the underlying signaling mechanisms of ER stress, especially in obesity and obesity-induced insulin resistance.

4.3 FABP4-2A-Cre-mediated recombination

The adipose tissue possess a central role in metabolism by serving not only as organ for excessive energy storage but also functions as an endocrine organ releasing hormones, that are termed adipokines (Ferris & Crowther, 2011). These adipokines, e.g. leptin, adiponectin and others, fulfill major functions in physiology and may contribute to the state of insulin resistance under obese conditions. Gene targeting strategies involving site-specific recombinases haven been described to gain insights into the function of adipose tissue specific gene expression.

Here, an adipose tissue-specific Cre mouse strain was characterized, expressing the Cre recombinase under the control of the endogenous FABP4-promotor. FABP4 (also termed aP2) is a 15 kDa adipocyte-specific lipid-chaperone, which facilitates lipid transport within the cell to specific compartments (Hunt *et al.*, 1986). As previously mentioned, using this promotor, several adipose tissue-specific Cre lines have been generated, so far (Abel *et al.*, 2001; Barlow *et al.*, 1997; Blüher *et al.*, 2002). In all of those approaches the integration of

the Cre transgenic DNA into the genome might interfere with tissue specific Cre expression due to random integration into the genome and the variability of copy numbers.

Here, for the first time an adipose tissue-specific Cre was generated by applying the properties of the foot-and-mouth-virus (FMDV)-derived 2A-technology (de Felipe, 2004). The 2A-technology allows a targeted knock-in into the endogenous gene locus and enables expression of Cre without interfering with endogenous gene expression, and hence is superior to IRES-technology in which a second protein is expressed from a second ribosomal entry site. This notion is achieved by the generation of one mRNA, that produces a fusion-protein in which FABP4 is linked to Cre by the 2A-peptide. The 2A-protein is a small peptide of 18 amino-acids and is needed by the FMDV to process the viral poly-protein (Halpin *et al.* , 1999). During translation, 2A induces the so termed “skipping” of the last peptide bond at the C-terminus of 2A by interacting with the exit tunnel of ribosome, and the ribosome continues translation after releasing the first protein fused to 2A at its C-terminus (de Felipe, 2004; Donnelly *et al.* , 2001; Sharma *et al.* , 2011). Hence, this process results in equimolar amounts of FABP4 and Cre.

Recently, Engert and colleagues generated a Sox17-2A-iCre, in which Cre expression is driven by the Sox17 promotor, whose expression is restricted to the developing endoderm, and to vascular endothelial cells of the cardiovascular and hematopoietic system (Engert *et al.* , 2009). In this approach, the 2A-peptide was derived from the *Thosea Aisgna* virus (Engert *et al.* , 2009).

Here, the FABP4-2A Cre mouse line was generated by Christoph Hees (Hees, n.d.) by targeted insertion of 2A and Cre into the endogenous FABP4 STOP-codon. To characterize this mouse strain, FABP4-2A-Cre mice were crossed on the one hand to ROSA26-FOXODN mice (Belgardt *et al.* , 2008) that express both FOXODN and eGFP upon Cre mediated recombination. On the other, FABP4-2A-Cre mice were crossed to IL-6R^{FL} mice (Wunderlich *et al.* , 2010) to confirm the excision specificity and efficiency on another loxP-flanked allele.

Analysis of FOXODN^{FABP4} mice revealed that FABP4-2A-Cre activity was found in adipose tissue, e.g. in white adipocytes, and white and brown adipose tissue, whereas no Cre activity was detected in skeletal muscle or brain. Furthermore, GFP expression in FOXODN^{FABP4} mice indicated Cre activity in peritoneal macrophages (95 % recombination frequency) and Kupffer cells (15 % recombination frequency). The Cre activity in

macrophages in the FABP4-2A-Cre mouse line is consistent with previous studies reporting expression of FABP4 also in macrophages (He *et al.* , 2003).

Thus using the novel FABP4_{2a}Cre line enables the specific inactivation of loxP-flanked target genes in WAT, BAT and macrophages. Nonetheless, when only adipose tissue specific gene inactivation is desired, replacing the myeloid compartment in FABP4-2A-Cre mice by WT by bone marrow transplantation (Kodama Y, 2009) would enable gene targeting specifically in adipocytes.

Moreover, the FABP4-2A-Cre mice were crossed with IL-6R α ^{FL/FL} mice (Wunderlich *et al.* , 2010) to verify excision specificity and efficiency on another loxP-flanked target gene. Strikingly, Cre-mediated recombination was observed in all investigated tissues that reached 100% efficiency, including skeletal muscle and liver indicating that FABP4-2A-Cre is expressed during early embryogenesis that subsequently leads to excision of the loxP-flanked exons of the IL-6R α gene in all following cells that originate from the initial Cre expressing cell.

However, such a differential outcome in the Cre-mediated recombination of target genes has been reported previously and might involve whether the Cre transgene transmits through either the female or male germline. Hafner and colleagues, reported that Keratin14-Cre-mediated deletion occurs in all tissues when the Cre allele was inherited by the mother (Hafner *et al.* , 2004), whereas only keratinocytes express Cre when the Cre allele comes from the father. Therefore, IL-6R α ^{FABP4} mice were investigated side by side in which the FABP4-2A-Cre allele was inherited by the mother and the father, respectively. However, independent from which gender the Cre allele was transmitted, always a complete excision of the loxP-flanked exons of the IL-6R α gene was observed in all tissues as revealed by Southern blot and PCR analysis. Since FABP4 is not expressed in skeletal muscle or liver, the FABP4-2A-Cre-mediated recombination has happened early during development.

Indeed, it was reported that FABP4 is expressed also in non-adipogenic tissues during embryonic development and Cre expression in those tissues leads to ectopic recombination (Martens *et al.* , 2010; Urs *et al.* , 2006). These data are consistent with findings that in adult mice FABP4 is expressed only in adipocytes and not in macrophages (He *et al.* , 2003), indicating that the observed GFP expression in peritoneal macrophages and

Kupffer cells remained from FABP4-2A-Cre mediated recombination during embryonic development.

Nevertheless, FABP4-2A-Cre mediated recombination was found in the adipose tissue and myeloid cell specific using the FOXODN-ROSA26 reporter mouse. Hence, the recombination efficiency of the loxP-flanked IL-6R α gene must contribute to the ubiquitous deletion observed in IL-6R α^{FABP4} mice. Vooijs and colleagues highlighted that the distance between two loxP sites alters recombination frequencies and efficiencies (Vooijs *et al.*, 2001). However, the distance between loxP sites was similar (e.g. 2kB) in IL-6R α^{FL} and ROSA-FOXODN mice, thereby excluding this possibility. Furthermore, differences in the expression level of the target gene or the local chromatin structure might also contribute to different recombination frequencies between two loxP sites (Vooijs *et al.*, 2001). Especially, Vooijs and colleagues demonstrated that loxP sites in the ROSA26 locus are less accessible than loxP sites in the retinoblastoma and Brca2 genes (Vooijs *et al.*, 2001).

Thus, as here ROSA26- and IL-6R α^{FL} alleles were analyzed with the FABP4-2A-Cre transgene, the aforementioned explanation might also account for FABP4-2A-Cre mice. Therefore, other loxP-flanked target genes than ROSA26 transgenic lines and the IL-6R α allele have to be used to verify the usefulness of the FABP4-2A-Cre mouse line in the WAT specific analysis of gene functions in mice.

Taken together, the 2A-technology was used for the first time to achieve an adipose tissue specific expression of the Cre recombinase driven by the FABP4-promotor. However, expression of FABP4 and hence, Cre activity was also found in peritoneal macrophages and to a lesser extent in Kupffer cells. Moreover, FABP4 expression is highly complex and is suggested also in early developmental stages, which may lead to ectopic expression of Cre that would lead to the complete excision of loxP-flanked target sequences. Noteworthy, Cre-mediated recombination depends on the target gene and the location of the loxP sites that must be taken into account when applying the newly developed FABP4-2A-Cre to analyze gene functions within the adipose tissue.

List of Figures

1.1	Obesity and physical inactivity are closely related	2
1.2	Schematic view of the insulin signaling pathway	4
1.3	Obesity induced JNK activation leads to inhibition of the insulin signaling cascade	7
1.4	Physical Exercise induced IL-6 activation in skeletal muscle	13
1.5	ER stress activates the UPR	15
1.6	Cre mediated recombination	17
2.1	JNK-2 and mXBP1s targeting vectors	24
2.2	Treadmill	38
3.1	JNK activity in skeletal muscle is elevated in HFD-induced obesity	41
3.2	General scheme of mice with a selective deletion of JNK-1 in skeletal muscle	42
3.3	Loss of JNK-1 specifically in skeletal muscle	43
3.4	Body weight of JNK-1 ^{SM-KO} mice	44
3.5	Unaltered adiposity in JNK-1 ^{SM-KO} mice	45
3.6	Body length of JNK-1 ^{SM-KO} mice	46
3.7	Food intake and energy expenditure of JNK-1 ^{SM-KO} mice	47
3.8	Unaltered glucose metabolism and insulin sensitivity in JNK-1 ^{SM-KO} mice	48
3.9	Insulin signaling in skeletal muscle and liver of JNK-1 ^{SM-KO} mice	49
3.10	JNK is activated in skeletal muscle of WT mice upon exercise	50
3.11	IL-6 mRNA expression is increased in skeletal muscle of WT mice upon exercise	51
3.12	IL-6 activation upon exercise is blunted in JNK-1 ^{SM-KO} mice	52
3.13	General scheme of mice with a selective constitutive activation of JNK-1 in skeletal muscle	55
3.14	Generation of a JNK-1 gain of function approach in skeletal muscle	56
3.15	Body weight and body length of JNK-1 ^{SM-C} mice	57
3.16	Unaltered adiposity in JNK-1 ^{SM-C} mice	57

List of Figures

3.17	Food intake and energy expenditure of JNK-1 ^{SM-C} mice	58
3.18	Unaltered insulin sensitivity in JNK-1 ^{SM-C} mice	59
3.19	Hepatic glucose production in JNK-1 ^{SM-C} mice	60
3.20	IL-6 mRNA expression is increased upon fasting	62
3.21	Expression pattern of JNK isoforms in tissues of WT mice	64
3.22	Generation of mice with a loxP-flanked allele of the murine JNK-2 gene	66
3.23	Generation of mice with targeted insertion of mXBP1s into the ROSA26 locus	69
3.24	General scheme of mice with a selective overexpression of mXBP1s in hippocampus (mXBP1s ^{CamKII} and liver (mXBP1s ^{Alfp}	71
3.25	XBP1s is overexpressed in hippocampi of mXBP1s ^{CamKII} mice	72
3.26	XBP1s is overexpressed in livers of mXBP1s ^{Alfp} mice	73
3.27	Expression of ER stress markers in skeletal muscle of mXBP1s ^{CamKII} and mXBP1s ^{Alfp} mice	74
3.28	The 2A-technology allows equivalent expression of FABP4 and Cre	77
3.29	Schematic view of crossing FABP4-2A-Cre mice to FOXODN mice to obtain FOXODN ^{FABP4} mice	78
3.30	FABP4-2A-Cre-mediated recombination in FOXODN ^{FABP4-Cre} mice	79
3.31	GFP expression in adipose tissue and macrophages of FOXODN ^{FABP4} mice	80
3.32	Schematic view of crossing FABP4-2A-Cre mice to IL-6R α ^{FL/FL} mice to obtain IL-6R α ^{FABP4} mice	81
3.33	FABP4-2A-Cre-mediated recombination in IL-6R α ^{FABP} mice	82
4.1	JNK-1 is required for exercise induced IL-6 activation in skeletal muscle	90

List of Tables

2.1	Chemicals	20
2.2	Enzymes	23
2.3	Primers used for genotyping	26
2.4	Primers used for the generation of Southern blot probes	27
2.5	Restriction enzymes used for the generation of Southern blot probes	28
2.6	Realtime PCR probes	29
2.7	Custom-made realtime PCR probes	29
2.8	Primary antibodies used for Western blot	32
2.9	Treadmill Protocol	38

Bibliography

- ABDELLI, S, PUYAL, J, BIELMANN, C, BUCHILLIER, V, ABDERRAHMANI, A, CLARKE, P G H, BECKMANN, J S, & BONNY, C. 2009. Jnk3 is abundant in insulin-secreting cells and protects against cytokine-induced apoptosis. *Diabetologia*, **52**(9), 1871–80.
- ABEL, E D, PERONI, O, KIM, J K, KIM, Y B, BOSS, O, HADRO, E, MINNEMANN, T, SHULMAN, G I, & KAHN, B B. 2001. Adipose-selective targeting of the glut4 gene impairs insulin action in muscle and liver. *Nature*, **409**(6821), 729–33.
- ACOSTA-ALVEAR, DIEGO, ZHOU, YIMING, BLAIS, ALEXANDRE, TSIKITIS, MARY, LENTS, NATHAN H, ARIAS, CAROLINA, LENNON, CHRISTEN J, KLUGER, YUVAL, & DYNLACHT, BRIAN DAVID. 2007. Xbp1 controls diverse cell type- and condition-specific transcriptional regulatory networks. *Mol cell*, **27**(1), 53–66.
- AGUIRRE, V, UCHIDA, T, YENUSH, L, DAVIS, R, & WHITE, M F. 2000. The c-jun nh(2)-terminal kinase promotes insulin resistance during association with insulin receptor substrate-1 and phosphorylation of ser(307). *J biol chem*, **275**(12), 9047–54.
- AKIRA, SHIZUO. 2003. Toll-like receptor signaling. *J biol chem*, **278**(40), 38105–8.
- AKIRA, SHIZUO, & TAKEDA, KIYOSHI. 2004. Toll-like receptor signalling. *Nat rev immunol*, **4**(7), 499–511.
- ALTHOFF, K, REDDY, P, VOLTZ, N, ROSE-JOHN, S, & MÜLLBERG, J. 2000. Shedding of interleukin-6 receptor and tumor necrosis factor alpha. contribution of the stalk sequence to the cleavage pattern of transmembrane proteins. *Eur j biochem*, **267**(9), 2624–31.
- ARKAN, MELEK C, HEVENER, ANDREA L, GRETEN, FLORIAN R, MAEDA, SHIN, LI, ZHI-WEI, LONG, JEFFREY M, WYNshaw-BORIS, ANTHONY, POLI, GIUSEPPE, OLEFSKY, JERROLD, & KARIN, MICHAEL. 2005. Ikk-beta links inflammation to obesity-induced insulin resistance. *Nat med*, **11**(2), 191–8.
- ARONSON, D, BOPPART, M D, DUFRESNE, S D, FIELDING, R A, & GOODYEAR, L J. 1998. Exercise stimulates c-jun nh2 kinase activity and c-jun transcriptional activity in human skeletal muscle. *Biochem biophys res commun*, **251**(1), 106–10.
- B. HOGAN, F. CONSTANTINI, E. LACEY. 1986. *Manipulating the mouse embryo: A laboratory manual*. Cold Spring Harbor Laboratory Press.
- BALON, T W, & NADLER, J L. 1994. Nitric oxide release is present from incubated skeletal muscle preparations. *J appl physiol*, **77**(6), 2519–21.
- BANTING, F G, BEST, C H, COLLIP, J B, CAMPBELL, W R, & FLETCHER, A A. 1962. Pancreatic extracts in the treatment of diabetes mellitus: Preliminary report. *Can med assoc j*, **87**(20), 1062–7.

- BANZET, SÉBASTIEN, KOULMANN, NATHALIE, SIMLER, NADINE, SANCHEZ, HERVÉ, CHAPOT, RACHEL, SERRURIER, BERNARD, PEINNEQUIN, ANDRÉ, & BIGARD, XAVIER. 2009. Control of gluconeogenic genes during intense/prolonged exercise: hormone-independent effect of muscle-derived il-6 on hepatic tissue and pepck mrna. *J appl physiol*, **107**(6), 1830–9.
- BARLOW, C, SCHROEDER, M, LEKSTROM-HIMES, J, KYLEFJORD, H, DENG, C X, WYNshaw-BORIS, A, SPIEGELMAN, B M, & XANTHOPOULOS, K G. 1997. Targeted expression of cre recombinase to adipose tissue of transgenic mice directs adipose-specific excision of loxp-flanked gene segments. *Nucleic acids res*, **25**(12), 2543–5.
- BARSH, G S, FAROOQI, I S, & O'RAHILLY, S. 2000. Genetics of body-weight regulation. *Nature*, **404**(6778), 644–51.
- BASTARD, J P, JARDEL, C, BRUCKERT, E, BLONDY, P, CAPEAU, J, LAVILLE, M, VIDAL, H, & HAINQUE, B. 2000. Elevated levels of interleukin 6 are reduced in serum and subcutaneous adipose tissue of obese women after weight loss. *J clin endocrinol metab*, **85**(9), 3338–42.
- BELGARDT, B. F, MAUER, J, WUNDERLICH, F. T, ERNST, M. B, PAL, M, SPOHN, G, BRONNEKE, H. S, BRODESSER, S, HAMPEL, B, SCHAUSS, A. C, & BRUNING, J. C. 2010a. Hypothalamic and pituitary c-jun n-terminal kinase 1 signaling coordinately regulates glucose metabolism. *Proceedings of the national academy of sciences*, **107**(13), 6028–6033.
- BELGARDT, BENGT F, HUSCH, ANDREAS, ROTHER, EVA, ERNST, MARIANNE B, WUNDERLICH, F THOMAS, HAMPEL, BRIGITTE, KLÖCKENER, TIM, ALESSI, DARIO, KLOPPENBURG, PETER, & BRÜNING, JENS C. 2008. Pdk1 deficiency in pomc-expressing cells reveals foxo1-dependent and -independent pathways in control of energy homeostasis and stress response. *Cell metab*, **7**(4), 291–301.
- BELGARDT, BENGT F, MAUER, JAN, & BRÜNING, JENS C. 2010b. Novel roles for jnk1 in metabolism. *Aging (albany ny)*, **2**(9), 621–6.
- BLÜHER, MATTHIAS, MICHAEL, M DODSON, PERONI, ODILE D, UEKI, KOHJIRO, CARTER, NATHAN, KAHN, BARBARA B, & KAHN, C RONALD. 2002. Adipose tissue selective insulin receptor knockout protects against obesity and obesity-related glucose intolerance. *Dev cell*, **3**(1), 25–38.
- BOLUYT, M O, LOYD, A M, ROTH, M H, RANDALL, M J, & SONG, E Y M. 2003. Activation of jnk in rat heart by exercise: effect of training. *Am j physiol heart circ physiol*, **285**(6), H2639–47.
- BOOTHBY, M, GRAVALLESE, E, LIOU, H C, & GLIMCHER, L H. 1988. A dna binding protein regulated by il-4 and by differentiation in b cells. *Science*, **242**(4885), 1559–62.

- BOPPART, M D, ARONSON, D, GIBSON, L, ROUBENOFF, R, ABAD, L W, BEAN, J, GOODYEAR, L J, & FIELDING, R A. 1999. Eccentric exercise markedly increases c-jun nh(2)-terminal kinase activity in human skeletal muscle. *J appl physiol*, **87**(5), 1668–73.
- BOPPART, M D, ASP, S, WOJTASZEWSKI, J F, FIELDING, R A, MOHR, T, & GOODYEAR, L J. 2000. Marathon running transiently increases c-jun nh2-terminal kinase and p38 activities in human skeletal muscle. *J physiol (lond)*, **526 Pt 3**(Aug), 663–9.
- BOULOUMIE, A, MARUMO, T, LAFONTAN, M, & BUSSE, R. 1999. Leptin induces oxidative stress in human endothelial cells. *Faseb j*, **13**(10), 1231–8.
- BRÜNING, J C, MICHAEL, M D, WINNAY, J N, HAYASHI, T, HÖRSCH, D, ACCILI, D, GOODYEAR, L J, & KAHN, C R. 1998. A muscle-specific insulin receptor knockout exhibits features of the metabolic syndrome of niddm without altering glucose tolerance. *Mol cell*, **2**(5), 559–69.
- BRUUNSGAARD, H, GALBO, H, HALKJAER-KRISTENSEN, J, JOHANSEN, T L, MACLEAN, D A, & PEDERSEN, B K. 1997. Exercise-induced increase in serum interleukin-6 in humans is related to muscle damage. *J physiol (lond)*, **499 (Pt 3)**(Mar), 833–41.
- CAREY, A L, BRUCE, C R, SACCHETTI, M, ANDERSON, M J, OLSEN, D B, SALTIN, B, HAWLEY, J A, & FEBBRAIO, M A. 2004. Interleukin-6 and tumor necrosis factor-alpha are not increased in patients with type 2 diabetes: evidence that plasma interleukin-6 is related to fat mass and not insulin responsiveness. *Diabetologia*, **47**(6), 1029–37.
- CAREY, ANDREW L, STEINBERG, GREGORY R, MACAULAY, S LANCE, THOMAS, WALTER G, HOLMES, ANNA G, RAMM, GEORG, PRELOVSEK, OJA, HOHNEN-BEHRENS, CORDULA, WATT, MATTHEW J, JAMES, DAVID E, KEMP, BRUCE E, PEDERSEN, BENTE K, & FEBBRAIO, MARK A. 2006. Interleukin-6 increases insulin-stimulated glucose disposal in humans and glucose uptake and fatty acid oxidation in vitro via amp-activated protein kinase. *Diabetes*, **55**(10), 2688–97.
- CASANOVA, E, FEHSENFELD, S, MANTAMADIOTIS, T, LEMBERGER, T, GREINER, E, STEWART, A F, & SCHÜTZ, G. 2001. A camkiialpha icre bac allows brain-specific gene inactivation. *Genesis*, **31**(1), 37–42.
- CHALFIE, M, TU, Y, EUSKIRCHEN, G, WARD, W W, & PRASHER, D C. 1994. Green fluorescent protein as a marker for gene expression. *Science*, **263**(5148), 802–5.
- CHAN, J M, RIMM, E B, COLDITZ, G A, STAMPFER, M J, & WILLETT, W C. 1994. Obesity, fat distribution, and weight gain as risk factors for clinical diabetes in men. *Diabetes care*, **17**(9), 961–9.
- CHAN, M H STANLEY, MCGEE, SEAN L, WATT, MATTHEW J, HARGREAVES, MARK, & FEBBRAIO, MARK A. 2004. Altering dietary nutrient intake that reduces glycogen content leads to phosphorylation of nuclear p38 map kinase in human skeletal muscle: association with il-6 gene transcription during contraction. *Faseb j*, **18**(14), 1785–7.

- CHANG, L, & KARIN, M. 2001. Mammalian map kinase signalling cascades. *Nature*, **410**(6824), 37–40.
- CHEATHAM, B, & KAHN, C R. 1995. Insulin action and the insulin signaling network. *Endocr rev*, **16**(2), 117–42.
- CHEN, XI, SHEN, JINGSHI, & PRYWES, RON. 2002. The luminal domain of atf6 senses endoplasmic reticulum (er) stress and causes translocation of atf6 from the er to the golgi. *J biol chem*, **277**(15), 13045–52.
- CLAUSS, I M, GRAVALLESE, E M, DARLING, J M, SHAPIRO, F, GLIMCHER, M J, & GLIMCHER, L H. 1993. In situ hybridization studies suggest a role for the basic region-leucine zipper protein hxbp-1 in exocrine gland and skeletal development during mouse embryogenesis. *Dev dyn*, **197**(2), 146–56.
- CLAUSS, I M, CHU, M, ZHAO, J L, & GLIMCHER, L H. 1996. The basic domain/leucine zipper protein hxbp-1 preferentially binds to and transactivates cre-like sequences containing an acgt core. *Nucleic acids res*, **24**(10), 1855–64.
- COURTOIS, GILLES, & ISRAËL, ALAIN. 2011. Ikk regulation and human genetics. *Curr top microbiol immunol*, **349**(Jan), 73–95.
- D CAI, M YUAN, DF FRANTZ PA MELENDEZ L HANSEN J LEE SE SHOELSON. 2005. Local and systemic insulin resistance resulting from hepatic activation of ikk-beta and nf-kappab. *Nat med.*, **11**(2), 183–90.
- DA LUZ, GABRIELLE, FREDERICO, MARISA J S, DA SILVA, SABRINA, VITTO, MARCELO F, CESCONETTO, PATRICIA A, DE PINHO, RICARDO A, PAULI, JOSÉ R, SILVA, ADELINO S R, CINTRA, DENNYS E, ROPELLE, EDUARDO R, & DE SOUZA, CLÁUDIO T. 2011. Endurance exercise training ameliorates insulin resistance and reticulum stress in adipose and hepatic tissue in obese rats. *European journal of applied physiology*, Jan.
- DAVIES, K J, QUINTANILHA, A T, BROOKS, G A, & PACKER, L. 1982. Free radicals and tissue damage produced by exercise. *Biochem biophys res commun*, **107**(4), 1198–205.
- DAVIS, R J. 2000. Signal transduction by the jnk group of map kinases. *Cell*, **103**(2), 239–52.
- DE FELIPE, PABLO. 2004. Skipping the co-expression problem: the new 2a "chysel" technology. *Genet vaccines ther*, **2**(1), 13.
- DOLMETSCH, R E, XU, K, & LEWIS, R S. 1998. Calcium oscillations increase the efficiency and specificity of gene expression. *Nature*, **392**(6679), 933–6.
- DONNELLY, M L, HUGHES, L E, LUKE, G, MENDOZA, H, TEN DAM, E, GANI, D, & RYAN, M D. 2001. The 'cleavage' activities of foot-and-mouth disease virus 2a site-directed mutants and naturally occurring '2a-like' sequences. *J gen virol*, **82**(Pt 5), 1027–41.

- EISENBARTH, G S, NAYAK, R C, & RABINOWE, S L. 1988. Type i diabetes as a chronic autoimmune disease. *J diabet complications*, **2**(2), 54–8.
- ENGERT, SILVIA, LIAO, W PERRY, BURTSCHER, INGO, & LICKERT, HEIKO. 2009. Sox17-2a-icre: a knock-in mouse line expressing cre recombinase in endoderm and vascular endothelial cells. *Genesis*, **47**(9), 603–10.
- F KÖNTGEN, CL STEWART. 1993. Simple screening procedure to detect gene targeting events in embryonic stem cells. *Methods enzymol.*, **225**, 878–90.
- FÄLDT, JENNY, WERNSTEDT, INGRID, FITZGERALD, SHARYN M, WALLENIUS, KRISTINA, BERGSTRÖM, GÖRAN, & JANSSON, JOHN-OLOV. 2004. Reduced exercise endurance in interleukin-6-deficient mice. *Endocrinology*, **145**(6), 2680–6.
- FEBBRAIO, MARK A, HISCOCK, NATALIE, SACCHETTI, MASSIMO, FISCHER, CHRISTIAN P, & PEDERSEN, BENTE K. 2004. Interleukin-6 is a novel factor mediating glucose homeostasis during skeletal muscle contraction. *Diabetes*, **53**(7), 1643–8.
- FERRIS, W F, & CROWTHER, N J. 2011. Once fat was fat and that was that: our changing perspectives on adipose tissue. *Cardiovasc j afr*, **22**(3), 147–54.
- FEUERER, MARKUS, HERRERO, LAURA, CIPOLLETTA, DANIELA, NAAZ, AFIA, WONG, JAMIE, NAYER, ALI, LEE, JONGSOON, GOLDFINE, ALLISON B, BENOIST, CHRISTOPHE, SHOELSON, STEVEN, & MATHIS, DIANE. 2009. Lean, but not obese, fat is enriched for a unique population of regulatory t cells that affect metabolic parameters. *Nat med*, **15**(8), 930–9.
- FIEDLER, BEATE, & WOLLERT, KAI C. 2004. Interference of antihypertrophic molecules and signaling pathways with the ca²⁺-calcineurin-nfat cascade in cardiac myocytes. *Cardiovasc res*, **63**(3), 450–7.
- FISCHER, JULIA, KOCH, LINDA, EMMERLING, CHRISTIAN, VIERKOTTEN, JEANETTE, PETERS, THOMAS, BRÜNING, JENS C, & RÜTHER, ULRICH. 2009. Inactivation of the fto gene protects from obesity. *Nature*, **458**(7240), 894–8.
- FRAYLING, TIMOTHY M, TIMPSON, NICHOLAS J, WEEDON, MICHAEL N, ZEGGINI, ELEFThERIA, FREATHY, RACHEL M, LINDGREN, CECILIA M, PERRY, JOHN R B, ELLIOTT, KATHERINE S, LANGO, HANA, RAYNER, NIGEL W, SHIELDS, BEVERLEY, HARRIES, LORNA W, BARRETT, JEFFREY C, ELLARD, SIAN, GROVES, CHRISTOPHER J, KNIGHT, BRIDGET, PATCH, ANN-MARIE, NESS, ANDREW R, EBRAHIM, SHAH, LAWLOR, DEBBIE A, RING, SUSAN M, BEN-SHLOMO, YOAV, JARVELIN, MARJORIITTA, SOVIO, ULLA, BENNETT, AMANDA J, MELZER, DAVID, FERRUCCI, LUIGI, LOOS, RUTH J F, BARROSO, INÊS, WAREHAM, NICHOLAS J, KARPE, FREDRIK, OWEN, KATHARINE R, CARDON, LON R, WALKER, MARK, HITMAN, GRAHAM A, PALMER, COLIN N A, DONEY, ALEX S F, MORRIS, ANDREW D, SMITH, GEORGE DAVEY, HATTERSLEY, ANDREW T, & MCCARTHY, MARK I. 2007. A common variant in the fto gene

- is associated with body mass index and predisposes to childhood and adult obesity. *Science*, **316**(5826), 889–94.
- FRIEDRICH, G, & SORIANO, P. 1991. Promoter traps in embryonic stem cells: a genetic screen to identify and mutate developmental genes in mice. *Genes dev*, **5**(9), 1513–23.
- FROST, ROBERT A, NYSTROM, GERALD J, & LANG, CHARLES H. 2003. Lipopolysaccharide and proinflammatory cytokines stimulate interleukin-6 expression in c2c12 myoblasts: role of the jun nh2-terminal kinase. *Am j physiol regul integr comp physiol*, **285**(5), R1153–64.
- GLADDEN, L B. 2004. Lactate metabolism: a new paradigm for the third millennium. *J physiol (lond)*, **558**(Pt 1), 5–30.
- GLADDEN, L BRUCE. 2008. Current trends in lactate metabolism: introduction. *Medicine and science in sports and exercise*, **40**(3), 475–6.
- GLIMCHER, L H. 2010. Xbp1: the last two decades. *Ann rheum dis*, **69 Suppl 1**(Jan), i67–71.
- GLUND, STEPHAN, DESHMUKH, ATUL, LONG, YUN CHAU, MOLLER, THEODORE, KOISTINEN, HEIKKI A, CAIDAHL, KENNETH, ZIERATH, JULEEN R, & KROOK, ANNA. 2007. Interleukin-6 directly increases glucose metabolism in resting human skeletal muscle. *Diabetes*, **56**(6), 1630–7.
- GOODYEAR, L J, CHANG, P Y, SHERWOOD, D J, DUFRESNE, S D, & MOLLER, D E. 1996. Effects of exercise and insulin on mitogen-activated protein kinase signaling pathways in rat skeletal muscle. *Am j physiol*, **271**(2 Pt 1), E403–8.
- GRANGE, R W, ISOTANI, E, LAU, K S, KAMM, K E, HUANG, P L, & STULL, J T. 2001. Nitric oxide contributes to vascular smooth muscle relaxation in contracting fast-twitch muscles. *Physiol genomics*, **5**(1), 35–44.
- GRANNER, D, ANDREONE, T, SASAKI, K, & BEALE, E. 1983. Inhibition of transcription of the phosphoenolpyruvate carboxykinase gene by insulin. *Nature*, **305**(5934), 549–51.
- HAFNER, MARTIN, WENK, JUTTA, NENCI, ARIANNA, PASPARAKIS, MANOLIS, SCHARFFETTER-KOCHANEK, KARIN, SMYTH, NEIL, PETERS, THORSTEN, KESS, DANIEL, HOLTKÖTTER, OLAF, SHEPHARD, PIERRE, KUDLOW, JEFFREY E, SMOLA, HANS, HAASE, INGO, SCHIPPERS, ANGELA, KRIEG, THOMAS, & MÜLLER, WERNER. 2004. Keratin 14 cre transgenic mice authenticate keratin 14 as an oocyte-expressed protein. *Genesis*, **38**(4), 176–81.
- HALPIN, C, COOKE, S E, BARAKATE, A, AMRANI, A EL, & RYAN, M D. 1999. Self-processing 2a-polyproteins—a system for co-ordinate expression of multiple proteins in transgenic plants. *Plant j*, **17**(4), 453–9.
- HARDING, H P, ZHANG, Y, & RON, D. 1999. Protein translation and folding are coupled by an endoplasmic-reticulum-resident kinase. *Nature*, **397**(6716), 271–4.

- HARRIS, ROBERT A, BOWKER-KINLEY, MELISSA M, HUANG, BOLI, & WU, PENGFEI. 2002. Regulation of the activity of the pyruvate dehydrogenase complex. *Adv enzyme regul*, **42**(Jan), 249–59.
- HE, WEIMIN, BARAK, YAACOV, HEVENER, ANDREA, OLSON, PETER, LIAO, DEBBIE, LE, JAMIE, NELSON, MICHAEL, ONG, ESTELITA, OLEFSKY, JERROLD M, & EVANS, RONALD M. 2003. Adipose-specific peroxisome proliferator-activated receptor gamma knockout causes insulin resistance in fat and liver but not in muscle. *Proc natl acad sci usa*, **100**(26), 15712–7.
- HE, YIN, SUN, SHENGYI, SHA, HAIBO, LIU, ZIYING, YANG, LIU, XUE, ZHEN, CHEN, HUI, & QI, LING. 2010. Emerging roles for xbp1, a super transcription factor. *Gene expr*, **15**(1), 13–25.
- HEES, CHRISTOPH. *Generierung von fett-spezifischen cre mäusen*. M.Phil. thesis, University of Cologne.
- HEIM, R, CUBITT, A B, & TSIEN, R Y. 1995. Improved green fluorescence. *Nature*, **373**(6516), 663–4.
- HEMISH, JILL, NAKAYA, NAOKI, MITTAL, VIVEK, & ENIKOLOPOV, GRIGORI. 2003. Nitric oxide activates diverse signaling pathways to regulate gene expression. *J biol chem*, **278**(43), 42321–9.
- HEPPNER, KRISTY M, HABEGGER, KIRK M, DAY, JONATHAN, PFLUGER, PAUL T, PEREZ-TILVE, DIEGO, WARD, BRIAN, GELFANOV, VASILY, WOODS, STEVE C, DIMARCHI, RICHARD, & TSCHÖP, MATTHIAS. 2010. Glucagon regulation of energy metabolism. *Physiol behav*, **100**(5), 545–8.
- HETZ, CLAUDIO, BERNASCONI, PAULA, FISHER, JILL, LEE, ANN-HWEE, BASSIK, MICHAEL C, ANTONSSON, BRUNO, BRANDT, GABRIEL S, IWAKOSHI, NEAL N, SCHINZEL, ANNA, GLIMCHER, LAURIE H, & KORSMEYER, STANLEY J. 2006. Proapoptotic bax and bak modulate the unfolded protein response by a direct interaction with ire1alpha. *Science*, **312**(5773), 572–6.
- HIBI, M, LIN, A, SMEAL, T, MINDEN, A, & KARIN, M. 1993. Identification of an oncoprotein- and uv-responsive protein kinase that binds and potentiates the c-jun activation domain. *Genes dev*, **7**(11), 2135–48.
- HILL, J O, & PETERS, J C. 1998. Environmental contributions to the obesity epidemic. *Science*, **280**(5368), 1371–4.
- HILL, JAMES O, WYATT, HOLLY R, REED, GEORGE W, & PETERS, JOHN C. 2003. Obesity and the environment: where do we go from here? *Science*, **299**(5608), 853–5.
- HIROSUMI, JIRO, TUNCMAN, GÜROL, CHANG, LUFEN, GÖRGÜN, CEM Z, UYSAL, K TEOMAN, MAEDA, KAZUHISA, KARIN, MICHAEL, & HOTAMISLIGIL, GÖKHAN S. 2002. A central role for jnk in obesity and insulin resistance. *Nature*, **420**(6913), 333–6.

- HO, RICHARD C, HIRSHMAN, MICHAEL F, LI, YANGFENG, CAI, DONGSHENG, FARMER, JOCELYN R, ASCHENBACH, WILLIAM G, WITCZAK, CAROL A, SHOELSON, STEVEN E, & GOODYEAR, LAURIE J. 2005. Regulation of ikappab kinase and nf-kappab in contracting adult rat skeletal muscle. *Am j physiol, cell physiol*, **289**(4), C794–801.
- HOESS, R, ABREMSKI, K, & STERNBERG, N. 1984. The nature of the interaction of the p1 recombinase cre with the recombining site loxp. *Cold spring harb symp quant biol*, **49**(Jan), 761–8.
- HOESS, R H, & ABREMSKI, K. 1984. Interaction of the bacteriophage p1 recombinase cre with the recombining site loxp. *Proc natl acad sci usa*, **81**(4), 1026–9.
- HOESS, R H, ZIESE, M, & STERNBERG, N. 1982. P1 site-specific recombination: nucleotide sequence of the recombining sites. *Proc natl acad sci usa*, **79**(11), 3398–402.
- HOTAMISLIGIL, G S, SHARGILL, N S, & SPIEGELMAN, B M. 1993. Adipose expression of tumor necrosis factor-alpha: direct role in obesity-linked insulin resistance. *Science*, **259**(5091), 87–91.
- HOTAMISLIGIL, GÖKHAN S. 2010. Endoplasmic reticulum stress and the inflammatory basis of metabolic disease. *Cell*, **140**(6), 900–17.
- HUMMASTI, SARAH, & HOTAMISLIGIL, GÖKHAN S. 2010. Endoplasmic reticulum stress and inflammation in obesity and diabetes. *Circ res*, **107**(5), 579–91.
- HUNT, C R, RO, J H, DOBSON, D E, MIN, H Y, & SPIEGELMAN, B M. 1986. Adipocyte p2 gene: developmental expression and homology of 5'-flanking sequences among fat cell-specific genes. *Proc natl acad sci usa*, **83**(11), 3786–90.
- ICHIJO, H, NISHIDA, E, IRIE, K, TEN DIJKE, P, SAITOH, M, MORIGUCHI, T, TAKAGI, M, MATSUMOTO, K, MIYAZONO, K, & GOTOH, Y. 1997. Induction of apoptosis by ask1, a mammalian mapkkk that activates sapk/jnk and p38 signaling pathways. *Science*, **275**(5296), 90–4.
- INOUE, HIROSHI, OGAWA, WATARU, ASAKAWA, AKIHIRO, OKAMOTO, YASUO, NISHIZAWA, AKIHIKO, MATSUMOTO, MICHIIHIRO, TESHIGAWARA, KIYOSHI, MATSUKI, YASUSHI, WATANABE, EIJIRO, HIRAMATSU, RYUJI, NOTOHARA, KENJI, KATAYOSE, KOJI, OKAMURA, HITOSHI, KAHN, C RONALD, NODA, TETSUO, TAKEDA, KIYOSHI, AKIRA, SHIZUO, INUI, AKIO, & KASUGA, MASATO. 2006. Role of hepatic stat3 in brain-insulin action on hepatic glucose production. *Cell metab*, **3**(4), 267–75.
- ISAKOFF, S J, YU, Y P, SU, Y C, BLAIKIE, P, YAJNIK, V, ROSE, E, WEIDNER, K M, SACHS, M, MARGOLIS, B, & SKOLNIK, E Y. 1996. Interaction between the phosphotyrosine binding domain of shc and the insulin receptor is required for shc phosphorylation by insulin in vivo. *J biol chem*, **271**(8), 3959–62.
- J. SAMBROOK, D.W. RUSSEL. 2001. *Molecular cloning: A laboratory manual*. CSHL Press.

- JAESCHKE, ANJA, CZECH, MICHAEL P, & DAVIS, ROGER J. 2004. An essential role of the jip1 scaffold protein for jnk activation in adipose tissue. *Genes dev*, **18**(16), 1976–80.
- JI, L L, GOMEZ-CABRERA, M-C, STEINHAFEL, N, & VINA, J. 2004. Acute exercise activates nuclear factor (nf)-kappab signaling pathway in rat skeletal muscle. *Faseb j*, **18**(13), 1499–506.
- JIMI, EIJIRO, & GHOSH, SANKAR. 2005. Role of nuclear factor-kappab in the immune system and bone. *Immunol rev*, **208**(Dec), 80–7.
- JOHNSON, J E, WOLD, B J, & HAUSCHKA, S D. 1989. Muscle creatine kinase sequence elements regulating skeletal and cardiac muscle expression in transgenic mice. *Mol cell biol*, **9**(8), 3393–9.
- JONES, S A, HORIUCHI, S, TOPLEY, N, YAMAMOTO, N, & FULLER, G M. 2001. The soluble interleukin 6 receptor: mechanisms of production and implications in disease. *Faseb j*, **15**(1), 43–58.
- JURCZAK, MICHAEL J, LEE, ANN-HWEE, JORNAYVAZ, FRANCOIS R, LEE, HUI-YOUNG, BIRKENFELD, ANDREAS L, GUIGNI, BLAS A, KAHN, MARIO, SAMUEL, VARMAN T, GLIMCHER, LAURIE H, & SHULMAN, GERALD I. 2012. Dissociation of inositol-requiring enzyme (ire1 α)-mediated c-jun n-terminal kinase activation from hepatic insulin resistance in conditional x-box-binding protein-1 (xbp1) knock-out mice. *J biol chem*, **287**(4), 2558–67.
- KAHN, C R, VICENT, D, & DORIA, A. 1996. Genetics of non-insulin-dependent (type-ii) diabetes mellitus. *Annu rev med*, **47**(Jan), 509–31.
- KASUGA, M, KARLSSON, F A, & KAHN, C R. 1982. Insulin stimulates the phosphorylation of the 95,000-dalton subunit of its own receptor. *Science*, **215**(4529), 185–7.
- KELLENDONK, C, OPPERK, C, ANLAG, K, SCHÜTZ, G, & TRONCHE, F. 2000. Hepatocyte-specific expression of cre recombinase. *Genesis*, **26**(2), 151–3.
- KELLY, MEGHAN, GAUTHIER, MARIE-SOLEIL, SAHA, ASISH K, & RUDERMAN, NEIL B. 2009. Activation of amp-activated protein kinase by interleukin-6 in rat skeletal muscle: association with changes in camp, energy state, and endogenous fuel mobilization. *Diabetes*, **58**(9), 1953–60.
- KIM, HYU-JEONG, HIGASHIMORI, TAKAMASA, PARK, SO-YOUNG, CHOI, HYEJEONG, DONG, JIANYING, KIM, YOON-JUNG, NOH, HYE-LIM, CHO, YOU-REE, CLINE, GARY, KIM, YOUNG-BUM, & KIM, JASON K. 2004. Differential effects of interleukin-6 and -10 on skeletal muscle and liver insulin action in vivo. *Diabetes*, **53**(4), 1060–7.
- KIM, YUHO, PARK, MIEJUNG, BOGHOSIAN, STÉPHANE, & YORK, DAVID A. 2010. Three weeks voluntary running wheel exercise increases endoplasmic reticulum stress in the brain of mice. *Brain res*, **1317**(Mar), 13–23.

- KIRÁLY, MICHAEL A, CAMPBELL, JON, PARK, EDWARD, BATES, HOLLY E, YUE, JESSICA T Y, RAO, VENKET, MATTHEWS, STEPHEN G, BIKOPOULOS, GEORGE, ROZAKIS-ADCOCK, MARIA, GIACCA, ADRIA, VRANIC, MLADEN, & RIDDELL, MICHAEL C. 2010. Exercise maintains euglycemia in association with decreased activation of c-jun nh2-terminal kinase and serine phosphorylation of irs-1 in the liver of zdf rats. *Am j physiol endocrinol metab*, **298**(3), E671–82.
- KLISCH, BRUNO. 2006. *Generierung cre-aktivierbarer transgene zur konditionalen expression in der maus*. M.Phil. thesis, University of Cologne.
- KODAMA Y, KISSALEVA T, IWASAKO K MIURA K DE MINICIS S OSTERREICHER CH SCHNABI B SEKI E BRENNER DA. 2009. c-jun n-terminal kinase-1 from hematopoietic cells mediates progression from hepatic steatosis to steatohepatitis and fibrosis in mice. *Gastroenterology*, **137**(4), 1467–1477.
- KÖNNER, A CHRISTINE, JANOSCHEK, RUTH, PLUM, LEONA, JORDAN, SABINE D, ROTHER, EVA, MA, XIAOSONG, XU, CHUN, ENRIORI, PABLO, HAMPEL, BRIGITTE, BARSH, GREGORY S, KAHN, C RONALD, COWLEY, MICHAEL A, ASHCROFT, FRANCES M, & BRÜNING, JENS C. 2007. Insulin action in agrp-expressing neurons is required for suppression of hepatic glucose production. *Cell metab*, **5**(6), 438–49.
- KÜHN, R, SCHWENK, F, AGUET, M, & RAJEWSKY, K. 1995. Inducible gene targeting in mice. *Science*, **269**(5229), 1427–9.
- LAU, K S, GRANGE, R W, CHANG, W J, KAMM, K E, SARELIUS, I, & STULL, J T. 1998. Skeletal muscle contractions stimulate cgmp formation and attenuate vascular smooth muscle myosin phosphorylation via nitric oxide. *Febs lett*, **431**(1), 71–4.
- LEE, ANN-HWEE, SCAPA, EREZ F, COHEN, DAVID E, & GLIMCHER, LAURIE H. 2008. Regulation of hepatic lipogenesis by the transcription factor xbp1. *Science*, **320**(5882), 1492–6.
- LEEM, YEA-HYUN, LIM, HWA-JA, SHIM, SUN-BO, CHO, JOON-YONG, KIM, BUM-SOO, & HAN, PYUNG-LIM. 2009. Repression of tau hyperphosphorylation by chronic endurance exercise in aged transgenic mouse model of tauopathies. *J neurosci res*, **87**(11), 2561–70.
- LIU, H C, BOOTHBY, M R, & GLIMCHER, L H. 1988. Distinct cloned class ii mhc dna binding proteins recognize the x box transcription element. *Science*, **242**(4875), 69–71.
- LIU, H C, BOOTHBY, M R, FINN, P W, DAVIDON, R, NABAVI, N, ZELEZNIK-LE, N J, TING, J P, & GLIMCHER, L H. 1990. A new member of the leucine zipper class of proteins that binds to the hla dr alpha promoter. *Science*, **247**(4950), 1581–4.
- LUMENG, CAREY N, MAILLARD, IVAN, & SALTIEL, ALAN R. 2009. T-ting up inflammation in fat. *Nat med*, **15**(8), 846–7.

- MACKIEWICZ, A, SCHOOLTINK, H, HEINRICH, P C, & ROSE-JOHN, S. 1992. Complex of soluble human il-6-receptor/il-6 up-regulates expression of acute-phase proteins. *J immunol*, **149**(6), 2021–7.
- MAJUMDAR, S K. 2001. Glimpses of the history of insulin. *Bull indian inst hist med hyderabad*, **31**(1), 57–70.
- MAKOWSKI, L, BOORD, J B, MAEDA, K, BABAIEV, V R, UYSAL, K T, MORGAN, M A, PARKER, R A, SUTTLES, J, FAZIO, S, HOTAMISLIGIL, G S, & LINTON, M F. 2001. Lack of macrophage fatty-acid-binding protein ap2 protects mice deficient in apolipoprotein e against atherosclerosis. *Nat med*, **7**(6), 699–705.
- MAO, X, FUJIWARA, Y, & ORKIN, S H. 1999. Improved reporter strain for monitoring cre recombinase-mediated dna excisions in mice. *Proc natl acad sci usa*, **96**(9), 5037–42.
- MARTENS, KATRIN, BOTTELBERGS, ASTRID, & BAES, MYRIAM. 2010. Ectopic recombination in the central and peripheral nervous system by ap2/fabp4-cre mice: implications for metabolism research. *Febs lett*, **584**(5), 1054–8.
- MATTHEWS, VANCE, SCHUSTER, BJÖRN, SCHÜTZE, STEFAN, BUSSMEYER, INGO, LUDWIG, ANDREAS, HUNDHAUSEN, CHRISTIAN, SADOWSKI, THORSTEN, SAFTIG, PAUL, HARTMANN, DIETER, KALLEN, KARL-JOSEF, & ROSE-JOHN, STEFAN. 2003. Cellular cholesterol depletion triggers shedding of the human interleukin-6 receptor by adam10 and adam17 (tace). *J biol chem*, **278**(40), 38829–39.
- MOKDAD, ALI H, FORD, EARL S, BOWMAN, BARBARA A, DIETZ, WILLIAM H, VINICOR, FRANK, BALES, VIRGINIA S, & MARKS, JAMES S. 2003. Prevalence of obesity, diabetes, and obesity-related health risk factors, 2001. *Jama*, **289**(1), 76–9.
- MOUNIER, CATHERINE, & POSNER, BARRY I. 2006. Transcriptional regulation by insulin: from the receptor to the gene. *Can j physiol pharmacol*, **84**(7), 713–24.
- MYERS, M G, BACKER, J M, SUN, X J, SHOELSON, S, HU, P, SCHLESSINGER, J, YOAKIM, M, SCHAFFHAUSEN, B, & WHITE, M F. 1992. Irs-1 activates phosphatidylinositol 3'-kinase by associating with src homology 2 domains of p85. *Proc natl acad sci usa*, **89**(21), 10350–4.
- MYERS, M G, SUN, X J, CHEATHAM, B, JACHNA, B R, GLASHEEN, E M, BACKER, J M, & WHITE, M F. 1993. Irs-1 is a common element in insulin and insulin-like growth factor-i signaling to the phosphatidylinositol 3'-kinase. *Endocrinology*, **132**(4), 1421–30.
- MYERS, M G, GRAMMER, T C, BROOKS, J, GLASHEEN, E M, WANG, L M, SUN, X J, BLENIS, J, PIERCE, J H, & WHITE, M F. 1995. The pleckstrin homology domain in insulin receptor substrate-1 sensitizes insulin signaling. *J biol chem*, **270**(20), 11715–8.
- NAKAE, J, KITAMURA, T, SILVER, D L, & ACCILI, D. 2001. The forkhead transcription factor foxo1 (fkhr) confers insulin sensitivity onto glucose-6-phosphatase expression. *J clin invest*, **108**(9), 1359–67.

- NEHLSSEN-CANNARELLA, S L, FAGOAGA, O R, NIEMAN, D C, HENSON, D A, BUTTERWORTH, D E, SCHMITT, R L, BAILEY, E M, WARREN, B J, UTTER, A, & DAVIS, J M. 1997. Carbohydrate and the cytokine response to 2.5 h of running. *J appl physiol*, **82**(5), 1662–7.
- NIELSEN, ANDERS RINNOV, MOUNIER, REMI, PLOMGAARD, PETER, MORTENSEN, OLE HARTVIG, PENKOWA, MILENA, SPEERSCHNEIDER, TOBIAS, PILEGAARD, HENRIETTE, & PEDERSEN, BENTE KLARLUND. 2007. Expression of interleukin-15 in human skeletal muscle effect of exercise and muscle fibre type composition. *J physiol (lond)*, **584**(Pt 1), 305–12.
- NIEMAN, D C, NEHLSSEN-CANNARELLA, S L, FAGOAGA, O R, HENSON, D A, UTTER, A, DAVIS, J M, WILLIAMS, F, & BUTTERWORTH, D E. 1998. Influence of mode and carbohydrate on the cytokine response to heavy exertion. *Medicine and science in sports and exercise*, **30**(5), 671–8.
- NIEMAN, D C, DAVIS, J M, HENSON, D A, WALBERG-RANKIN, J, SHUTE, M, DUMKE, C L, UTTER, A C, VINCI, D M, CARSON, J A, BROWN, A, LEE, W J, MCANULTY, S R, & MCANULTY, L S. 2003. Carbohydrate ingestion influences skeletal muscle cytokine mrna and plasma cytokine levels after a 3-h run. *J appl physiol*, **94**(5), 1917–25.
- OLIVEIRA, ALEXANDRE G, CARVALHO, BRUNO M, TOBAR, NATÁLIA, ROPELLE, EDUARDO R, PAULI, JOSÉ R, BAGAROLLI, RENATA A, GUADAGNINI, DIOZE, CARVALHEIRA, JOSÉ B C, & SAAD, MARIO J A. 2011. Physical exercise reduces circulating lipopolysaccharide and tlr4 activation and improves insulin signaling in tissues of diabetic rats. *Diabetes*, **60**(3), 784–96.
- ONO, S J, LIOU, H C, DAVIDON, R, STROMINGER, J L, & GLIMCHER, L H. 1991. Human x-box-binding protein 1 is required for the transcription of a subset of human class ii major histocompatibility genes and forms a heterodimer with c-fos. *Proc natl acad sci usa*, **88**(10), 4309–12.
- OSTROWSKI, K, ROHDE, T, ZACHO, M, ASP, S, & PEDERSEN, B K. 1998. Evidence that interleukin-6 is produced in human skeletal muscle during prolonged running. *J physiol (lond)*, **508** (Pt 3)(May), 949–53.
- OSTROWSKI, K, ROHDE, T, ASP, S, SCHJERLING, P, & PEDERSEN, B K. 1999. Pro- and anti-inflammatory cytokine balance in strenuous exercise in humans. *J physiol (lond)*, **515** (Pt 1)(Feb), 287–91.
- OZCAN, LALE, ERGIN, AYSE SEDA, LU, ALLEN, CHUNG, JASON, SARKAR, SUMIT, NIE, DUYU, MYERS, MARTIN G, & OZCAN, UMUT. 2009. Endoplasmic reticulum stress plays a central role in development of leptin resistance. *Cell metab*, **9**(1), 35–51.
- OZCAN, UMUT, CAO, QIONG, YILMAZ, ERKAN, LEE, ANN-HWEE, IWAKOSHI, NEAL N, OZDELEN, ESRA, TUNCMAN, GÜROL, GÖRGÜN, CEM, GLIMCHER, LAURIE H, & HOTAMISLIGIL, GÖKHAN S. 2004. Endoplasmic reticulum stress links obesity, insulin action, and type 2 diabetes. *Science*, **306**(5695), 457–61.

- OZCAN, UMUT, YILMAZ, ERKAN, OZCAN, LALE, FURUHASHI, MASATO, VAILLANCOURT, ERIC, SMITH, ROSS O, GÖRGÜN, CEM Z, & HOTAMISLIGIL, GÖKHAN S. 2006. Chemical chaperones reduce er stress and restore glucose homeostasis in a mouse model of type 2 diabetes. *Science*, **313**(5790), 1137–40.
- PAL, MARTIN. 2008. *Generation of loxp-flanked c-jun n-terminal kinases alleles in murine embryonic stem cells*. M.Phil. thesis, University of Heidelberg and Cologne.
- PATTI, M E, & KAHN, C R. 1998. The insulin receptor—a critical link in glucose homeostasis and insulin action. *J basic clin physiol pharmacol*, **9**(2-4), 89–109.
- PEDERSEN, BENTE K, & FEBBRAIO, MARK A. 2008. Muscle as an endocrine organ: focus on muscle-derived interleukin-6. *Physiol rev*, **88**(4), 1379–406.
- PEDERSEN, BENTE KLARLUND. 2011. Muscles and their myokines. *J exp biol*, **214**(Pt 2), 337–46.
- PENG SHEN, CHANG, TSIMBERG, YELENA, SALVADORE, CHRISTOPHER, & MELLER, EMANUEL. 2004. Activation of erk and jnk mapk pathways by acute swim stress in rat brain regions. *Bmc neurosci*, **5**(Sep), 36.
- PODOLSKY, DANIEL K. 2002. Inflammatory bowel disease. *N engl j med*, **347**(6), 417–29.
- POSSEMATO, RICHARD, EGGAN, KEVIN, MOELLER, BENJAMIN J, JAENISCH, RUDOLF, & JACKSON-GRUSBY, LAURIE. 2002. Flp recombinase regulated lacz expression at the rosa26 locus. *Genesis*, **32**(2), 184–6.
- PRAGER, R, WALLACE, P, & OLEFSKY, J M. 1987. Direct and indirect effects of insulin to inhibit hepatic glucose output in obese subjects. *Diabetes*, **36**(5), 607–11.
- RAJEWSKY, K, GU, H, KÜHN, R, BETZ, U A, MÜLLER, W, ROES, J, & SCHWENK, F. 1996. Conditional gene targeting. *J clin invest*, **98**(3), 600–3.
- RAO, R V, ELLERBY, H M, & BREDESEN, D E. 2004. Coupling endoplasmic reticulum stress to the cell death program. *Cell death differ*, **11**(4), 372–80.
- REIMOLD, A M, ETKIN, A, CLAUSS, I, PERKINS, A, FRIEND, D S, ZHANG, J, HORTON, H F, SCOTT, A, ORKIN, S H, BYRNE, M C, GRUSBY, M J, & GLIMCHER, L H. 2000. An essential role in liver development for transcription factor xbp-1. *Genes dev*, **14**(2), 152–7.
- RIZZUTO, R, BRINI, M, PIZZO, P, MURGIA, M, & POZZAN, T. 1995. Chimeric green fluorescent protein as a tool for visualizing subcellular organelles in living cells. *Curr biol*, **5**(6), 635–42.
- RODRÍGUEZ, C I, BUCHHOLZ, F, GALLOWAY, J, SEQUERRA, R, KASPER, J, AYALA, R, STEWART, A F, & DYMECKI, S M. 2000. High-efficiency deleter mice show that flpe is an alternative to cre-loxp. *Nat genet*, **25**(2), 139–40.

- ROSS, S R, GRAVES, R A, GREENSTEIN, A, PLATT, K A, SHYU, H L, MELLOVITZ, B, & SPIEGELMAN, B M. 1990. A fat-specific enhancer is the primary determinant of gene expression for adipocyte p2 in vivo. *Proc natl acad sci usa*, **87**(24), 9590–4.
- SABAPATHY, K, JOCHUM, W, HOCHEDLINGER, K, CHANG, L, KARIN, M, & WAGNER, E F. 1999. Defective neural tube morphogenesis and altered apoptosis in the absence of both jnk1 and jnk2. *Mech dev*, **89**(1-2), 115–24.
- SABIO, G, DAS, M, MORA, A, ZHANG, Z, JUN, J. Y, KO, H. J, BARRETT, T, KIM, J. K, & DAVIS, R. J. 2008. A stress signaling pathway in adipose tissue regulates hepatic insulin resistance. *Science*, **322**(5907), 1539–1543.
- SABIO, GUADALUPE, & DAVIS, ROGER J. 2010. cjun nh2-terminal kinase 1 (jnk1): roles in metabolic regulation of insulin resistance. *Trends biochem sci*, **35**(9), 490–6.
- SABIO, GUADALUPE, CAVANAGH-KYROS, JULIE, KO, HWI JIN, JUNG, DAE YOUNG, GRAY, SUSAN, JUN, JOHN Y, BARRETT, TAMERA, MORA, ALFONSO, KIM, JASON K, & DAVIS, ROGER J. 2009. Prevention of steatosis by hepatic jnk1. *Cell metab*, **10**(6), 491–8.
- SABIO, GUADALUPE, KENNEDY, NORMAN J, CAVANAGH-KYROS, JULIE, JUNG, DAE YOUNG, KO, HWI JIN, ONG, HELENA, BARRETT, TAMERA, KIM, JASON K, & DAVIS, ROGER J. 2010. Role of muscle c-jun nh2-terminal kinase 1 in obesity-induced insulin resistance. *Mol cell biol*, **30**(1), 106–15.
- SALTIEL, A R, & KAHN, C R. 2001. Insulin signalling and the regulation of glucose and lipid metabolism. *Nature*, **414**(6865), 799–806.
- SCHWARTZ, GARY J. 2004. Biology of eating behavior in obesity. *Obes res*, **12 Suppl 2**(Nov), 102S–6S.
- SCHWARTZ, MICHAEL W. 2006. Central nervous system regulation of food intake. *Obesity (silver spring)*, **14 Suppl 1**(Feb), 1S–8S.
- SHARMA, A M. 1998. The thrifty-genotype hypothesis and its implications for the study of complex genetic disorders in man. *J mol med*, **76**(8), 568–71.
- SHARMA, PAMILA, YAN, FU, DORONINA, VICTORIA A, ESCUIN-ORDINAS, HELENA, RYAN, MARTIN D, & BROWN, JEREMY D. 2011. 2a peptides provide distinct solutions to driving stop-carry on translational recoding. *Nucleic acids res*, Dec.
- SHI, Y, VATTEM, K M, SOOD, R, AN, J, LIANG, J, STRAMM, L, & WEK, R C. 1998. Identification and characterization of pancreatic eukaryotic initiation factor 2 alpha-subunit kinase, pek, involved in translational control. *Mol cell biol*, **18**(12), 7499–509.
- SIDRAUSKI, C, & WALTER, P. 1997. The transmembrane kinase ire1p is a site-specific endonuclease that initiates mrna splicing in the unfolded protein response. *Cell*, **90**(6), 1031–9.
- SILVER, L.M. 1995. *Mouse genetics: Concepts and applications*. Oxford University Press.

- SOLINAS, GIOVANNI, & KARIN, MICHAEL. 2010. Jnk1 and ikkbeta: molecular links between obesity and metabolic dysfunction. *Faseb j*, **24**(8), 2596–611.
- SORIANO, P. 1999. Generalized lacz expression with the rosa26 cre reporter strain. *Nat genet*, **21**(1), 70–1.
- STEENBERG, A, VAN HALL, G, OSADA, T, SACCHETTI, M, SALTIN, B, & PEDERSEN, B KLARLUND. 2000. Production of interleukin-6 in contracting human skeletal muscles can account for the exercise-induced increase in plasma interleukin-6. *J physiol (lond)*, **529 Pt 1**(Nov), 237–42.
- STEENBERG, ADAM, KELLER, CHARLOTTE, HILLIG, THORE, FRØSIG, CHRISTIAN, WOJTASZEWSKI, JØRGEN F P, PEDERSEN, BENTE KLARLUND, PILEGAARD, HENRIETTE, & SANDER, MIKAEL. 2007. Nitric oxide production is a proximal signaling event controlling exercise-induced mrna expression in human skeletal muscle. *Faseb j*, **21**(11), 2683–94.
- STERNBERG, N, & HAMILTON, D. 1981. Bacteriophage p1 site-specific recombination. i. recombination between loxp sites. *J mol biol*, **150**(4), 467–86.
- STERNBERG, N, SAUER, B, HOESS, R, & ABREMSKI, K. 1986. Bacteriophage p1 cre gene and its regulatory region. evidence for multiple promoters and for regulation by dna methylation. *J mol biol*, **187**(2), 197–212.
- STOLLER, JASON Z, DEGENHARDT, KARL R, HUANG, LI, ZHOU, DIANE D, LU, MIN MIN, & EPSTEIN, JONATHAN A. 2008. Cre reporter mouse expressing a nuclear localized fusion of gfp and beta-galactosidase reveals new derivatives of pax3-expressing precursors. *Genesis*, **46**(4), 200–4.
- TAGA, T, HIBI, M, HIRATA, Y, YAMASAKI, K, YASUKAWA, K, MATSUDA, T, HIRANO, T, & KISHIMOTO, T. 1989. Interleukin-6 triggers the association of its receptor with a possible signal transducer, gp130. *Cell*, **58**(3), 573–81.
- TOBIUME, K, MATSUZAWA, A, TAKAHASHI, T, NISHITOH, H, MORITA, K, TAKEDA, K, MINOWA, O, MIYAZONO, K, NODA, T, & ICHIJO, H. 2001. Ask1 is required for sustained activations of jnk/p38 map kinases and apoptosis. *Embo rep*, **2**(3), 222–8.
- TOURNIER, C, WHITMARSH, A J, CAVANAGH, J, BARRETT, T, & DAVIS, R J. 1999. The mkk7 gene encodes a group of c-jun nh2-terminal kinase kinases. *Mol cell biol*, **19**(2), 1569–81.
- TOURNIER, C, DONG, C, TURNER, T K, JONES, S N, FLAVELL, R A, & DAVIS, R J. 2001. Mkk7 is an essential component of the jnk signal transduction pathway activated by proinflammatory cytokines. *Genes dev*, **15**(11), 1419–26.
- UM, HYUN-SUB, KANG, EUN-BUM, KOO, JUNG-HOON, KIM, HYUN-TAE, JIN-LEE, KIM, EUNG-JOON, YANG, CHUN-HO, AN, GIL-YOUNG, CHO, IN-HO, & CHO, JOON-YONG. 2011. Treadmill exercise represses neuronal cell death in an aged transgenic mouse model of alzheimer's disease. *Neurosci res*, **69**(2), 161–73.

- UNGER, R H. 1971. Glucagon and the insulin: glucagon ratio in diabetes and other catabolic illnesses. *Diabetes*, **20**(12), 834–8.
- URANO, F, WANG, X, BERTOLOTTI, A, ZHANG, Y, CHUNG, P, HARDING, H P, & RON, D. 2000. Coupling of stress in the er to activation of jnk protein kinases by transmembrane protein kinase ire1. *Science*, **287**(5453), 664–6.
- URS, SUMITHRA, HARRINGTON, ANNE, LIAW, LUCY, & SMALL, DEENA. 2006. Selective expression of an ap2/fatty acid binding protein 4-cre transgene in non-adipogenic tissues during embryonic development. *Transgenic res*, **15**(5), 647–53.
- UYSAL, K T, WIESBROCK, S M, MARINO, M W, & HOTAMISLIGIL, G S. 1997. Protection from obesity-induced insulin resistance in mice lacking tnf-alpha function. *Nature*, **389**(6651), 610–4.
- VALLERIE, SARA N, & HOTAMISLIGIL, GÖKHAN S. 2010. The role of jnk proteins in metabolism. *Sci transl med*, **2**(60), 60rv5.
- VAN HALL, GERRIT, STEENSBERG, ADAM, SACCHETTI, MASSIMO, FISCHER, CHRISTIAN, KELLER, CHARLOTTE, SCHJERLING, PETER, HISCOCK, NATALIE, MØLLER, KIRSTEN, SALTIN, BENGT, FEBBRAIO, MARK A, & PEDERSEN, BENTE K. 2003. Interleukin-6 stimulates lipolysis and fat oxidation in humans. *J clin endocrinol metab*, **88**(7), 3005–10.
- VANHAESEBROECK, B, & ALESSI, D R. 2000. The pi3k-pdk1 connection: more than just a road to pkb. *Biochem j*, **346 Pt 3**(Mar), 561–76.
- VARONA-SANTOS, J L, PILEGGI, A, MOLANO, R D, SANABRIA, N Y, IJAZ, A, ATSUSHI, M, ICHII, H, PASTORI, R L, INVERARDI, L, RICORDI, C, & FORNONI, A. 2008. c-jun n-terminal kinase 1 is deleterious to the function and survival of murine pancreatic islets. *Diabetologia*, **51**(12), 2271–80.
- VOOIJIS, M, JONKERS, J, & BERNS, A. 2001. A highly efficient ligand-regulated cre recombinase mouse line shows that loxp recombination is position dependent. *Embo rep*, **2**(4), 292–7.
- VOZAROVA, B, WEYER, C, HANSON, K, TATARANNI, P A, BOGARDUS, C, & PRATLEY, R E. 2001. Circulating interleukin-6 in relation to adiposity, insulin action, and insulin secretion. *Obes res*, **9**(7), 414–7.
- WALLENIUS, VILLE, WALLENIUS, KRISTINA, AHRÉN, BO, RUDLING, MATS, CARLSTEN, HANS, DICKSON, SUZANNE L, OHLSSON, CLAES, & JANSSON, JOHN-OLOV. 2002. Interleukin-6-deficient mice develop mature-onset obesity. *Nat med*, **8**(1), 75–9.
- WEISBERG, STUART P, MCCANN, DANIEL, DESAI, MANISHA, ROSENBAUM, MICHAEL, LEIBEL, RUDOLPH L, & FERRANTE, ANTHONY W. 2003. Obesity is associated with macrophage accumulation in adipose tissue. *J clin invest*, **112**(12), 1796–808.

- WEISSENBACH, J, CHERNAJOVSKY, Y, ZEEVI, M, SHULMAN, L, SOREQ, H, NIR, U, WALLACH, D, PERRICAUDET, M, TIOLLAIS, P, & REVEL, M. 1980. Two interferon mRNAs in human fibroblasts: in vitro translation and escherichia coli cloning studies. *Proc natl acad sci usa*, **77**(12), 7152–6.
- WESTON, CLAIRE R, & DAVIS, ROGER J. 2007. The jnk signal transduction pathway. *Curr opin cell biol*, **19**(2), 142–9.
- WHITE, MORRIS F. 2003. Insulin signaling in health and disease. *Science*, **302**(5651), 1710–1.
- WHITHAM, MARTIN, CHAN, M H STANLEY, PAL, MARTIN, MATTHEWS, VANCE B, PRELOVSEK, OJA, LUNKE, SEBASTIAN, EL-OSTA, ASSAM, BROENNEKE, HELLA, ALBER, JENS, BRUNING, JENS C, WUNDERLICH, F THOMAS, LANCASTER, GRAEME I, & FEBBRAIO, MARK A. 2012. Contraction-induced il-6 gene transcription in skeletal muscle is regulated by c-jun terminal kinase/activator protein -1. *J biol chem*, Feb.
- WHITMAN, M, DOWNES, C P, KEELER, M, KELLER, T, & CANTLEY, L. 1988. Type i phosphatidylinositol kinase makes a novel inositol phospholipid, phosphatidylinositol-3-phosphate. *Nature*, **332**(6165), 644–6.
- WILD, SARAH, ROGLIC, GOJKA, GREEN, ANDERS, SICREE, RICHARD, & KING, HILARY. 2004. Global prevalence of diabetes: estimates for the year 2000 and projections for 2030. *Diabetes care*, **27**(5), 1047–53.
- WOLSK, EMIL, MYGIND, HELENE, GRØNDAHL, THOMAS S, PEDERSEN, BENTE K, & VAN HALL, GERRIT. 2010. Il-6 selectively stimulates fat metabolism in human skeletal muscle. *Am j physiol endocrinol metab*, **299**(5), E832–40.
- WUNDERLICH, F T, WILDNER, H, RAJEWSKY, K, & EDENHOFER, F. 2001. New variants of inducible cre recombinase: a novel mutant of cre-pr fusion protein exhibits enhanced sensitivity and an expanded range of inducibility. *Nucleic acids res*, **29**(10), E47.
- WUNDERLICH, F THOMAS, STRÖHLE, PETER, KÖNNER, A CHRISTINE, GRUBER, SABINE, TOVAR, SULAY, BRÖNNEKE, HELLA S, JUNTTI-BERGGREN, LISA, LI, LUOSHENG, VAN ROOIJEN, NICO, LIBERT, CLAUDE, BERGGREN, PER-OLOF, & BRÜNING, JENS C. 2010. Interleukin-6 signaling in liver-parenchymal cells suppresses hepatic inflammation and improves systemic insulin action. *Cell metab*, **12**(3), 237–49.
- WUNDERLICH, THOMAS. 2004. *Generation of inducible cre systems for conditional gene inactivation in mice*. Ph.D. thesis, University of Cologne.
- Y WANG, B SU, VP SAH JH BROWN J HAN KR CHIEN. 1998. Cardiac hypertrophy induced by mitogen-activated protein kinase kinase 7, a specific activator for c-jun nh2-terminal kinase in ventricular muscle cells. *Journal of biological chemistry*, **273**(10), 5423–5426.

Bibliography

- ZHANG, XIAOQING, ZHANG, GUO, ZHANG, HAI, KARIN, MICHAEL, BAI, HUA, & CAI, DONGSHENG. 2008. Hypothalamic ikkbeta/nf-kappab and er stress link overnutrition to energy imbalance and obesity. *Cell*, **135**(1), 61–73.
- ZHOU, YINGJIANG, LEE, JUSTIN, RENO, CANDACE M, SUN, CHENG, PARK, SANG WON, CHUNG, JASON, LEE, JAEMIN, FISHER, SIMON J, WHITE, MORRIS F, BIDDINGER, SUDHA B, & OZCAN, Umut. 2011. Regulation of glucose homeostasis through a xbp-1-foxo1 interaction. *Nat med*, **17**(3), 356–65.
- ZIMMET, P, ALBERTI, K G, & SHAW, J. 2001. Global and societal implications of the diabetes epidemic. *Nature*, **414**(6865), 782–7.

Danksagung

Dieser Abschnitt bietet mir die Möglichkeit, mich bei diesen Personen zu bedanken, die entscheidend zum guten Gelingen dieser Arbeit beigetragen haben. Im Besonderen bedanke ich mich bei

- **PD Dr. Thomas Wunderlich** für all seine Unterstützung und sein Verständnis in den letzten Jahren. Er stand mir immer und bei jedem Problem mit Rat und Tat zur Seite, ohne ihn wäre vieles nicht möglich gewesen. Ihm gebührt mein größter Dank.
- **Prof. Dr. Jens Brüning** dafür, dass ich seit so vielen Jahren ein Teil der AG-Brüning sein darf und er mir zusammen mit Thomas Wunderlich diese Dissertation ermöglicht hat.
- **Prof. Dr. Peter Kloppenburg** dafür, dass er sich dazu bereit erklärt hat, den Vorsitz meiner Disputation zu übernehmen.
- **Dr. Claudia Wunderlich** für ihre Bereitschaft gemeinsam mit den oben genannten Personen mein Prüfungskomitee zu formen. Weiterhin danke ich ihr für das unermüdliche Korrekturlesen meiner Arbeit und den Spaß, den wir gemeinsam mit **Sabine Gruber** in unserem Labor auf der "Schäl Sick" haben!
- den Kollegen **Sonja Becker** und **Patrick Jankowski** für die Blastozysten-Injektionen, sowie bei **Brigitte Hampel** und **Pia Scholl** für ihre Hilfe bei Schnitten und Färbungen. Ferner danke ich **Dr. Hella Brönnecke** und **Jens Alber** für ihre Unterstützung bei den Messungen im Phenomaster und auf dem Laufband. Schließlich bedanke ich mich bei meinen Laborkolleginnen **Anke Lietzau** und **Rele Ringeisen** für ihre großartige technische Unterstützung in allen Situationen.
- **Dr. Simon Heß** für seine Unterstützung bei all den Problemen, die das Schreiben mit LaTeX mit sich bringt.
- **Dr. Hayley Nichols** for helpful and most desired suggestions on writing a "super hammer geil" manuscript.
- **Dr. Peter Ströhle** und **Dr. Denis Delic** für gründliches Korrekturlesen und den vielen Spaß, den wir zusammen mit **Justus Ackermann** nicht zuletzt dank Comunio und TGIF haben.
- allen Kollegen der **AG Brüning**, die hier namentlich unerwähnt bleiben und dennoch großen Anteil an der besonderen Atmosphäre des Brüning-Labs haben, und mir bei jedem Problem und jeder Frage sofort in großartiger Weise zur Seite standen.

- bei den lieben Menschen und Freunden, die mich außerhalb meiner Arbeit begleiten. Im besonderen bei **Thomas Stratmann** für die gute Zeit vor, während und nach dem Triathlon-Sport in den letzten Jahren. Ebenso danke ich **Jörg Lambertz** u.a. für die mehr oder weniger regelmäßige sonntägliche Laufrunde durch das Grefrather Marienfeld.
- meiner **Familie**, meinen Eltern **Ursula und Karl Pal**, die mich jederzeit bedingungslos unterstützt haben und größten Dank verdienen, sowie meinen Brüdern **Thomas und Stefan Pal** und **Peter Pal**. Genauso danke ich **Yvonne und Ingo Reibe**, die mich stets unterstützen, und **Dustin Reibe** nicht zuletzt für die herzliche Leihgabe seines Apple.

Die letzte Worte gehören der besten Person in meinem Leben, **Dr. Saskia Reibe**. Sie war nicht nur zu den leichten Zeiten an meiner Seite, sondern stand auch grade in schwierigeren Zeiten hinter mir und hat mir immer wieder gezeigt wofür es sich lohnt zu kämpfen.

**It's so hard to get on without a cause, I don't want to perish like a fading horse,
youth's like diamonds in the sun and diamonds are forever**

Alphaville, 1984

Erklärung

Ich versichere, dass ich die von mir vorgelegte Dissertation selbständig angefertigt, die benutzten Quellen und Hilfsmittel vollständig angegeben und die Stellen der Arbeit – einschließlich Tabellen, Karten und Abbildungen –, die anderen Werken im Wortlaut oder dem Sinn nach entnommen sind, in jedem Einzelfall als Entlehnung kenntlich gemacht habe; dass diese Dissertation noch keiner anderen Fakultät oder Universität zur Prüfung vorgelegen hat; dass sie – abgesehen von unten angegebenen Teilpublikationen – noch nicht veröffentlicht worden ist sowie, dass ich eine solche Veröffentlichung vor Abschluss des Promotionsverfahrens nicht vornehmen werde.

Die Bestimmungen der Promotionsordnung sind mir bekannt. Die von mir vorgelegte Dissertation ist von Prof. Dr. Jens Brüning und PD Dr. Thomas Wunderlich betreut worden.

Köln, den 27.02.2012

(Martin Pal)

Teilpublikationen

WHITHAM M, CHAN MHS, PAL M, MATTHEWS VB, PRELOVSEK O, LUNKE S, EL-OSTA A, BRÖNNEKE HS, ALBER J, BRÜNING JC, WUNDERLICH FT, LANCASTER GI, FEBBRAIO M. 2012. Contraction-induced IL-6 gene transcription in skeletal muscle is regulated by c-jun terminal kinase/Activator-protein -1. *J. Biol. Chem.*, **Epub ahead of print.**

BELGARDT BF, MAUER J, WUNDERLICH FT, ERNST MB, PAL M, SPOHN G, BRÖNNEKE HS, BRODESSER S, HAMPEL B, SCHAUSS AC, BRÜNING JC. 2010. Hypothalamic and pituitary c-Jun N-terminal kinase 1 signaling coordinately regulates glucose metabolism. *PNAS*, **107(13)**, 6028-33.

Curriculum Vitae

Dipl. Biol. Martin Pal

University of Cologne
Institute for Genetics
Zuelpicher Str. 47b
50674 Cologne
Tel.: +49 (0)221 470-1552
Email: mpal@uni-koeln.de
Birthday/ -place: 01-11-1983 in Cologne
Nationality: german

EDUCATION

- 2008 – 2012 **University of Cologne, Institute for Genetics**
PhD-thesis in the laboratory of Prof. Dr. Jens Brüning and PD Dr. Thomas Wunderlich. Topic: "Stress Signaling Pathways in Metabolic Disorders".
- 2007 – 2008 **University of Cologne, Institute for Genetics**
Diploma-thesis in the laboratory of Prof. Dr. Jens Brüning. Topic: "Generation of loxP flanked c-Jun N-terminal kinase alleles 2 and 3 in murine embryonic stem cells"
- 2003 – 2008 **University of Heidelberg**
Study of Biological Sciences. Graduation: Diplom
- 2002 – 2003 **Military Service, Wachbataillon**
Brueckberg-Baracks, Siegburg
- 1993 – 2002 **Elisabeth-von-Thueringen-Gymnasium, Koeln-Suelz**
Graduation: Abitur
- 1989 – 1993 **Kath. Grundschule Berrenrather Str., Koeln-Suelz**

Cologne, 27. February 2012 _____
(Martin Pal)

Curriculum Vitae

Dipl. Biol. Martin Pal

Universität zu Köln
Institut für Genetik
Zülpicher Straße 47b
50674 Köln
Tel.: +49 (0)221 470-1552
Email: mpal@uni-koeln.de
Geburtsdatum/ -ort: 11.01.1983 in Köln
Staatsangehörigkeit: deutsch

AUSBILDUNG

- 2008 – 2012 **Universität zu Köln, Institut für Genetik**
Doktorarbeit im Labor von Prof. Dr. Jens Brüning und PD Dr. Thomas Wunderlich. Thema: „Stress Signaling Pathways in Metabolic Diseases“.
- 2007 – 2008 **Universität zu Köln, Institut für Genetik**
Diplomarbeit im Labor von Prof. Dr. Jens Brüning. Thema:
"Generation of loxP flanked c-Jun N-terminal kinase alleles 2 and 3 in murine embryonic stem cells"
- 2003 – 2008 **Universität zu Heidelberg**
Studium der Biologie. Abschluss: Diplom
- 2002 – 2003 **Wehrdienst, Wachbataillon**
Brückberg-Kaserne, Siegburg
- 1993 – 2002 **Elisabeth-von-Thüringen-Gymnasium, Köln-Sülz**
Abschluss: Abitur (Fachhochschulreife)
- 1989 – 1993 **Kath. Grundschule Berrenrather Str., Köln-Sülz**

Köln, den 27. Februar 2012 _____
(Martin Pal)